

COOL SUBDWARF INVESTIGATIONS. I. NEW THOUGHTS ON THE SPECTRAL TYPES OF K AND M SUBDWARFS

WEI-CHUN JAO¹, TODD J. HENRY¹, THOMAS D. BEAULIEU¹, AND JOHN P. SUBASAVAGE¹

Department of Physics and Astronomy, Georgia State University, Atlanta, GA 30302-4106, USA; jao@chara.gsu.edu, thenry@chara.gsu.edu, beaulieu@chara.gsu.edu, and subasavage@chara.gsu.edu

Received 2007 July 11; accepted 2008 May 16; published 2008 July 14

ABSTRACT

Using new spectra of 88 K- and M-type subdwarfs, we consider novel methods for assigning their spectral types and take steps toward developing a comprehensive spectral sequence for subdwarf types K3.0 to M6.0. The types are assigned based on the overall morphology of spectra covering 6000–9000 Å. The types and sequence presented link the spectral types of cool subdwarfs to their main-sequence counterparts, with emphasis on the relatively opacity-free region from 8200–9000 Å. When available, supporting abundance, kinematic, and trigonometric parallax information is used to provide more complete portraits of the observed subdwarfs. We find that the CaHn ($n = 1-3$) and TiO5 indices often used for subdwarf spectral typing are affected in complicated ways by combinations of the subdwarfs' temperatures, metallicities, and gravities, and we use model grids to evaluate the trends in all three parameters. Because of the complex interplay of these three characteristics, it is not possible to identify a star as an “extreme” subdwarf simply based on very low metallicity, and we suggest that the modifiers “extreme” or “ultra” only outline locations on spectroscopic indices plots, and should not be used to imply low or very low metallicity stars. In addition, we propose that “VI” be used to identify a star as a subdwarf, rather than the confusing “sd” prefix, which is also used for hot O and B subdwarfs that are unrelated to the cool subdwarfs discussed in this paper.

Key words: stars: abundances – stars: fundamental parameters – stars: late-type – subdwarfs

Online-only material: color figures

1. INTRODUCTION

The H-R diagram is the most important map in stellar astronomy. It provides a relatively straightforward method for separating different stellar luminosity classes, e.g., supergiants, bright giants, giants, subgiants, main-sequence dwarfs, and white dwarfs, using their colors and luminosities. However, spectroscopic and trigonometric parallax results have revealed a seventh distinct stellar luminosity class—the subdwarfs—that lie below the main-sequence dwarfs on the H-R diagram.

The realm of the subdwarfs has been previously explored by Sandage & Eggen (1959), Hartwick et al. (1984), Monet et al. (1992), Gizis (1997), and Jao et al. (2005), to name a few. Subdwarfs' locations on the H-R diagram are in part due to having metallicity abundances lower than most field stars, which causes their opacities to differ from those of regular dwarfs. Subdwarfs are sometimes called low metallicity halo stars or Galactic thick disk stars based on their spectroscopic features, kinematics, and/or ages (Digby et al. 2003; Lépine et al. 2003; Burgasser et al. 2003; Reid & Gizis 2005; Monteiro et al. 2006). Regardless of how they are described, subdwarfs are fundamentally different from their main-sequence cousins.

Because of their generally high intrinsic velocities in the Galaxy, many subdwarfs have been selected using high-proper-motion efforts, such as the Lowell proper motion (Giclas et al. 1971, 1978), the Luytens Half-Second (LHS) (Luyten 1979), and Lépine-Shara Proper Motion-North (LSPM; Lépine & Shara 2005a) catalogs. Recently, subdwarfs have been selected by colors and spectroscopic observations via the Sloan Digital Sky Survey (SDSS; West et al. 2004). After initial flagging as a

potential subdwarf, spectroscopic and astrometric (i.e., trigonometric parallax work) followup efforts are typically carried out to confirm or refute candidates as true subdwarfs. Past subdwarf identification efforts include Bessell & Wickramasinghe (1979), Ryan & Norris (1991), Monet et al. (1992), Carney et al. (1994), Gizis (1997), Lépine et al. (2003), West et al. (2004), Reid & Gizis (2005), and Burgasser & Kirkpatrick (2006). Most of these studies confirmed subdwarfs spectroscopically, but only Monet et al. (1992) provide the crucial trigonometric parallaxes that allow subdwarfs to be placed on the H-R diagram.

Gizis (1997) presented a pioneering effort to assign numeric subtypes for cool subdwarfs of spectral types K and M. First, he used the flux ratio of molecular band features, CaHn ($n = 1-3$; we will use “CaH” to indicate all three bands or index values throughout this paper, unless otherwise specified) and TiO5 with pseudo-continuum points to calculate spectroscopic indices ($f_{\text{bands}}/f_{\text{continuum}}$). On TiO5 versus CaH1 or TiO5 versus CaH2 + CaH3 plots, two high-order polynomial lines can be used to separate a continuous distribution of stars into three categories: regular dwarfs, subdwarfs, and extreme subdwarfs. Numerical subclasses were then assigned using two independent linear fits for subdwarfs and extreme subdwarfs. For a decade, this methodology has been used to assign spectral types for cool subdwarfs.

However, the current method of assigning subdwarf spectral types is not directly linked to either their main-sequence or giant counterparts, as is typically (but not always) the case with normal dwarfs and giants. In addition, we have found that many subdwarfs are assigned different subtypes even though their differences are limited to CaH. If these limitations can be overcome, a well-defined spectral sequence would benefit many research areas beyond classification efforts, including attempts to estimate effective temperatures and distances, as well as providing insight into understanding Galactic structure.

¹ Visiting Astronomer, Cerro Tololo Inter-American Observatory. CTIO is operated by AURA, Inc., under contract to the National Science Foundation.

In this work, we first provide clarification and recommendations for subdwarf terminology by addressing the usage of the confusing spectral prefix “sd.” We then discuss our spectroscopic observations of 88 subdwarfs, generally targeting high-proper-motion stars in the southern sky. We next outline how synthetic spectra can assist us in understanding cool subdwarf spectral features. The bulk of this work describes a detailed effort to provide a subdwarf spectral sequence for stars having spectral types K3.0 through M6.0. We then apply this spectral typing method to those subdwarfs found in the SDSS database. Once we have a detailed understanding of what makes a star a subdwarf, we then discuss (1) why it is premature to assign precise parameters to subdwarf spectra, (2) misunderstandings related to the terms “extreme” and “ultra” subdwarfs, (3) why the old method works for dwarfs, but not subdwarfs, and finally (4) the recent set of subdwarf spectral standards from Lépine et al. (2007).

2. “VI” SUBDWARFS ARE DIFFERENT FROM “sd” SUBDWARFS

The first subluminescent objects fainter than main-sequence stars were reported by Adams & Joy (1922) when they were trying to determine the luminosities of A-type stars. In Adams et al. (1935) they called these stars “intermediate white dwarfs” to separate them from typical white dwarfs, and in the same paper reported the first six “intermediate white dwarfs”—now known as LHS 405 (sdF3), LHS 540 (F8IV), LHS 1501 (A4p), LHS 2194 (sdF5), HD 132475 (F5/F6V), and HIP 68321 (A4). All six have either A or F types (spectral types are from SIMBAD) in the modern MK spectral classification system. However, the term “subdwarfs” was not suggested until Kuiper (1939). He expected three classes of objects to be found in his spectroscopic survey of high-proper-motion stars—white dwarfs, stars of large spectroscopic parallaxes, and a class that was 2 or 3 mag less luminous than main-sequence stars of the same color.² He suggested the name “subdwarfs” be used to represent this final, independent, class of stars. This name paralleled the use of the term “subgiants” to describe stars that fall below the giants on the H-R diagram. The name also eliminated the confusion with white dwarfs, which are much less luminous than main-sequence stars (and we now know they are a completely different type of object). A year later, Kuiper (1940) reported the first three M-type subdwarfs—Kapteyn’s star, LHS 20, and LHS 64 (Gizis 1997 confirmed that all are M subdwarfs). Although they were termed subdwarfs, he used the same spectral classification as dwarfs (M0 and M2; see Kuiper 1940 Table 1). The “sd” spectral classification prefix for subdwarfs did not appear until Joy (1947), when he used the strengthening of the Lindblad depression around 4226 Å.

In the late 1940s through 1960s, the term “subdwarfs” also began to be used for a class of underluminous blue stars (Humason & Zwicky 1947; Feige 1958; Greenstein 1966; Greenstein & Münch 1966). The terminology was based on the understanding that if these were high luminosity blue stars, their distances would be outside the Milky Way, so it was surmised that these stars should be underluminous, and therefore closer. Although their temperatures are similar to O and B dwarfs, their spectral features are, in fact, quite different. Generally, O-type

subdwarfs (sdO) and B-type subdwarfs (sdB) both have broad Balmer absorption. sdBs have weak or no He II lines, while sdOs have strong He II (4686 Å) or other He II lines (Heber 1992). Since Feige (1958), such blue objects have been called sdO-, sdB-, or sdOB-type stars.

Thus, we are left with the unfortunate situation that there are two different classes of stars called “subdwarfs.” One is located at the cool end of the H-R diagram while the other is at the hot end. The two classes of stars are subluminescent for completely different astrophysical reasons but share the same “sd” spectral classification prefix. Cool subdwarfs usually have low metallicity (Chamberlain & Aller 1951; Greenstein & Eggen 1966; Mould 1976; Allard & Hauschildt 1995), so their opacities are different from those of dwarfs. For example, Allard & Hauschildt (1995) discussed the possible opacity sources for a solar-type dwarf and a $[m/H] = -2.5$ subdwarf. TiO dominates the opacity sources in the optical band. However, because of the decreasing metallicity for subdwarfs, TiO opacity decreases dramatically. Hence, this less blanketing from TiO bands causes more continuum flux radiated from deeper and hotter layer of stellar atmosphere and their spectrum falls closer overall to that of a blackbody, so these subdwarfs appear bluer than dwarfs, as shown in Figure 1.³ In contrast, hot blue subdwarfs of types O and B are progenitors of white dwarfs, and their subluminescent nature is not caused by metallicity at all. Instead, hot subdwarfs represent a stage in the stellar evolution cycle of an evolved star, and they happen to be crossing the main sequence at the moment of observation.

Because they *are* different kinds of stellar objects, we suggest that the two classes should not share the same spectral classification notation, “sd.” Roman (1955) argued that for types later than G0, the spectral notation “VI” should be used for stars that are $\sim 1\text{--}2$ mag less luminous than main-sequence stars. Although Jaschek & Jaschek (1987) stated that “this designation (VI) should definitely be abandoned,” no specific reasons were actually given. Here we propose that the luminosity class “VI” should be adopted for cool subdwarfs, especially for K and M types. The three primary reasons are as follows.

1. Cool subdwarfs of types K and M lie clearly below main-sequence stars on the H-R diagram, forming an additional class of objects. Assigning their types as VI continues the progression outlined by other classes. Like the family of giants, which includes luminous supergiants (I), bright giants (II), normal giants (III), and subgiants (IV), the family of dwarfs includes main-sequence dwarfs (V) and their subdwarf (VI) counterparts.
2. Cool subdwarfs and OB subdwarfs are completely differently types of objects with different origins. The notation “sd” is suitable for OB subdwarfs, which have not yet as a group been established to have any sort of sequence on the H-R diagram, at least when using parallaxes from the Yale Parallax Catalog, *Hipparcos*, and more recent efforts. On the other hand, there are dozens of cool subdwarfs with parallax measurements, and they do form a coherent group below the main sequence on the H-R diagram, making a Roman numeral designation reasonable.
3. Historically, the Roman numerals used for luminosity categorization track with different gravities for the stars classified, with higher gravities being assigned higher Roman

² Kuiper assumed all of these high-proper-motion stars had V_{tan} less than 474 km s^{-1} . Under this assumption, he could then make crude estimates of their absolute magnitudes without having trigonometric parallaxes. The results placed some stars 3 mag below the main sequence.

³ The details of these synthetic spectra, the “GAIA model grids,” are discussed in Section 4.

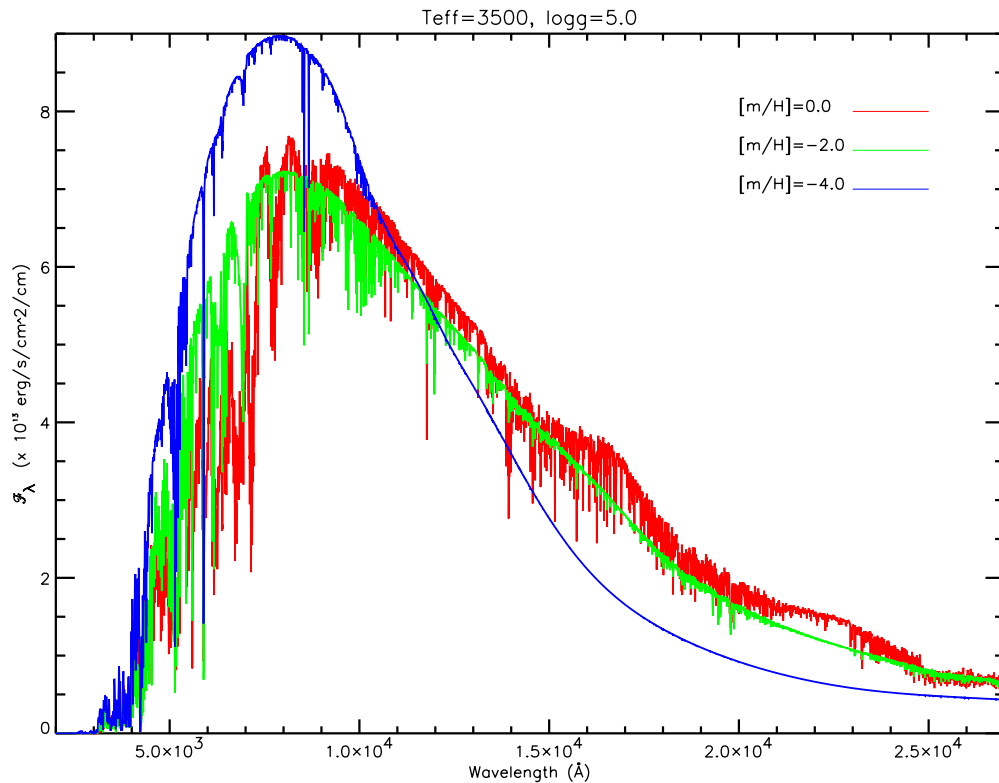


Figure 1. Synthetic spectra for stars having $T_{\text{eff}} = 3500$ K and $\log g = 5.0$. The red, green, and blue lines represent different metallicities, 0.0, -2.0 , and -4.0 . Note that the relative amounts of blue and red fluxes trend toward bluer objects at lower metallicities. (A color version of this figure is available in the online journal.)

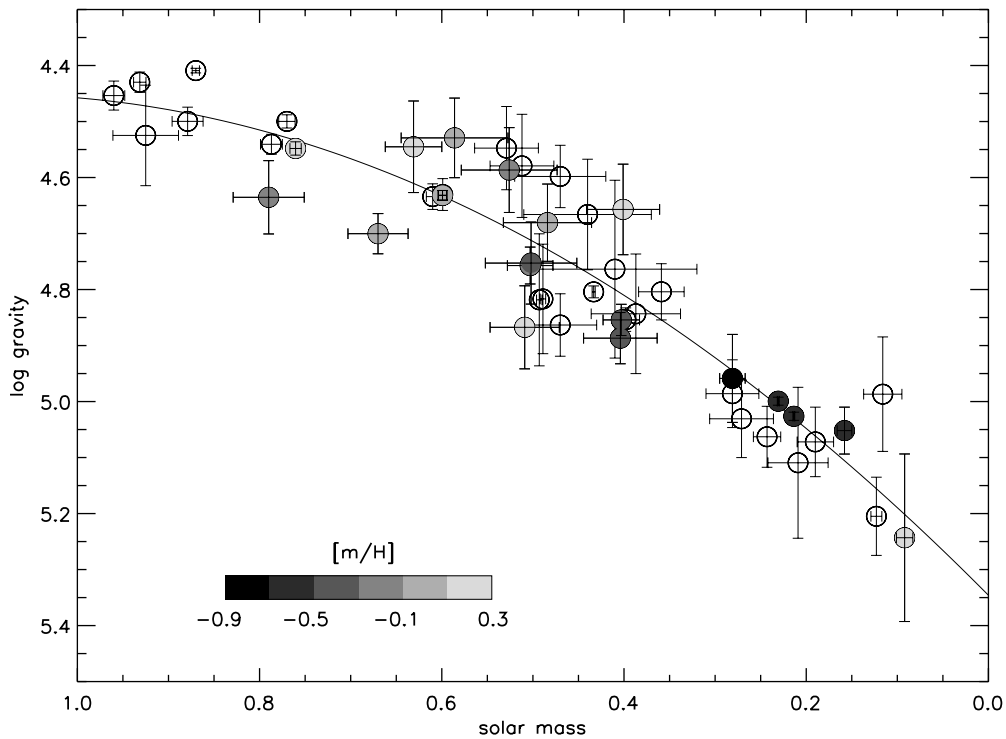


Figure 2. Mass–gravity relation using data from Table 1 of López-Morales (2007). A solid line represents a polynomial fit to all of the points, simply to be used as a guide. Different shades for the points represent different metallicity measurements. Stars with unknown metallicities are plotted as the open circles.

numerals. We find that assigning “VI” for subdwarfs appropriately continues this trend. Figure 2 shows the mass–gravity relation using data from Table 1 of López-Morales (2007). In the best-represented mass regime from $0.35 M_{\odot}$

to $0.70 M_{\odot}$, a crude trend indicates that lower metallicity stars do indeed have higher gravities. Although much more data are needed to understand clearly how metallicity affects the mass–gravity relation, current evidence supports

using the “VI” designation for low metallicity subdwarfs, which tend to exhibit higher gravities.

Thus, in order to separate the OB subdwarfs from the cool subdwarfs, we suggest the “sd” prefix should not be used for low-metallicity (and/or high gravity, as will be shown below) subdwarfs.

3. OBSERVATIONS AND REDUCTIONS

3.1. Observations

Our subdwarf targets were selected from several different efforts, including lists of spectroscopically identified subdwarfs (Gizis 1997; Reid & Gizis 2005), subdwarfs with parallax measurements (Jao et al. 2005; Costa et al. 2005, 2006), candidates from proper-motion catalogs (Deacon et al. 2005; Subasavage et al. 2005a, 2005b), and stars with metallicity measurements (Carney et al. 1994; Cayrel de Strobel et al. 2001; Nordström et al. 2004). We define our subdwarfs of interest to be those with $V - K_s \geq 2.0$, $[M/H] \leq -0.5$, or having absolute magnitudes at least 1 mag less luminous in M_{K_s} than a fit to main-sequence stars of comparable color with trigonometric parallaxes from the Research Consortium on Nearby Stars (RECONS) 10 pc sample (Henry et al. 2006).

Spectroscopic observations were made with the 1.5 m and 4.0 m telescopes at Cerro Tololo Inter-American Observatory (CTIO). For the observations on the 1.5 m from 2002 to 2006, the R-C spectrograph with a Loral 1200 × 800 CCD camera was used with the #32 grating (in first order) at tilt 15.1°. The order-blocking filter OG570 was utilized to provide spectra covering the range 6000–9500 Å with a resolution of 8.6 Å. The only variation in observing parameters was that during the 2006 May and December observing runs a larger slit width of 6" and 4", respectively, was used instead of the 2" slit used in previous runs, in order to minimize the differential color refraction (because the slit orientation was not changed during observations). For observations on the 4.0 m in 2002, the R-C spectrograph with a Loral 3K × 1K CCD was used with the #181 grating (in first order) at tilt 58.8°. The order-blocking filter OG515 was utilized to provide spectra covering the range from 5500 Å to 10000 Å with a resolution of 6 Å. Fringing at wavelengths longer than ~7000 Å in the 4.0 m data was removed by customized IDL routines. Bias frames and dome flats (and sky flats at the 1.5 m) were taken at the beginning of each night for calibration. At least two exposures were taken for each object to permit cosmic ray rejection. If stars were faint, additional observations were sometimes made. A 10 s Ne + He + Ar or Ne only arc lamp spectrum was recorded after each target to permit wavelength calibration. Several spectroscopic flux standard stars found in the IRAF spectroscopy reduction packages were observed during each observing run, usually nightly. Reductions were carried out in the standard way using IRAF reduction packages. Wavelength and flux calibrations were done using *onedspec.dispcor* and *onedspec.calibrate* within IRAF, respectively.

Many of the subdwarfs discussed in this paper have new trigonometric parallaxes and *VRI* photometry acquired during our southern nearby star program, Cerro Tololo Inter-American Observatory Parallax Investigation (CTIOPI; see Jao et al. 2005). In a future paper in this subdwarf series, we will present the astrometric (particularly trigonometric parallaxes) and photometric results.

3.2. Identifying Subdwarfs

During our five-year spectroscopic campaign, we have acquired spectra for more than 900 objects. To glean subdwarfs from our spectroscopic database, we calculated their spectroscopic indices listed in Table 1 (targets listed alphabetically), mimicking the methodology outlined by Gizis (1997).

Figure 3 shows TiO5 plotted against CaH1 and CaH2 + CaH3 for various samples of stars. Our subdwarfs are shown with solid circles. For comparison, small dots indicate main-sequence stars from Hawley et al. (1996), while the open triangles and squares represent subdwarfs and “extreme” subdwarfs from Gizis (1997) and Reid & Gizis (2005). Some stars (solid circles) having indices located near or in the main-sequence regions in these plots have been manually checked to confirm that they are subdwarfs. Using the H-R diagram in Figure 4, we confirm the low luminosities of our spectroscopically selected subdwarfs ($V - K_s > 2.7$) that have accurate trigonometric parallaxes.

Although we focus primarily on the K and M subdwarfs for this study, we include a few G-type subdwarfs among those selected from metallicity measurements in the literature. For reference, we consider early K-type stars to have types K0 to K2, mid-K-types to be K3 to K5, and late K-types to be K6 and later. We find that it is difficult, but possible, to separate late G from early K-type stars using our spectral coverage and resolution. Their continuum slopes have only slight differences across our wavelength window coverage, and there are no noticeable absorption differences beyond 7500 Å. Spectra for G1V to K5V types from Jacoby et al. (1984) (resolution ~4 Å) and Silva & Cornell (1992) (resolution ~11 Å) are plotted in Figure 5. The only strong features are the absorption lines of Ba I (6497 Å)⁴ and H α (6563 Å), with gradually increasing Ba I absorption and decreasing H α absorption as the effective temperature drops. These effects can be seen in both sequences, regardless of the spectral resolution. Our spectral resolution of 6–9 Å falls between the resolution of the two sequences shown, so we can use the relative absorption strengths of Ba I and H α to separate G- and K-type stars. In total, we have identified 88 K and M subdwarfs and five G-type subdwarfs, using spectra with coverage from 6000 Å to 9000 Å.

3.3. Sorting Spectra

After reduction, the spectra were sorted into different bins based upon similarity in overall slope and features. This assured that stars in each bin had approximately the same temperature. However, several impediments to clean sorting were encountered.

1. All mid-K-type subdwarfs had spectra virtually indistinguishable from dwarf standard stars, yet they had low-metallicity measurements and/or were found below the main sequence on the H-R diagram (see top figure in Figure 6).
2. Many subdwarf spectra placed into the same bin showed differences only in CaH (see the middle figure in Figure 6).
3. Many subdwarf spectra matched different dwarf standards at the blue ($\lambda < 7570$ Å) and red ($\lambda > 8200$ Å) ends (see the bottom figure in Figure 6).

⁴ Turnshek et al. (1985) noted that this feature at 6497 Å is a blend of different atomic lines, including Fe I, Ba I, Ca I, Mn I, Co I, Ti I and II, and Ni I. Ba I is likely the dominant absorber because it has the largest Einstein coefficient in the NIST atomic spectra database.

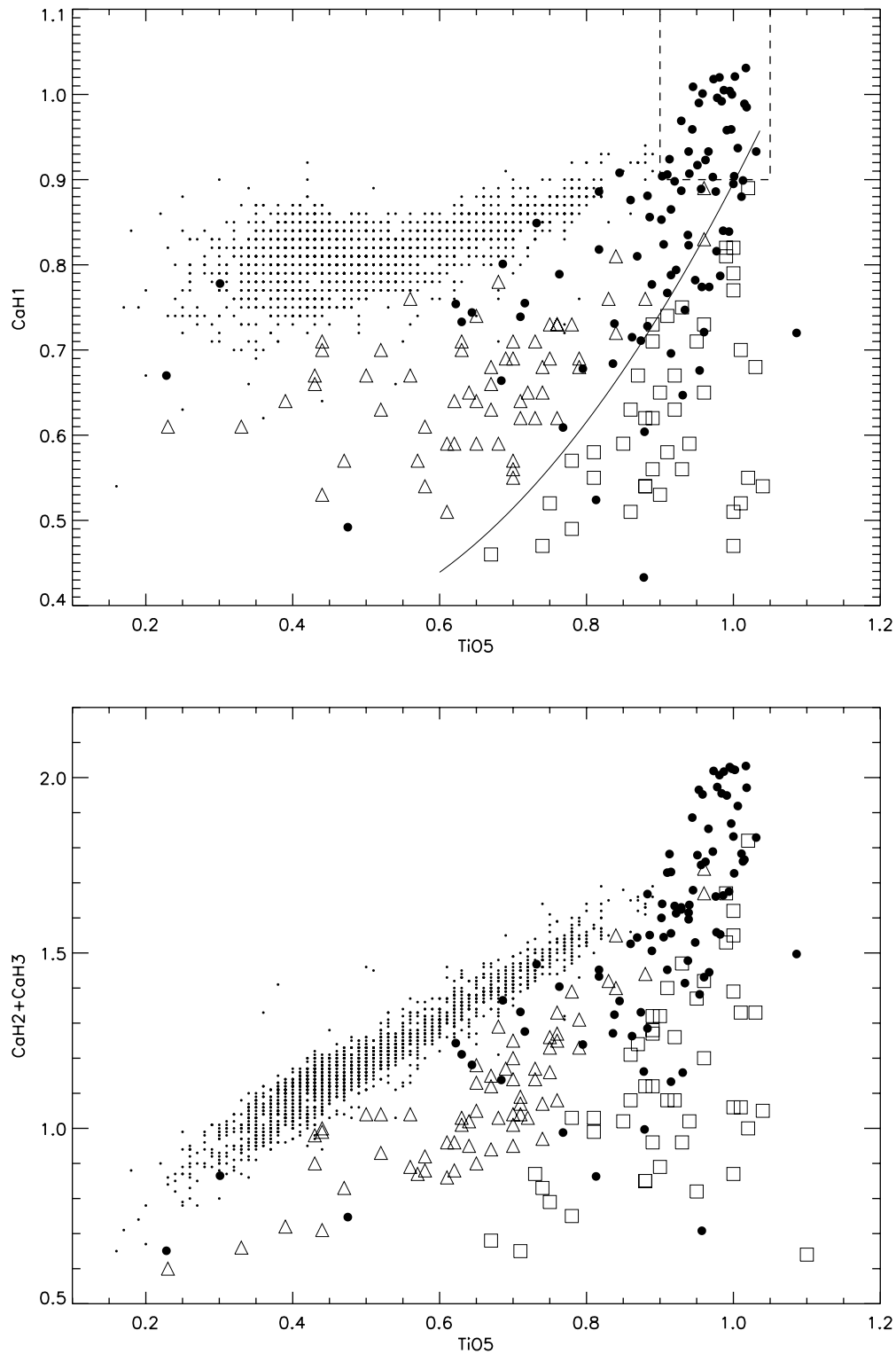


Figure 3. CaH1 and CaH2+CaH3 vs. TiO5 indices plotted for our identified subdwarfs (solid circles). For comparison, known cool dwarfs (dots), subdwarfs (open triangles), and “extreme” subdwarfs (open boxes) from Hawley et al. (1996), Gizis (1997), and Reid & Gizis (2005) are also shown. The dashed box indicates subdwarfs that do not exhibit strong spectroscopic indices, but which are either below the main sequence on the H-R diagram or have published metallicities $[m/H]$ less than or equal to -0.5 . A solid line indicates the separation between regular subdwarfs and extreme subdwarfs adopted by Gizis (1997).

In order to understand what factors caused these anomalies, we next examine theoretical studies that provide synthetic spectra that can be compared directly to the observed spectra.

4. GRIDS OF SYNTHETIC SPECTRA

We use grids of synthetic spectra computed with PHOENIX codes (hereafter, *GAIA* model grids) to understand how

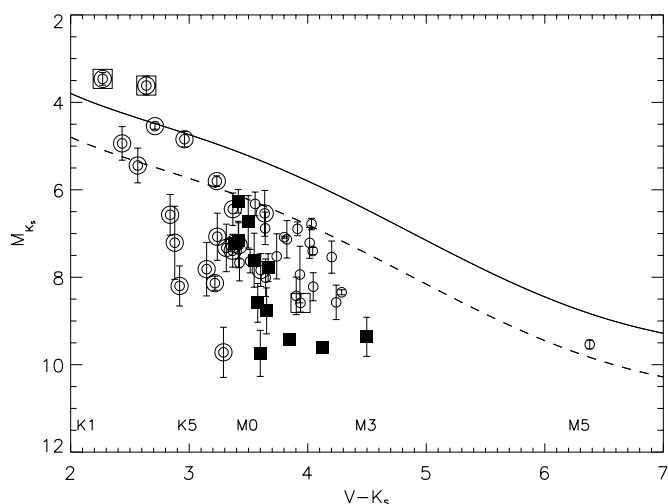


Figure 4. H-R diagram for subdwarfs listed in Table 1 and shown in Figure 3 that have trigonometric parallaxes. The open circles indicate subdwarfs and the filled boxes indicate “extreme” subdwarfs based on spectroscopic indices. The concentric circles indicate stars with CaH1 index greater than 0.9 that are difficult to distinguish from main-sequence stars at our spectral resolution. The open boxes indicate confirmed spectroscopic binaries. A solid line indicates a fit to main-sequence dwarfs, primarily from Henry et al. (2004) with extra dwarf standard stars from Gray et al. (2003). The dashed line is 1 mag fainter than this solid line. Note that the K-type subdwarf sequence merges with the K dwarf sequence at the blue end of this (M_{K_s} vs. $V - K_s$) plot. The single point at $V - K_s = 6.4$ is LHS 2067A. The spectral types for dwarfs are given at the bottom of the figure as references.

subdwarfs’ physical parameters (temperature, metallicity, and gravity) affect their spectra. The most recently released *GAIA*

model grids (Brott & Hauschildt 2005) are available at an FTP site in Hamburg.⁵ Gizis (1997), Woolf & Wallerstein (2005), and Burgasser & Kirkpatrick (2006) have all used these synthetic model grids to characterize subdwarfs, but an older version of the grids was used in all three cases. The version we employ here, 2.6.1, was released in late 2004. A comparison of one pre-2004 spectral model (provided by V. Woolf 2007, private communication) and a new spectral model (from the *GAIA* model grids) for a cool subdwarf is shown in Figure 7. Improvements to the new models include (1) an enlarged and enhanced version of the equation of state, (2) more atomic, ionic, and molecular line opacities, (3) inclusion of the formation of dust particles for cool stars, and (4) microturbulence calculations. Additional water and TiO opacities and the inclusion of dust are enhancements particularly applicable to the low-mass stars discussed here.

The two spectra shown in Figure 7 are virtually identical redward of 7000 Å, but there are significant differences between 6500 Å and 7000 Å, where the CaH2 and CaH3 bands are found, and these differences will certainly affect evaluations done with the older models. The new model in this region has much shallower absorptions than the old one, which will affect metallicity and gravity estimates. A few narrow absorption features (Li I at 6103 Å, Ca I at 6122 Å and 6162 Å) are also changed. As outlined in the discussion section, Section 9, even the latest version of the model grids does not provide ideal matches to real spectra, so further progress can still be made.

⁵ [ftp://ftp.hs.uni-hamburg.de/pub/outgoing/phoenix/GAIA/v2.6.1/](http://ftp.hs.uni-hamburg.de/pub/outgoing/phoenix/GAIA/v2.6.1/).

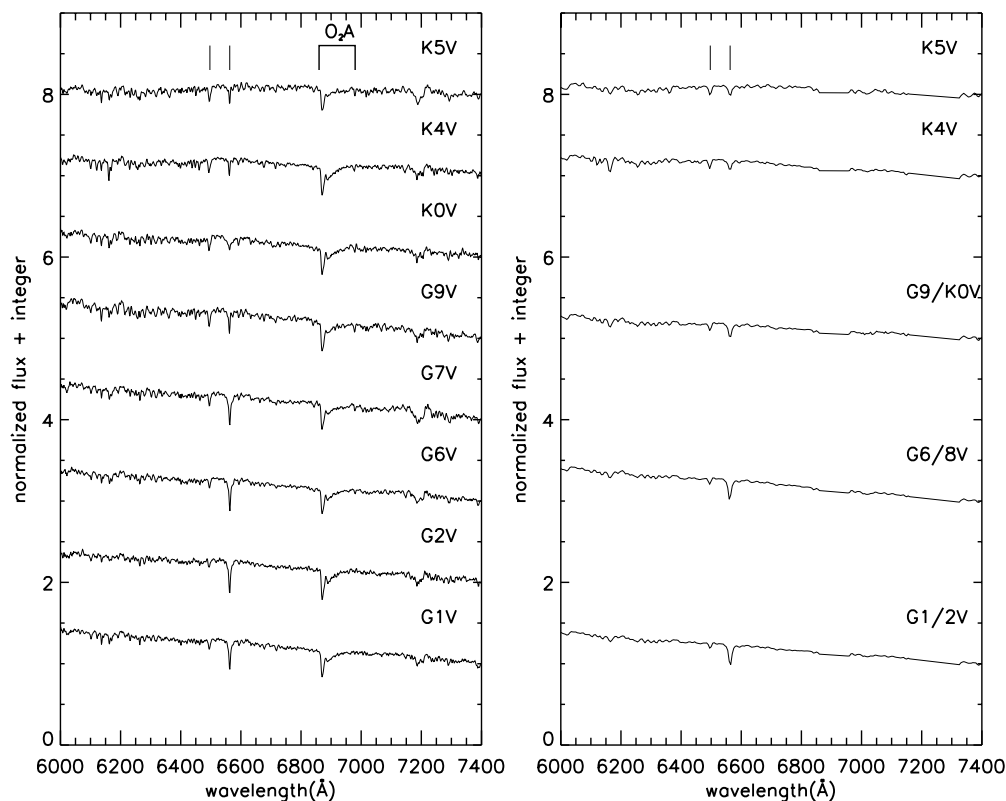


Figure 5. Spectra for G- and K-type stars from Jacoby et al. (1984) (left panel, 4 Å resolution) and Silva & Cornell (1992) (right panel, 11 Å resolution). Because the red cutoff is 7400 Å in Jacoby et al. (1984), the results from Silva & Cornell (1992) are also plotted to 7400 Å, and both sets of spectra are normalized at 7400 Å. The two tick marks indicate the Ba I (left) and H α (right) absorption features. Silva & Cornell (1992) have removed telluric absorption features.

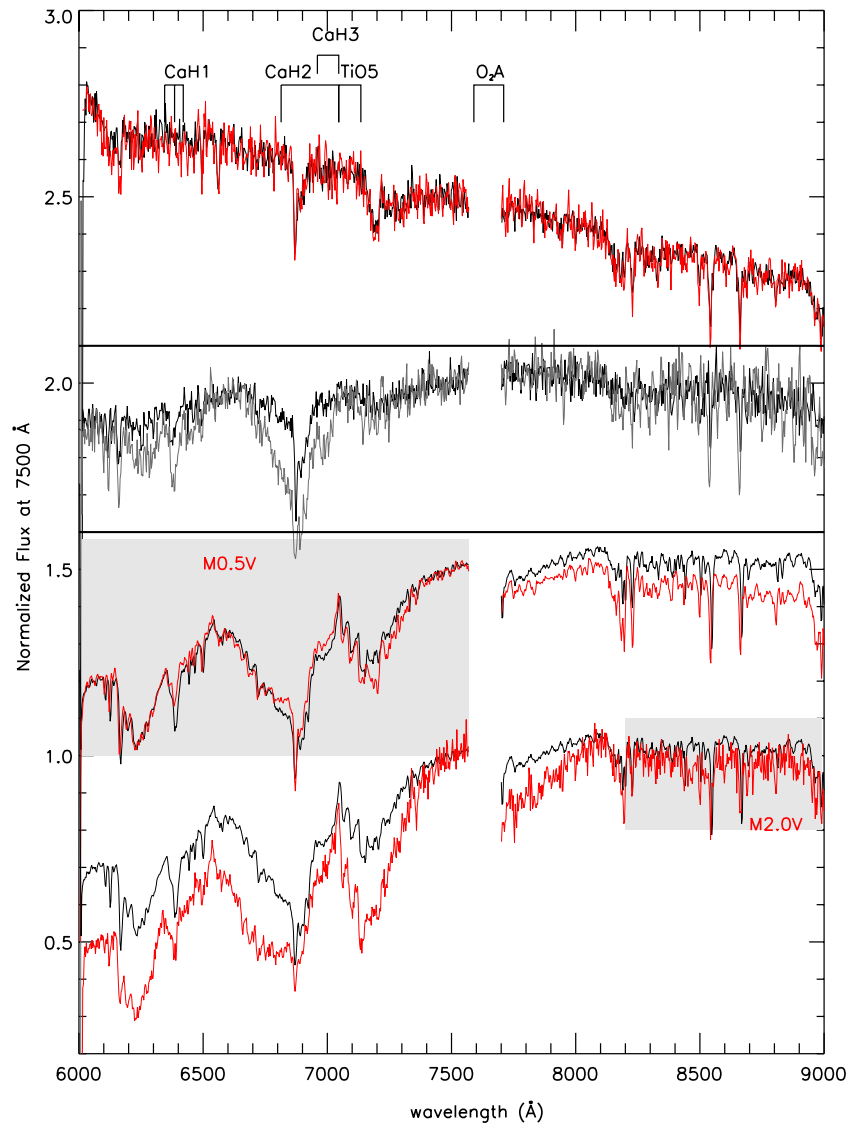


Figure 6. Top: a mid-K subdwarf spectrum (black) is virtually identical to a mid-K dwarf (red). Middle: the spectra of two early M subdwarfs differ only at CaH. Bottom: one subdwarf’s spectrum (black) matches an M0.5V spectral standard (red) at the blue end, but matches an M2.0V spectral standard (red) at the red end. The deep telluric band, O₂ A (7570–7700 Å), has been removed.

(A color version of this figure is available in the online journal.)

4.1. Identifying Mid-K-type Subdwarfs

We use the latest *GAIA* model grids⁶ to calculate predicted CaH band strengths and plot the derived indices against effective temperatures in Figure 8. We evaluate stars with T_{eff} between 2700 K and 4500 K and $[m/H]$ between 0.0 and -3.0 . For the moment, we adopt $\log g = 5.0$ generically for subdwarfs. This gravity value does not apply to all types of subdwarfs, but we are presently interested in outlining the behavior of the CaH features with metallicity alone.

When T_{eff} is less than about 3300 K, Figure 8 shows that the CaH1 index decreases (stronger absorption) when metallicity decreases from 0.0 to -2.0 at fixed T_{eff} . However, the trend reverses for $[m/H] = -2.5$ and -3.0 . When T_{eff} is between 3300 K and 3500 K, there is a very weak relation between metallicity and the CaH1 index, but from 0.0 to -1.0 , the

relation (CaH1 index decreases when metallicity decreases) still holds. This relationship is degenerate for lower metallicities. For temperatures hotter than 3500 K, the CaH1 index increases (weaker absorption) as metallicity decreases, in contrast to the low-temperature region. For the CaH2 + CaH3 index, the trends are generally the same, except that (1) at temperatures less than 3200 K the index decreases (stronger absorption) only for 0.0 to -1.0 , with a reversal for lower metallicities and (2) the trend for higher temperature stars (increasing index, weaker absorption with lower metallicity) is the same, but the turnover is near 3200 K rather than 3500 K.

Even more important than these subtleties is that overall, the hotter the subdwarf, the weaker its CaH bands. Note the collapse of any differences between indices for hotter stars of various metallicities in Figure 8. This collapse makes separating mid-K-type subdwarfs from dwarfs based only on spectroscopic indices difficult using our spectral coverage (6000–9000 Å) and resolution (6–8.6 Å). An alternative method, such as the H-R diagram shown in Figure 4, sufficiently solves the

⁶ *GAIA* model grids also provide various values of α -elements (O, Ne, Mg, Si, S, Ar, Ca, and Ti), which yield abundance ratios such as O/Fe, Ne/Fe, etc. We select models with $[\alpha/\alpha_{\odot}] = 0.0$ throughout this manuscript.

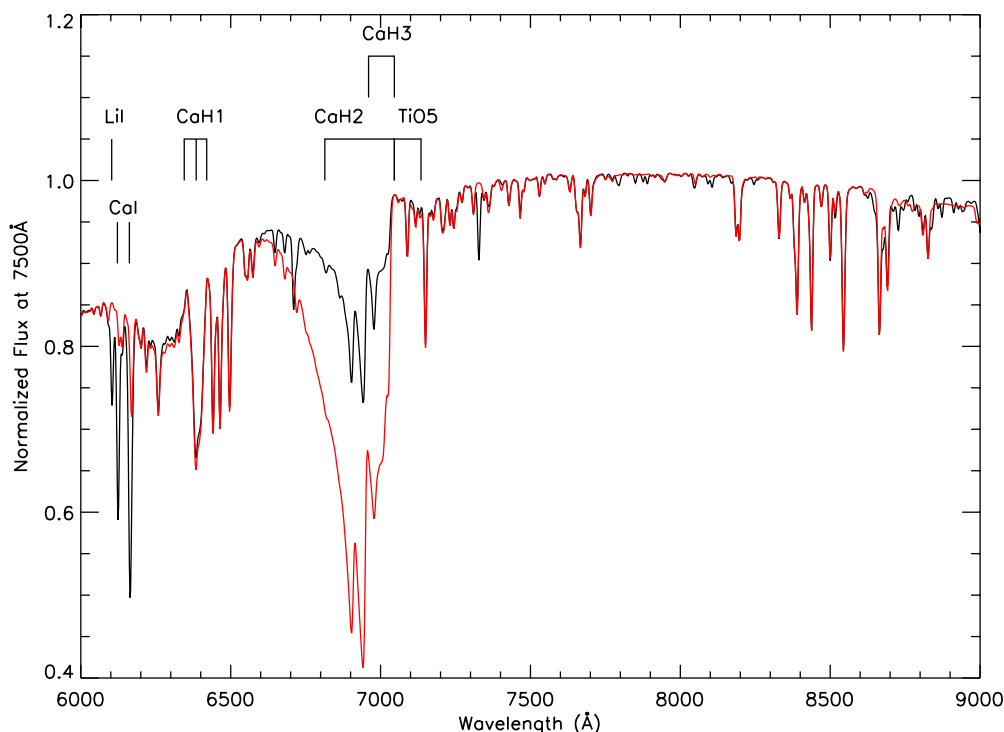


Figure 7. Two synthetic spectra from old (red) and new (black) model grids. The physical parameters for both models are $T_{\text{eff}} = 3600$ K, $\log g = 5.0$, and $[m/H] = -2.0$. Major differences are seen between 6500 Å and 7000 Å, and in the absorption lines of Li I (6103 Å) and Ca I (6122 Å and 6162 Å). (A color version of this figure is available in the online journal.)

problem for mid-K-type subdwarfs and will be discussed in the next section. Independent metallicity measurements via high-resolution spectroscopic observations (Bonfils et al. 2005; Bean et al. 2006) can also be utilized. Our own spectra are not of sufficiently high resolution to measure metallicities, but all selected K-type subdwarfs have measured $[m/H] \leq -0.5$ from other publications.

4.2. Mid-K-type Subdwarf Sample from Our Observations

There are 31 subdwarfs having CaH1 indices larger than 0.9 enclosed by the dashed box in Figure 3. In this region, there are no subdwarfs with previously measured CaH/TiO5 indices to compare to our new sample of mid-K-type stars, making it difficult to separate the dwarfs and subdwarfs based on the CaH1 index alone. Fortunately, 21 of these 31 stars have trigonometric parallaxes, and are plotted with concentric circles in Figure 4. At least 15 of these stars are subdwarfs based on their locations one or more magnitudes below the main sequence on the H-R diagram. The star with the largest offset is DEN0515-7211,⁷ located at $(V - K) = 3.3$, $M_{K_s} = 9.7$. This star is a full 4.5 mag less luminous than the main sequence, but has no CaH or TiO5 features. Two additional stars (G016-009AB and G026-009ACD) above the main sequence are known to be double-line spectroscopic binaries with $[m/H] < -0.5$. These individual targets are discussed in Section 6.2. The dwarf/subdwarf status of only four stars of the 21 remain ambiguous—we suspect that most of them are also subdwarfs, perhaps with as yet undetected companions elevating them into main-sequence territory.

Generally, the spectroscopic index method fails to distinguish subdwarfs from dwarfs if the derived CaH1 index is greater than 0.9. With the benefit of additional trigonometric parallax information and/or metallicity measurements, however, we can conclude that nearly all of these mid-K-type stars are indeed subdwarfs.

5. LATE K-TYPE AND M-TYPE SUBDWARFS FROM GAIA MODEL GRIDS

For late K-type (redder than K5.0) and M-type stars, we use the GAIA model grids to understand how the effective temperatures, metallicities, and gravities affect the shapes and features of subdwarfs' spectra. This analysis allows us to develop a spectral sequence for cool subdwarfs of types K6.0 to M6.0, which is tentatively extended blueward to K3.0 when additional information is incorporated. We plot GAIA synthetic noiseless spectra in Figure 9, at increments of 200 K (cooler than 4000 K) and 400 K (hotter than 4000 K) for stars with metallicities of $[m/H] = 0.0, -1.0, \text{ and } -2.0$. Because gravities have very limited impact on the overall shapes of the spectra (shown in the top panel of Figure 10), we do not show gravity plots with fixed temperatures and metallicities (of course, some features do change markedly with gravity, but not the overall slopes of the spectra). Based on the synthetic spectra from GAIA model grids, cool subdwarf spectra between 6000 Å and 9000 Å exhibit the following trends.

1. The effects of metallicity are minimal in low-resolution subdwarf spectra for stars with temperatures of 4400 K and hotter. This makes it difficult to separate dwarfs and subdwarfs using low-resolution spectra (as discussed in Section 4.1). However, from these noiseless spectra, we can still identify a few metallic lines showing metallicity

⁷ This star was first reported in Costa et al. (2006) as reference star #4 in the LHS 1749 parallax field. We identify it henceforth as DEN0515-7211 (DENIS-P J051545.1-721122).

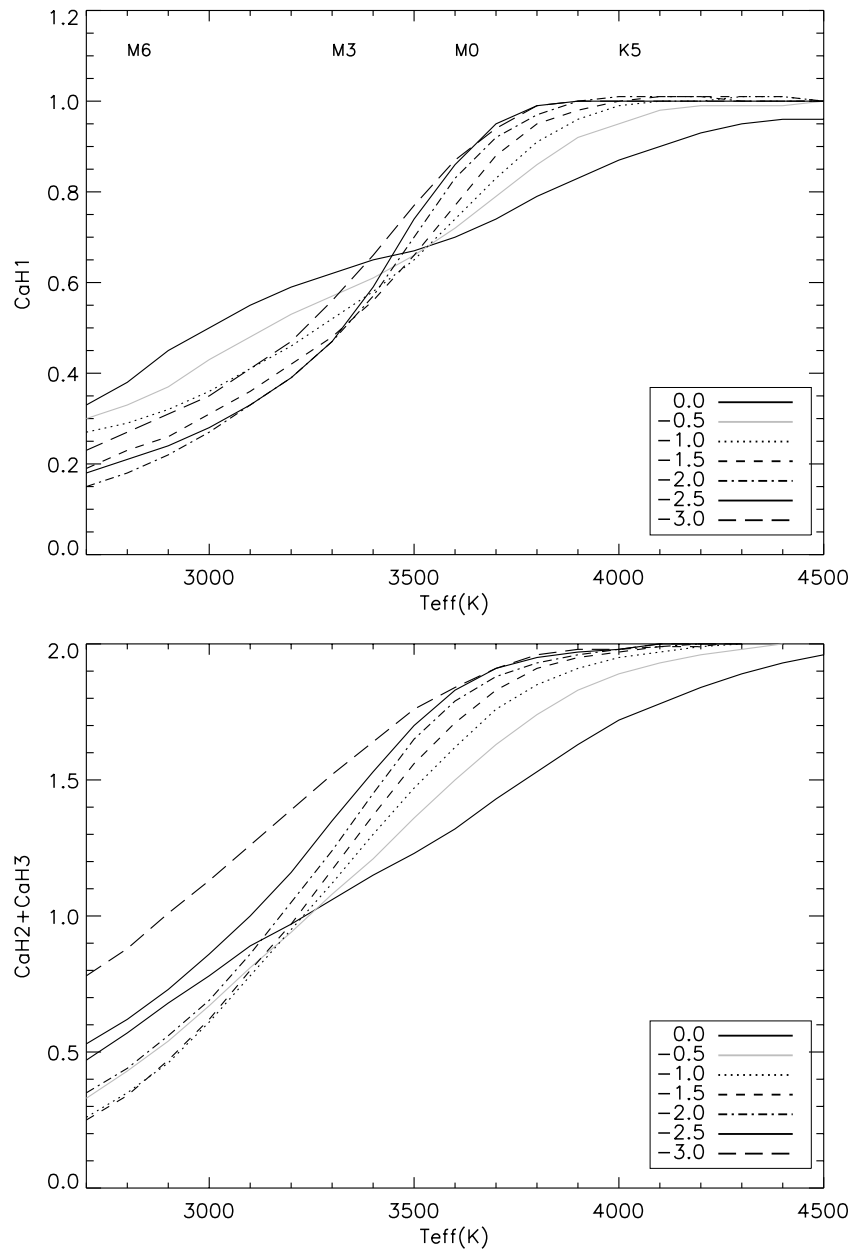


Figure 8. CaH1 (top) and CaH2 + CaH3 (bottom) indices from *GAIA* model grids plotted against T_{eff} . The different line styles represent different $[m/H]$. The spectral types for dwarfs are given at the top of the figure as references.

trends. The most prominent feature is marked #1 at 6256 Å in Figure 9. Unfortunately, we do not see this feature in any of our K-type spectra (nor is it listed in Table 1 of Turnshek et al. 1985), so we consider its validity questionable. The next prominent feature, marked #2 in Figure 9, is Ca I (6162 Å). This line can possibly be used to distinguish subdwarfs from dwarfs (see examples discussed in Section 7.2), but in practice it is somewhat difficult to evaluate in real spectra (with noise) at our resolution.

2. For stars with temperatures of 2800–4000 K, metallicity strongly affects the spectra between 6000 Å and 8200 Å. This is the region that has been historically used to assign spectral types. In effect, subdwarfs with decreased metallicities have spectra that are “brightened” or “less blanketed” at the blue end, relative to solar metallicity stars. However, the continuum at wavelengths longer than 8200 Å for temperatures 3400–4800 K is nearly free

of metallicity effects. We can therefore use the 8200–9000 Å region to establish subtypes in the subdwarf spectral sequence because the slope is a function of temperature. This also allows us to mirror the spectral sequence for dwarfs, providing a useful link between the dwarf and subdwarf sequences.

3. The TiO5 band strength at 7050–7150 Å is very sensitive to metallicity for temperatures cooler than 4000 K. As shown in the top panel of Figure 10, the TiO5 band strength is effectively independent of gravity. We can therefore use the TiO5 feature to separate subdwarfs with different metallicities if their continua (8200–9000 Å) are the same, regardless of their gravities.
4. For a star of given temperature, stronger CaH bands could be caused by lower metallicity, as shown in Figure 9, or higher gravity, as shown in the top panel of Figure 10. If two subdwarfs have the same continua from 8200 to

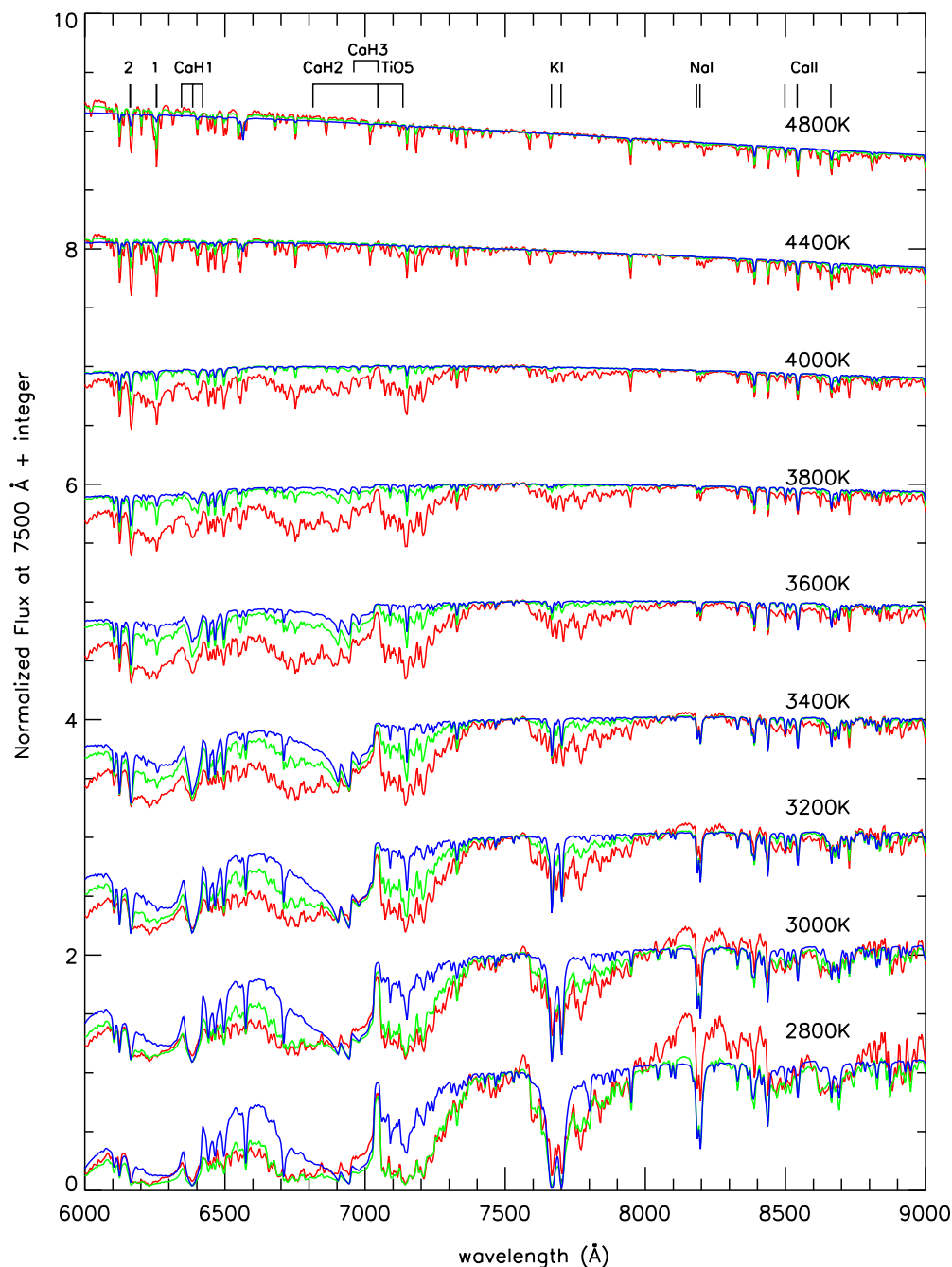


Figure 9. *GAIA* synthetic spectra from 4800 K to 2800 K. All spectra are noiseless and have $\log g = 5.0$. The red, green, and blue lines represent $[m/H] = 0.0, -1.0,$ and -2.0 , respectively. Effective temperatures for each set of spectra are given above each group of lines. The feature marked #2 is seen in our spectra. The Ca I (6162 Å) feature marked #1 is not seen in any of our spectra.

(A color version of this figure is available in the online journal.)

9000 Å and the same TiO5 band strength, but their CaH bands are different, we can rank them by their relative gravities.

Consequently, the impediments to sorting cool subdwarf spectra at our resolution discussed in Section 3.3 can be overcome by understanding the trends revealed in *GAIA* synthetic spectra: (1) the mid-K-type dwarfs have the same spectra as dwarfs for our spectral coverage and resolution, (2) CaH features are affected by both metallicity and gravity, while the TiO5 band is affected by metallicity but not gravity, and (3) the continuum from 8200 Å to 9000 Å is not strongly affected by

either metallicity or gravity, so can therefore be used for spectral sequencing.

6. ADDITIONAL EVIDENCE SUPPORTING THE METALLICITY AND GRAVITY TRENDS INDICATED BY THE *GAIA* MODELS

To investigate the metallicity trends seen in *GAIA* models, we compare our available spectra to metallicity measurements provided independently by others. Measuring M dwarf metallicities is difficult, but several recent attempts have made progress (Valenti et al. 1998; Woolf & Wallerstein 2005; Bonfils et al.

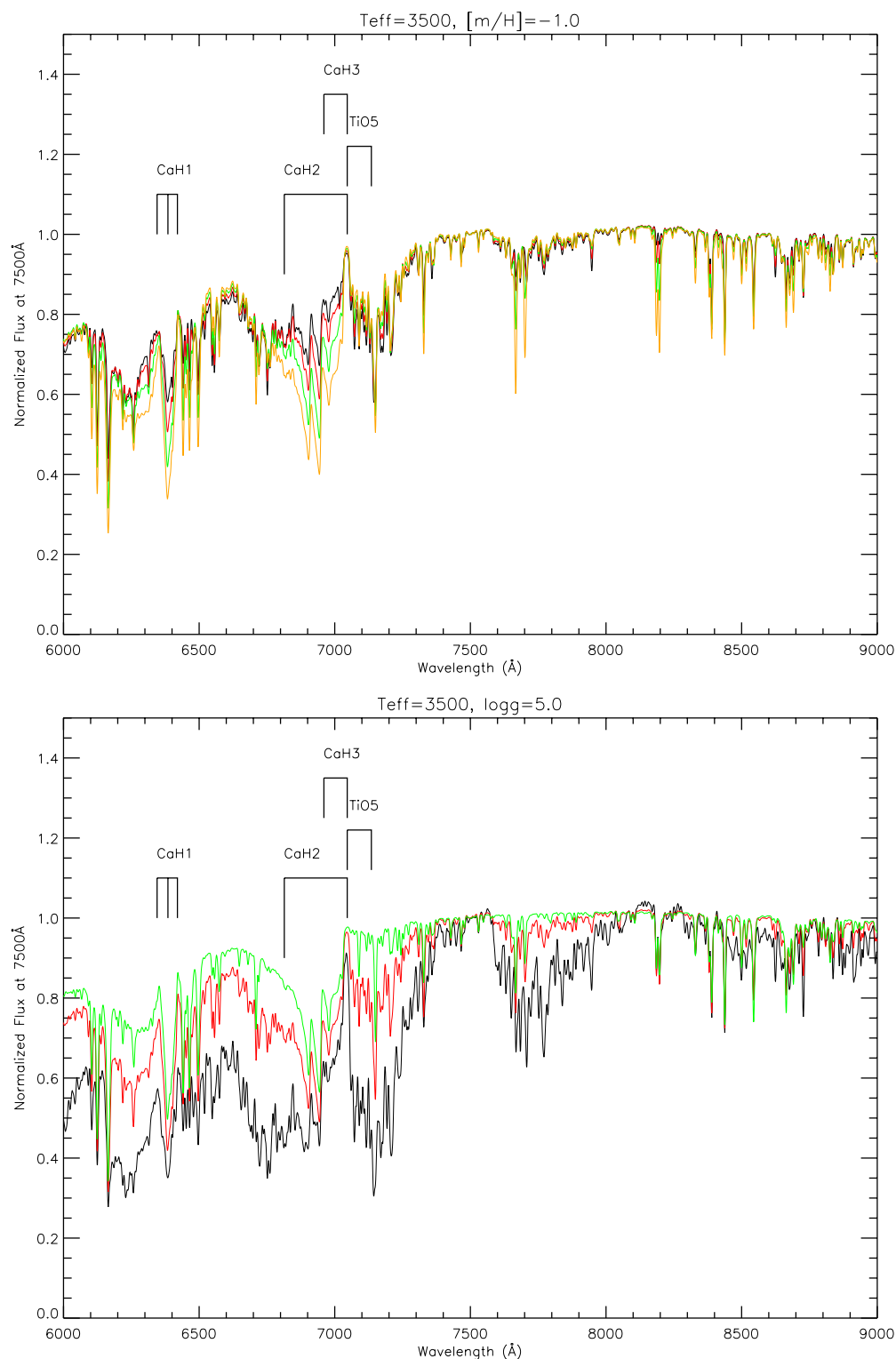


Figure 10. The top plot shows *GAIA* model grids at fixed metallicity ($[m/H] = -1.0$) and effective temperature (3500 K). The black, red, green, and yellow lines represent various $\log g = 4.0, 4.5, 5.0,$ and 5.5 , respectively. It is clear that CaH bands will be affected by changing gravity but TiO5 is not. The bottom plot shows model grids at fixed $\log g = 5.0$ and $T = 3500$ K. The black, red, and green lines represent various $[m/H] = 0.0, -1.0,$ and -2.0 , respectively. Note that model grids do not have telluric lines.

(A color version of this figure is available in the online journal.)

2005; Bean et al. 2006). Six red dwarfs that we have observed are included in the study by Bonfils et al. (2005), comprising three pairs of M dwarfs of types M1.0V, M2.5V, and M3.0V shown in Figure 11. Each pair includes a relatively low-metallicity dwarf

(gray) and a relatively high-metallicity dwarf (black). The red ends (from 8200 Å to 9000 Å) of each pair match one another, but the blue ends of the lower-metallicity members are brighter in each case, as predicted by the *GAIA* models. The effect is

Table 1
Spectroscopic Indices

Object	TiO5	CaH1	CaH2	CaH3	CaH2 + CaH3
DEN0515–7211	1.002	1.021	1.019	1.003	2.022
G016–009AB	0.973	1.018	1.021	0.998	2.019
G022–015	0.978	0.996	0.989	0.984	1.973
G026–009ACD	0.953	0.990	0.975	0.990	1.965
GJ0191	0.860	0.876	0.678	0.848	1.526
GJ0223.1	0.958	1.001	0.981	0.971	1.952
LEHPM1628	0.954	0.676	0.628	0.754	1.382
LEHPM3861	0.957	0.774	0.340	0.368	0.709
LHS0012	0.883	0.881	0.779	0.889	1.668
LHS0073	0.972	0.903	0.862	0.927	1.789
LHS0109	0.939	0.823	0.752	0.863	1.616
LHS0125	0.981	1.020	1.014	0.993	2.007
LHS0127	0.716	0.755	0.537	0.739	1.276
LHS0144	0.768	0.609	0.396	0.592	0.987
LHS0148	0.977	0.816	0.729	0.830	1.560
LHS0158	0.732	0.849	0.639	0.829	1.469
LHS0161	0.889	0.777	0.689	0.817	1.506
LHS0162	0.838	0.731	0.577	0.747	1.324
LHS0164	0.987	1.005	1.000	1.017	2.017
LHS0165	0.956	0.889	0.841	0.910	1.751
LHS0186	0.710	0.739	0.568	0.764	1.332
LHS0189AB	0.630	0.733	0.492	0.719	1.211
LHS0193A	0.944	0.959	0.920	0.966	1.886
LHS0227	1.000	0.895	0.883	0.949	1.832
LHS0228	0.644	0.744	0.480	0.701	1.181
LHS0232	0.998	1.000	1.020	1.005	2.025
LHS0244	0.902	0.853	0.731	0.869	1.601
LHS0272	0.862	0.715	0.527	0.736	1.264
LHS0299	0.903	0.904	0.756	0.884	1.641
LHS0300AB	1.031	0.933	0.886	0.943	1.830
LHS0318	0.934	0.747	0.617	0.797	1.413
LHS0326	0.948	0.782	0.689	0.841	1.530
LHS0327	0.995	1.004	1.025	1.005	2.030
LHS0334	0.475	0.492	0.277	0.470	0.747
LHS0335	0.960	0.721	0.640	0.791	1.431
LHS0360	0.986	0.840	0.778	0.886	1.664
LHS0367	1.011	0.880	0.854	0.929	1.783
LHS0375	0.879	0.604	0.414	0.583	0.997
LHS0381	0.883	0.728	0.555	0.730	1.285
LHS0385	0.982	0.787	0.712	0.841	1.553
LHS0398	0.910	0.767	0.644	0.808	1.452
LHS0401	0.997	0.959	0.911	0.958	1.869
LHS0406	0.686	0.801	0.576	0.789	1.365
LHS0418	0.913	0.924	0.858	0.924	1.782
LHS0424	0.951	0.917	0.852	0.927	1.778
LHS0440	0.763	0.789	0.608	0.796	1.404
LHS0507	0.991	0.958	0.969	0.980	1.949
LHS0515	0.813	0.524	0.355	0.508	0.863
LHS0518	0.966	0.933	0.903	0.951	1.854
LHS0521	1.006	0.937	0.950	0.969	1.919
LHS0541	0.795	0.678	0.538	0.701	1.239
LHS1490	0.301	0.778	0.296	0.569	0.865
LHS1970	0.878	0.433	0.476	0.686	1.162
LHS2067A	0.228	0.670	0.199	0.452	0.651
LHS2467	1.017	1.031	1.019	1.014	2.033
LHS2734A	1.018	0.985	0.984	0.987	1.972
LHS2734B	1.086	0.720	0.669	0.828	1.497
LHS3620	0.836	0.684	0.544	0.727	1.271
SCR0242–5935	0.910	0.906	0.838	0.891	1.728
SCR0406–6735	1.015	0.989	0.829	0.937	1.766
SCR0433–7740	0.929	0.887	0.760	0.864	1.624
SCR0529–3950	0.817	0.886	0.637	0.815	1.452
SCR0629–6938	0.845	0.908	0.579	0.784	1.363
SCR0654–7358	0.938	0.835	0.653	0.825	1.478
SCR0701–0655	0.976	0.886	0.780	0.881	1.662
SCR0708–4709	0.984	0.992	0.979	0.976	1.955

Table 1
(Continued)

Object	TiO5	CaH1	CaH2	CaH3	CaH2 + CaH3
SCR0709–4648	1.013	0.899	0.846	0.915	1.761
SCR1107–4135	0.994	0.839	0.783	0.892	1.675
SCR1433–3847	1.001	0.904	0.797	0.930	1.726
SCR1455–3914	0.915	0.788	0.707	0.849	1.555
SCR1457–3904	0.905	0.824	0.707	0.838	1.545
SCR1613–3040	0.920	0.898	0.749	0.885	1.634
SCR1739–8222	0.945	1.009	0.797	0.882	1.679
SCR1740–5646	0.915	0.696	0.496	0.637	1.133
SCR1756–5927	0.922	0.794	0.757	0.856	1.613
SCR1822–4542	0.817	0.818	0.624	0.809	1.433
SCR1843–7849	0.869	0.810	0.715	0.829	1.545
SCR1913–1001	0.962	0.923	0.835	0.925	1.760
SCR1916–3638	0.931	0.647	0.493	0.666	1.159
SCR1958–5609	0.915	0.865	0.805	0.926	1.731
SCR2018–6606	0.886	0.856	0.715	0.836	1.550
SCR2101–5437	0.929	0.969	0.726	0.904	1.630
SCR2104–5229	0.940	0.907	0.772	0.865	1.638
SCR2109–5226	0.967	0.774	0.646	0.799	1.445
SCR2204–3347	0.874	0.711	0.569	0.762	1.331
SIP1342–3534	0.684	0.664	0.462	0.676	1.138
WT0135	0.622	0.754	0.512	0.731	1.243
WT0233	0.939	0.933	0.739	0.857	1.596

rather subtle, but the derived metallicities for each pair are not wildly different (none of the six stars is a subdwarf), and yet the trend is confirmed in all three cases. One caveat is that the metallicities from these six stars were determined from the polynomial relation in Bonfils et al. (2005), not measured directly from spectra, but this appears to be the best that can be done given the available data. We conclude that the metallicity trend revealed in the *GAIA* models (see Figure 9) is sound because it appears to be confirmed in real M dwarf spectra.

Contrary to the evidence for the metallicity trend, we have found no direct spectroscopic results to support the gravity trend in dwarfs and subdwarfs. Direct gravity measurements are difficult because (1) stars must have both mass and radius measurements and (2) clean spectra without contamination from companions must be obtained. This limits the available target lists to eclipsing binaries such as those discussed in López-Morales (2007) with cleanly deconvolved spectra or visual binaries in which individual radii can be measured via long-baseline interferometry. Neither class of objects yet provides a rich dataset for cool dwarfs or subdwarfs.

Hence, we rely on other observational or theoretical efforts to investigate the gravity trend. The top panel of Figure 10 indicates that other than some sharp metallic lines, CaH bands show the most prominent changes when gravity varies (TiO is unaffected by changing gravity). Öhman (1934) demonstrated that the CaH2 band is found in the spectra of M-type dwarfs, but is not observed in the spectra of M-type giants, thus identifying the CaH2 band as a gravity indicator to separate dwarfs and giants. In addition to the *GAIA* models, Mould (1976) also showed that for stars with effective temperatures of 3250 K, a spectrum from his atmospheric model with $\log g = 5.75$ has stronger CaH2 than a spectrum with $\log g = 4.75$. If the CaH2 band is a gravity indicator, we may presume that the same gravity effects for CaH1 and CaH3 bands will be seen.

As shown in the two panels of Figure 10, the *GAIA* models imply that the CaH band strengths are indicators of both gravity and metallicity differences. In reality, if two red subdwarfs have spectra with the same overall continua and slopes, as well as

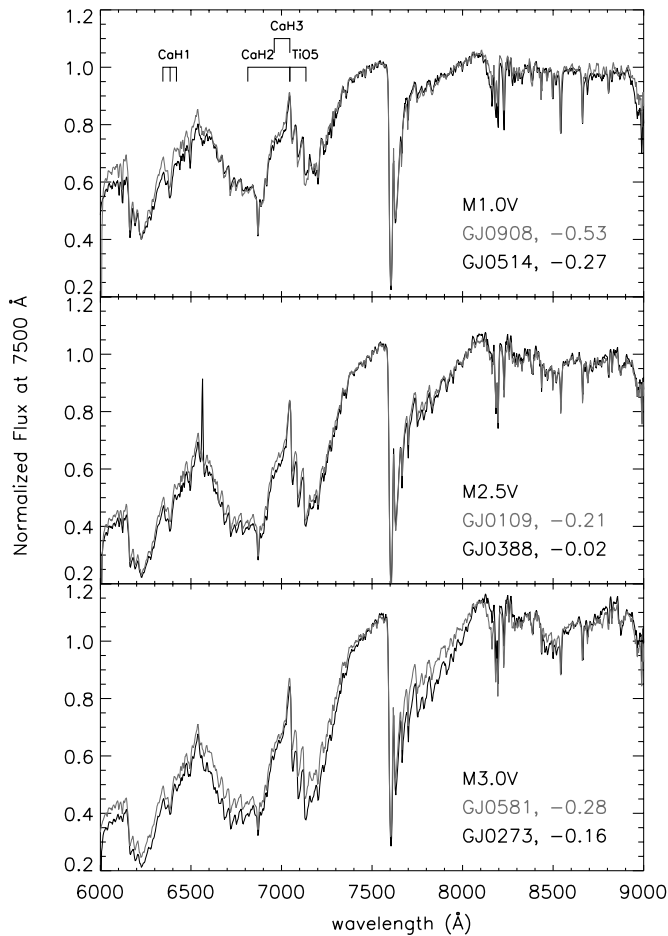


Figure 11. Using our spectra and metallicities measured independently by others, three different types of M dwarfs show the metallicity trend predicted by *GAIA* models. The gray lines represent lower metallicity stars in each pair. Metallicities from Bonfils et al. (2005) are given in each panel for the stars.

matching TiO band strengths (e.g., the middle panel in Figure 6), the only remaining discrepancies will be at the CaH bands. We believe that such differences are caused by different gravities.

Obviously, there is not yet a wealth of accurate direct observational results of red dwarfs and subdwarfs that can be used to stress test the metallicity and gravity trends seen in *GAIA* models. Nonetheless, what little we do have supports the trends, so we use these trends to assist us in establishing the subdwarf spectral sequence discussed below.

7. SUBDWARF SPECTRAL SEQUENCE

7.1. Procedures

In addition to presenting 88 subdwarfs, a goal of this project is to establish a subdwarf spectral sequence that mirrors the sequence for dwarfs and considers the latest available synthetic models. Although synthetic models are not yet capable of fully representing the complicated spectra of these cool stars, the models can be used to investigate the primary factors that affect subdwarfs' spectra. Specifically, we examine the spectra in the framework of what appear to be the three main drivers of the trends observed—temperature, metallicity, and gravity.

We first separate our available subdwarf spectra into several groups that have similar overall slopes. Known subdwarfs such as LHS 12, GJ 161, and LHS 2734A are used as anchor points. Within each group, several stars that have high surface gravities

are obvious because their spectra match except in CaH, implying nearly identical temperatures and metallicities.

We then compare each subdwarf's spectrum with our sequence of dwarf spectral standards⁸ that span types from K0.0 to M9.0 using an IDL program to find the closest match to the continuum slope in the region 8200–9000 Å. Visual checks of the matches between all subdwarf and standard dwarf spectra are also made to ensure match quality.

7.2. Results and Notes on Objects

Based on the 88 confirmed cool subdwarf spectra we have, we present a sequence of subdwarfs with spectral types spanning K3.0 to M6.0, listed in Table 2. We also identify five additional G-type subdwarfs. After the five G-type subdwarfs, we sort the cool subdwarfs from K3.0[VI] to M6.0VI, using double lines in Table 2 to separate each type.

As discussed in Section 4.1, because mid-K subdwarfs are virtually indistinguishable from K dwarfs at our spectral resolution, we use [VI] to indicate their questionable luminosity classes, which are currently based on their metallicities, kinematics, or locations on the H-R diagram. We anticipate that higher-resolution spectra will reveal these stars to be subdwarfs. A colon after the type indicates that we have had difficulty in assigning a subtype, metallicity, or gravity.

Within each type for which sufficient spectra are available, we sort targets by their metallicities (lowest metallicity first). A letter “m” indicates a star having the same metallicity as a main-sequence dwarf, while more negative signs indicate lower metallicities, e.g., m– is more metal poor than m–. We use as many as six negative signs, because in the case of the M1.0VI type, we have 23 stars that fall into seven different metallicity categories. Gravities are indicated by “g” with additional plus signs for higher gravities, e.g., g++ is higher gravity than g+. A baseline subdwarf of low metallicity is assigned m– and g. If a subdwarf has a similar metallicity but higher gravity, the designations are m– and g+. A few stars appear to have solar metallicity and are subluminous only because of high gravities; these stars are assigned m and g+. We have removed any stars from this study that might have gravities lower than main-sequence stars, i.e. slightly evolved stars such as subgiants, that would have gravity g–.

Note that values for metallicity and gravity are not comparable across all spectral types, i.e. M1.0VI with metallicity “m–” is not equivalent to M2.0VI with metallicity “m–,” nor is “g+” for M1.0VI the same as “g+” for M2.0VI. We can hope to formalize a definitive subdwarf spectral sequence that includes temperature, metallicity, and gravity trends when hundreds of systematically consistent subdwarf spectra and improved model

⁸ Our dwarf standard sequence is a hybrid of cool dwarf standards from Gray et al. (2006) for K stars, and Boeshaar (1976) and Kirkpatrick et al. (1991) for M stars. The dwarf standard sequence is the topic of a future publication of the RECONS group. Our spectral sequencing efforts began before the recent spectral sequence from SDSS (Bochanski et al. 2007) was released. We continue to use our standard sequence because (1) stars in our sequence have trigonometric parallaxes so we can understand how metallicities and gravities affect stars' positions on the H-R diagram, (2) the SDSS sequence does not include K-type stars, (3) we have acquired spectra for many K-type stars from Gray et al. (2003, 2006) so we have benchmark K dwarf spectral standards to link to the M dwarf sequence, (4) SDSS standard stars have telluric lines removed (It is difficult for us to make comparisons to SDSS spectra in the 6800–7100 Å region, which includes O₂ and H₂O absorption. This region overlaps with the CaH3 and TiO5 bands. Thus, all subdwarfs would appear to have high gravity when compared to the SDSS standards.), and (5) our dwarf spectra have been acquired using the same telescope/instrument/observing protocols as used for the subdwarfs, and the data have been reduced identically, so they are systematically consistent.

Table 2
Spectral Types

R.A.	Decl.	Object	K_s	$V - K_s$	M_{K_s}	V_{\tan}	Old type	New type	Metallicity	Gravity	Ref.			
											π	V	spect	
						km s ⁻¹								
12 06 00.9	+14 38 56.8	G012-016	7.931 ± 0.018	2.16	4.12	98.4	K2	GVI	(-0.52) ^a	g	H	2	2	
01 04 26.4	-02 21 59.8	G070-035	7.116 ± 0.020	2.04	4.15	55.8	G5	GVI	(-0.67) ^a	g	H	4	H	
02 25 49.8	+05 53 39.5	G073-056	10.427 ± 0.023	2.06	8.64	44.9		GVI	(-1.18) ^b	g	H	4		
07 54 34.1	-01 24 44.3	G112-054	5.425 ± 0.023	2.00	4.01	23.7	K1	GVI	(-0.94) ^c	g	H	1	2	
16 13 48.6	-57 34 13.8	LHS0413	5.293 ± 0.024	2.24	4.60	106.5	G8/K0V(W)	GVI	(-1.35) ^c	g	H	1	10	
15 45 52.4	+05 02 26.6	G016-009AB	6.880 ± 0.024	2.27	3.46	59.2	K2V	K3.0[VI]	m-, (-0.77) ^d	g	H	H	3	
00 50 17.0	-39 30 08.3	LHS0125	11.452 ± 0.026	2.88	7.73	342.6		K4.0[VI]	m-	g	R	R		
07 35 46.3	+03 29 36.0	LHS0232	10.841 ± 0.024	2.84	6.57	346.0		K4.0[VI]	m-	g	Y	R		
12 25 50.7	-24 33 17.8	LHS0327	10.144 ± 0.021	2.57	5.44	418.3	K0V	K4.0[VI]	m-	g	R	R	2	
11 52 32.0	+27 30 51.3	LHS2467	9.806 ± 0.017	2.43	4.94	437.0	G7V	K4.0[VI]	m-	g	H	R	2	
19 07 02.0	+07 36 57.3	G022-015	6.469 ± 0.018	2.71	4.54	97.2	K5V	K5.0[VI]	m-, (-0.61) ^e	g	H	H	2	
21 32 11.9	+00 13 18.0	G026-009ACD	7.082 ± 0.029	2.64	3.62	96.9	K2V	K5.0[VI]	m-, (-1.05) ^f	g	H	H	2	
05 54 34.1	-09 23 33.7	GJ0223.1	7.760 ± 0.020	2.96	4.84	82.1	K4V	K5.0[VI]	m-, (-0.62) ^e	g	H	1	9	
04 32 36.6	-39 02 03.4	LHS0193A	8.427 ± 0.023	3.23	5.80	147.3		K6.0VI	m-	g	R	16		
23 43 16.7	-24 11 16.4	LHS0073	9.393 ± 0.021	3.42	7.27	322.3	K5V	K6.0VI	m-	g+	Y	19	2	
07 13 40.6	-13 27 57.1	LHS0227	11.036 ± 0.023	3.41	7.15	362.5		K6.0VI	m-	g+	Y	R		
02 52 45.7	+01 55 49.4	LHS0161	10.995 ± 0.019	3.65	8.01	272.6	esdM2	K6.0VI	m-	g++	Y	R	8	
03 01 40.6	-34 57 56.5	LHS0164	10.641 ± 0.024	2.92	8.20	192.6		K7.0VI	m--	g	R	R		
05 15 45.1	-72 11 22.2	DEN0515-7211	13.211 ± 0.040	3.29	9.72	4.7		K7.0VI:	m--	g	7	7		
07 08 32.0	-47 09 30.5	SCR0708-4709	10.764 ± 0.025	3.05		K7.0VI:	m--	g		R		
13 25 14.0	-21 27 06.0	LHS2734A	12.896 ± 0.037	3.23	too far	> 280		K7.0VI	m-	g	R	R		
03 06 28.7	-07 40 41.5	LHS0165	11.006 ± 0.025	3.42	7.67	333.1		M0.0VI	m----	g+:	Y	R		
11 11 13.7	-41 05 32.7	LHS0300A	9.802 ± 0.023	3.38	7.23	197.5		M0.0VI:	m--	g	11	16		
16 25 14.0	+15 40 54.2	LHS0418	10.072 ± 0.018	3.37	6.44	301.5	K7V	M0.0VI	m--	g	Y	R	8	
16 37 05.6	-01 32 01.6	LHS0424	10.803 ± 0.022	3.37	7.39	279.6		M0.0VI	m--	g	Y	R		
08 13 27.8	-09 27 56.6	LHS0244	10.729 ± 0.023	3.64	6.88	412.7		M0.0VI	m-	g++:	Y	19		
22 27 59.0	-30 09 30.0	LHS0521	11.463 ± 0.019	3.22	8.14	222.1		M0.5VI:	m----	g	11	11		
21 21 34.8	-19 03 38.6	LHS0507	12.053 ± 0.026	3.15	7.81	355.2	K/M sd	M0.5VI	m----	g+	Y	R	Y	
15 39 39.0	-55 09 10.0	LHS0401	9.407 ± 0.019	3.31	7.33	142.2		M0.5VI	m----	g++	Y	R		
02 42 26.3	-59 35 01.6	SCR0242-5935	12.783 ± 0.031	3.40		M0.5VI	m--	g		R		
07 09 37.2	-46 48 58.8	SCR0709-4648	11.491 ± 0.026	3.41		M0.5VI	m--	g		R		
11 07 55.8	-41 35 52.7	SCR1107-4135	11.474 ± 0.019	3.49		M0.5VI	m--	g		R		
17 39 45.4	-82 22 02.2	SCR1739-8222	12.190 ± 0.026	3.48		M0.5VI	m--	g		R		
02 02 52.2	+05 42 21.0	LHS0012	8.684 ± 0.020	3.56	6.32	342.1	sdM0	M0.5VI	m-	g	Y	13	8	
11 11 22.6	-06 31 56.4	LHS0299	11.143 ± 0.024	3.64	6.54	437.3		M0.5VI:	m-	g	Y	R		
14 18 20.4	-52 24 12.6	LHS0367	9.786 ± 0.019	3.41	6.26	268.6		M0.5VI:	m-	g	7	7		
04 06 06.7	-67 35 28.8	SCR0406-6735	12.804 ± 0.031	3.54		M0.5VI	m-	g		R		
04 33 26.5	-77 40 09.7	SCR0433-7740	13.361 ± 0.034	3.50		M0.5VI	m-	g		R		
14 33 03.3	-38 46 59.6	SCR1433-3847	13.592 ± 0.046	3.62		M0.5VI	m-	g		R		
18 43 35.7	-78 49 02.5	SCR1843-7849	12.591 ± 0.026	3.55		M0.5VI	m-	g		R		
19 58 31.2	-56 09 10.6	SCR1958-5609	12.525 ± 0.033	3.51		M0.5VI	m-	g		R		
13 46 55.5	+05 42 56.4	LHS0360	11.662 ± 0.023	3.50	6.73	524.0		M0.5VI:	m-	g+	7	7		
22 20 27.0	-24 21 49.3	LHS0518	10.393 ± 0.021	3.24	7.07	230.7		M1.0VI	m-----	g	11	11		
07 01 17.7	-06 55 49.3	SCR0701-0655	12.996 ± 0.030		M1.0VI	m-----	g+				
01 53 09.0	-33 25 02.1	LHS0148	12.832 ± 0.032	3.59	8.59	374.8		M1.0VI	m-----	g+:	6	6		
01 53 09.0	-33 25 02.1	SCR1913-1001	11.929 ± 0.028	3.69		M1.0VI	m-----	g		R		
00 17 40.0	-10 46 16.9	LHS0109	10.366 ± 0.021	3.51	7.63	176.1	K5	M1.0VI	m-----	g+	Y	R	2	
21 04 00.5	-52 29 43.5	SCR2104-5229	12.763 ± 0.024	3.53		M1.0VI	m-----	g+		R		
14 55 35.8	-15 33 44.0	LHS0385	11.062 ± 0.023	3.55	7.61	403.4	M0	M1.0VI	m-----	g++	Y	R	Y	
14 55 51.5	-39 14 33.1	SCR1455-3914	11.788 ± 0.024	3.65		M1.0VI	m-----	g++		R		
12 34 53.1	+05 03 54.1	LHS0335	13.000 ± 0.030	3.60	9.74	247.2		M1.0VI	m-----	g+++	Y	R		
21 09 02.5	-52 26 17.8	SCR2109-5226	13.049 ± 0.036	3.66		M1.0VI	m-----	g+++		R		
01 31 04.1	-50 24 54.3	LEHPM1628	13.459 ± 0.038	3.70		M1.0VI	m-----	g++++		R		
06 54 06.3	-73 58 03.6	SCR0654-7358	13.285 ± 0.048		M1.0VI	m-----	g		R		
14 57 49.0	-39 04 51.4	SCR1457-3904	12.984 ± 0.030	3.69		M1.0VI	m-----	g		R		
16 13 53.5	-30 40 58.4	SCR1613-3040	12.383 ± 0.031	3.66		M1.0VI	m-----	g		R		
17 56 27.9	-59 27 18.2	SCR1756-5927	12.686 ± 0.030	3.61		M1.0VI	m-----	g		R		
20 18 28.7	-66 06 44.5	SCR2018-6606	12.990 ± 0.030		M1.0VI	m-----	g		R		

Table 2
(Continued)

R.A.	Decl.	Object	K_s	$V - K_s$	M_{K_s}	V_{tan}	Old type	New type	Metallicity	Gravity	Ref		
											π	V	spect
05 29 40.9	-39 50 25.6	SCR0529-3950	11.651 ± 0.021		M1.0VI	m--	g			
21 01 45.6	-54 37 31.9	SCR2101-5437	12.078 ± 0.026	3.70		M1.0VI	m-	g		R	
08 01 29.0	+10 43 04.2	LHS1970	13.875 ± 0.032	3.84	9.43	374.8	esdM2.5	M1.0VI:	m-	g+:	Y	R	8
13 25 14.0	-21 27 06.0	LHS2734B	14.932 ± 0.136	3.90	too far	> 280		M1.0VI:	m-	g+:	R	R	
02 42 02.9	-44 30 58.7	LHS0158	9.726 ± 0.021	3.91	6.89	191.4		M1.0[VI]	m	g	11	11	
17 18 35.0	-43 26 24.0	LHS0440	8.948 ± 0.023	4.03	6.78	135.6	M1V	M1.0VI:	m	g+:	11	11	2
18 22 58.7	-45 42 45.3	SCR1822-4542	12.879 ± 0.027	3.92		M1.0VI:	m	g+:		R	
07 56 13.4	-67 05 20.6	WT0233	12.627 ± 0.024	3.60	7.84	326.8	M0.0VI	M2.0VI	m---	g	6	6	6
11 56 54.8	+26 39 56.3	LHS0318	11.797 ± 0.018	3.65	8.77	263.8		M2.0VI:	m---	g	18	R	
05 11 40.6	-45 01 06.0	GJ0191	5.049 ± 0.021	3.80	7.08	161.0	sdM1.0	M2.0VI	m--(-0.99) ^e	g	Y	13	8
02 56 13.2	-35 08 26.9	LHS0162	11.536 ± 0.021	3.82	7.13	364.1	M1.0VI	M2.0VI	m--	g+	6	6	6
21 04 25.5	-27 52 48.5	LHS3620	12.696 ± 0.027	3.93	7.94	414.6		M2.0VI	m--	g+	R	R	
04 03 38.4	-05 08 05.4	LHS0186	10.854 ± 0.024	4.02	7.21	295.6		M2.0VI	m-	g	Y	R	
15 43 18.3	-20 15 33.0	LHS0406	9.018 ± 0.021	4.04	7.40	117.4	M1.0V	M2.0VI	m-	g	11	11	2
00 55 43.8	-21 13 05.5	LHS0127	11.733 ± 0.023	4.06		M2.0VI	m-	g+		R	
06 29 56.4	-69 38 13.4	SCR0629-6938	12.901 ± 0.034		M2.0VI	m-	g+		R	
12 24 26.8	-04 43 36.7	LHS0326	11.234 ± 0.023	3.67	7.69	304.9		M3.0VI	m--	g	R	R	
15 34 27.7	+02 16 47.5	LHS0398	11.502 ± 0.025	3.74	7.52	354.3		M3.0VI	m--	g	Y	19	
23 17 05.0	-13 51 04.1	LHS0541	12.414 ± 0.026	4.05	8.22	420.0	sdM3.0	M3.0VI	m--	g+	Y	1	8
22 04 02.2	-33 47 38.9	SCR2204-3347	11.601 ± 0.027	3.84		M3.0VI	m--	g+		R	
17 40 46.9	-56 46 58.0	SCR1740-5646	13.195 ± 0.040		M3.0VI	m--	g++		R	
19 16 46.5	-36 38 05.8	SCR1916-3638	12.947 ± 0.034	3.88		M3.0VI	m--	g++		R	
04 25 38.4	-06 52 37.0	LHS0189AB	10.311 ± 0.037	3.94	8.59	128.3		M3.0VI:	m-	g	7	7	
07 16 27.7	+23 42 10.4	LHS0228	11.298 ± 0.018	4.20	7.54	300.6	sdM2.0	M3.0VI	m-	g	Y	R	14
13 42 21.2	-35 34 50.7	SIP1342-3534	12.935 ± 0.030	4.37		M3.0VI	m-:	g		R	
04 11 27.1	-44 18 09.0	WT0135	9.834 ± 0.020	4.33		M3.0VI	m-:	g		5	
09 43 46.2	-17 47 06.2	LHS0272	8.874 ± 0.021	4.29	8.34	86.3	sdM3.0	M3.0VI	m-:	g+	Y	R	8
14 50 28.8	-08 38 36.8	LHS0381	11.237 ± 0.021	3.90	8.43	274.9	K7.0V	M3.5VI	m--	g	Y	19	Y
14 31 38.4	-25 25 33.9	LHS0375	11.507 ± 0.022	4.12	9.61	157.5	esdM4	M3.5VI	m--	g+	Y	R	8
01 38 49.0	+11 21 36.7	LHS0144	12.080 ± 0.026	4.24	8.57	386.6		M3.5VI	m-	g	Y	R	
21 55 48.0	-11 21 42.1	LHS0515	12.912 ± 0.032	4.50	9.36	264.5	esdM5	M3.5VI	m-	g+	Y	R	17
05 00 15.3	-54 06 09.0	LEHPM3861	13.967 ± 0.059	4.47	esdM6	M4.0VI	m-	g		R	15
03 02 06.3	-39 50 51.8	LHS1490	9.885 ± 0.023	4.37		M5.0VI	m-	g		R	
12 34 15.7	+20 37 05.7	LHS0334	13.044 ± 0.029	4.98	sdM4.5	M6.0VI	m--	g		R	17
08 53 57.0	-24 46 54.0	LHS2067A	11.571 ± 0.023	6.38	9.54	76.2	subdwarf	M6.0VI	m-	g	R	R	12

Notes.

The last three columns provide references for parallaxes, V -band photometry, and previous spectroscopy results. “:” indicates a questionable subtype, metallicity, or gravity. All K_s magnitudes are from the Two Micron All Sky Survey (2MASS) database. LHS2734A and B have zero parallax so we list them as “too far” in the table.

^a Metallicity data are from Carney et al. (1994).

^b Metallicity data are from Nordström et al. (2004).

^c Metallicity data are from Cayrel de Strobel et al. (2001). There are multiple metallicities reported for G112-054, so a mean value is presented.

^d Cayrel de Strobel et al. (2001), Goldberg et al. (2002), and Laird et al. (1988) report different metallicities, so a mean value is given.

^e Metallicity data are from Woolf & Wallerstein (2005).

^f Morrison et al. (2003) and Allen et al. (2000) report different metallicities, so a mean value is given.

References.

(1) Bessel (1990); (2) Bidelman (1985); (3) Cayrel de Strobel et al. (1997); (4) Carney et al. (1994); (5) Costa & Méndez (2003); (6) Costa et al. (2005); (7) Costa et al. (2006); (8) Gizis (1997); (9) Hawley et al. (1996); (10) Houk & Cowley (1975); (11) Jao et al. (2005); (12) Kirkpatrick et al. (1995); (13) Leggett (1992); (14) Lépine et al. (2007); (15) Lodieu et al. (2005); (16) Monteiro et al. (2006); (17) Reid & Gizis (2005); (18) Smart et al. (2007); (19) Weis (1996); (H) ESA (1997); (R) W.-C. Jao (2008, in preparation); (Y) van Altena et al. (1995).

grids are available. Objects with virtually identical spectra are listed in alphabetical and/or numerical order.

We discuss each spectral subtype from K3.0[VI] to M6.0VI in the following sections and highlight noteworthy subdwarfs of various types. The order of the highlighted targets is based on

their metallicities or gravities. Colored spectra in the figures in these sections are illustrative only—they do not represent any numeric metallicities or gravities, so a red-lined spectrum in one type does not necessarily have similar attributes as a red-lined spectrum in another type.

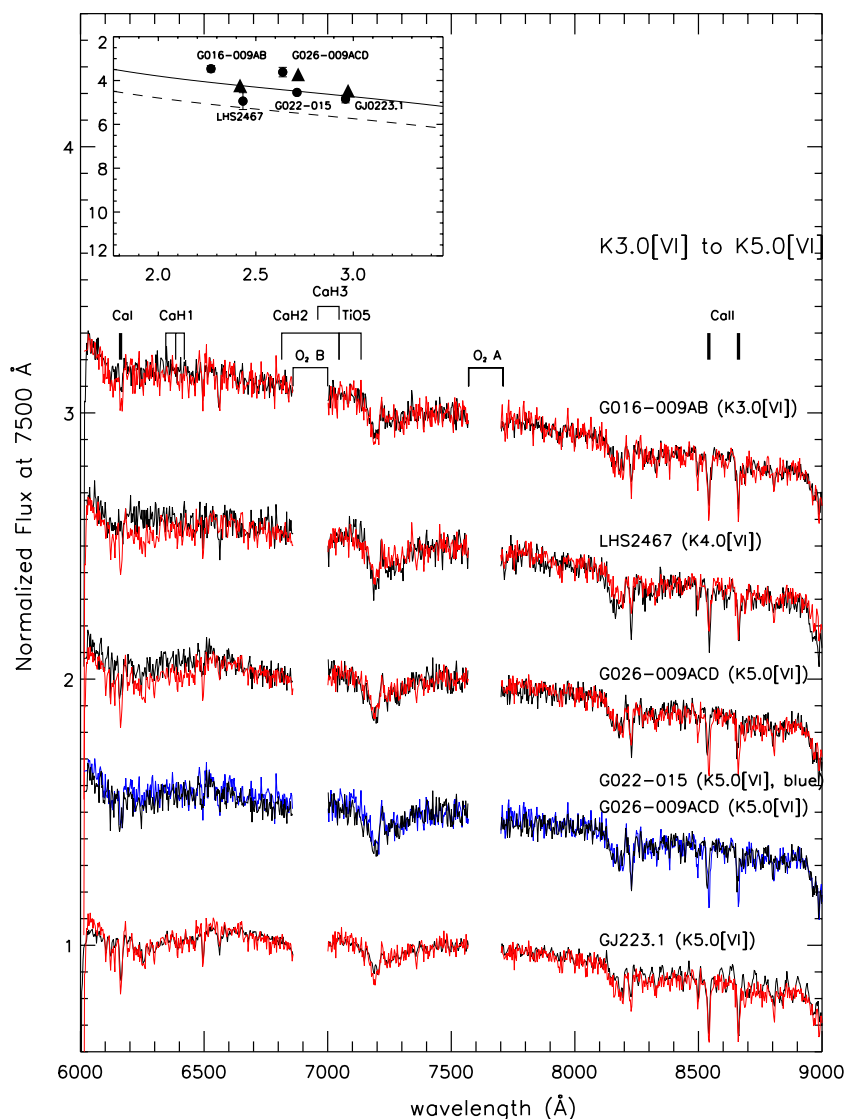


Figure 12. K3.0[VI] to K5.0[VI] spectra compared to K dwarf standard spectra (red). The two telluric bands (O₂ A and B) have been removed for clarity. The three thick tick marks represent the locations of Ca I (6162 Å) and Ca II (8542 Å and 8662 Å) absorption features. The inset plot shows the locations of the stars on the H-R diagram, where the filled circles represent subdwarfs and triangles represent main-sequence standards of types K3.0V, K4.0V, and K5.0V (left to right). For clarity, the axis labels for the inset plot are not shown but are always $V - K_s$ vs. M_{K_s} . The errors in absolute magnitudes are shown. However, because the errors for $V - K_s$ are equal to or smaller than the filled circles, they are not shown. The solid line represents a fitted main-sequence line and the dashed line is 1 mag fainter than the solid line.

(A color version of this figure is available in the online journal.)

7.2.1. K3.0[VI] to K5.0[VI] types

We begin with K3.0[VI], for which it is still difficult to separate subdwarfs from dwarfs at our spectral resolution. Figure 9 shows how similar mid-K-type subdwarfs and dwarfs are (temperatures 4400 K and 4800 K). For these stars, we use other independent published measurements, e.g. $[m/H]$ values, to confirm their subdwarf natures. We currently call stars with $[m/H] \leq -0.5$ subdwarfs. The K3.0[VI] to K5.0[VI] spectra are shown in Figure 12.

G 016-009AB (K3.0[VI]). Goldberg et al. (2002) reported this star to be a double-lined spectroscopic binary with $P = 9.9$ days, $T_{\text{eff}} = 5903$ K, and having a mass ratio (M_1/M_2) of ~ 1.22 . Given that the components are presumably coeval, the combined spectrum should represent the metallicity for each component. Although their estimated temperature is that of a

G-type star, our spectrum has the same slope as a K3.0V. Cayrel de Strobel et al. (2001) and Goldberg et al. (2002) reported measurements of $[Fe/H] = -0.7$ and -1.0 , respectively, while Laird et al. (1988) found $[m/H] = -1.11$. Apparently, it is a low-metallicity star and its location on the H-R diagram is elevated because of multiplicity. This system is also reported to be a photometrically variable system in Kazarovets et al. (2006). This system demonstrates that low-metallicity subdwarfs do not have different spectra from their main-sequence counterparts at our wavelength coverage and resolution, so we assign its luminosity class as [VI] as a result of its low-metallicity measurements.

LHS 2467 (K4.0[VI]). Our spectrum shows that it is a K4.0[VI], rather than a G7V type, as reported in Bidelman (1985). Its continuum is not as blue as K0.0V and its Ba I/H α lines are not as weak/strong as shown in Figure 5 for a

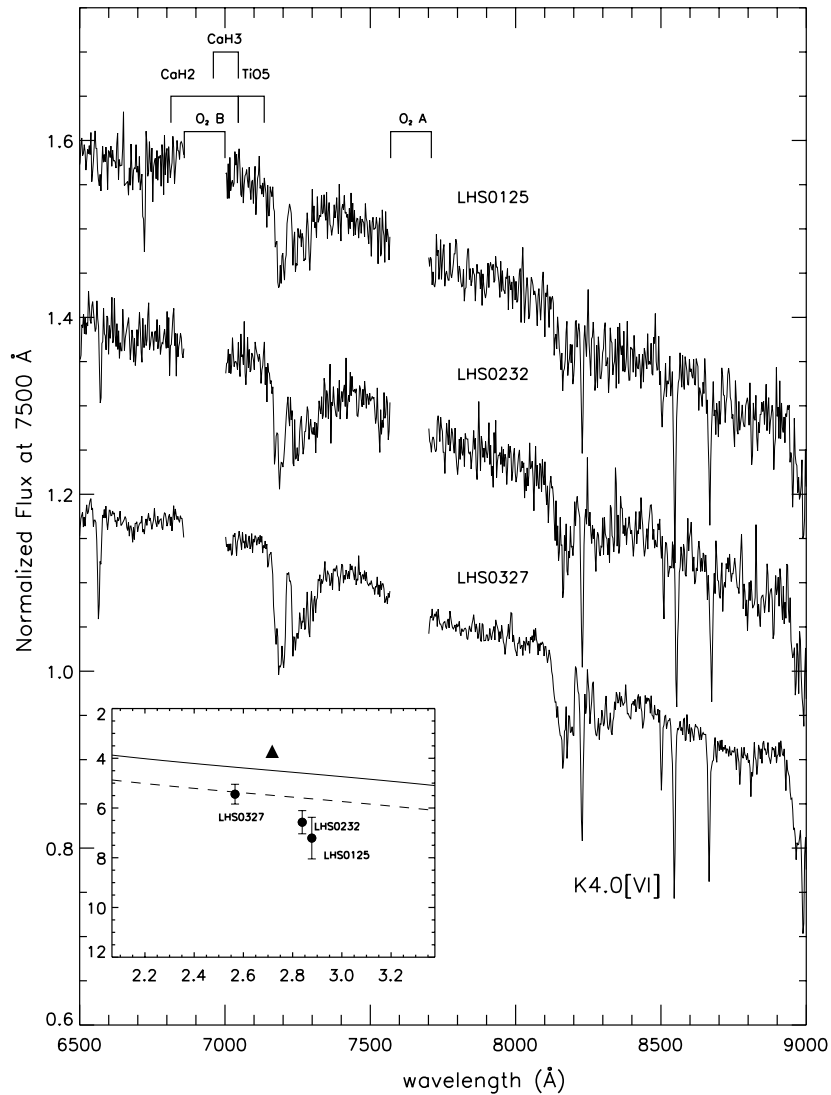


Figure 13. Spectra of LHS 125, LHS 232, and LHS 327 (all K4.0[V]). Note that the blue end of these spectra are at 6500 Å because of problems with these particular spectra between 6000 Å and 6500 Å. The two telluric O₂ A and B bands have been removed. The triangle in the inset plot represents a K4.0V standard star. The symbols and lines have the same meanings as in Figure 12.

G-type star. Its weighted mean parallax from ESA (1997) and van Altena et al. (1995) is 10.63 ± 1.88 mas and its proper motion is $0''.98 \text{ yr}^{-1}$ (Luyten 1979), indicating $V_{\text{tan}} = 437 \text{ km s}^{-1}$. Ryan & Norris (1991) reported the star to have $V_{\text{rad}} = 44 \text{ km s}^{-1}$. After removing the solar motion, LHS 2467 has $(U, V, W) = (281.4, -304.8, -41.9) \text{ km s}^{-1}$. The extremely high tangential and space velocities are indicative of a subdwarf.

G 026–009ACD (K5.0[V]). The wide ($132''$, corresponding to 6520 AU at the system's distance of 49.4 pc) common proper-motion companion, B, in this quadruple system is a white dwarf known as G026–010 or G026–009B, that during its planetary nebula phase should have had limited impact on the metallicity of the close ACD triple. Peterson et al. (1980) reported G026–009AC to be double-lined spectroscopic binary with $P = 3.75$ days, with a mass ratio (M_1/M_2) ~ 1.25 . Allen et al. (2000) reported a third component, D, $0''.7$ away from G026–009AC. Morrison et al. (2003) and Allen et al. (2000) both report the system (ACD) to have low metallicity, measuring $[\text{Fe}/\text{H}] = -0.91$ and -1.19 , respectively. Both the V and K_s magnitudes include three stars, causing the point to be improperly placed on the H-R diagram.

G 022–015 (K5.0[V]). Woolf & Wallerstein (2005) reported this system to have $[\text{Fe}/\text{H}] = -0.61$. G022–015's spectrum is virtually identical to G026–009ACD, as shown by plotting both together in Figure 12.

GJ 223.1 (K5.0[V]). This star has the same slope as the K5.0V standard and its location on the H-R diagram is on the main-sequence line. Nonetheless, Woolf & Wallerstein (2005) reported it to have $[m/\text{H}] = -0.62$, so we tentatively consider it to be a subdwarf until further information indicates otherwise.

Although not definitive, the Ca I line at 8500 Å in these spectra seems to show the metallicity trend seen in the noiseless model spectra plotted in Figure 9 and discussed in Section 5. LHS 2467 has a much weaker Ca I line, and G016–009AB and G026–009AB have slightly weaker Ca I lines than seen in the dwarfs' spectra. However, G022–015 and GJ223.1 both have approximately the same Ca I line strengths as dwarfs. Contrary to the Ca I line, the Ca II lines at (8542 Å and 8662 Å) do not show any metallicity trend from our spectra. Because these prominent lines fail to separate subdwarfs from dwarfs at our resolution and signal-to-noise ratio (S/N), other evidence, i.e. kinematics, parallaxes or independent metallicity

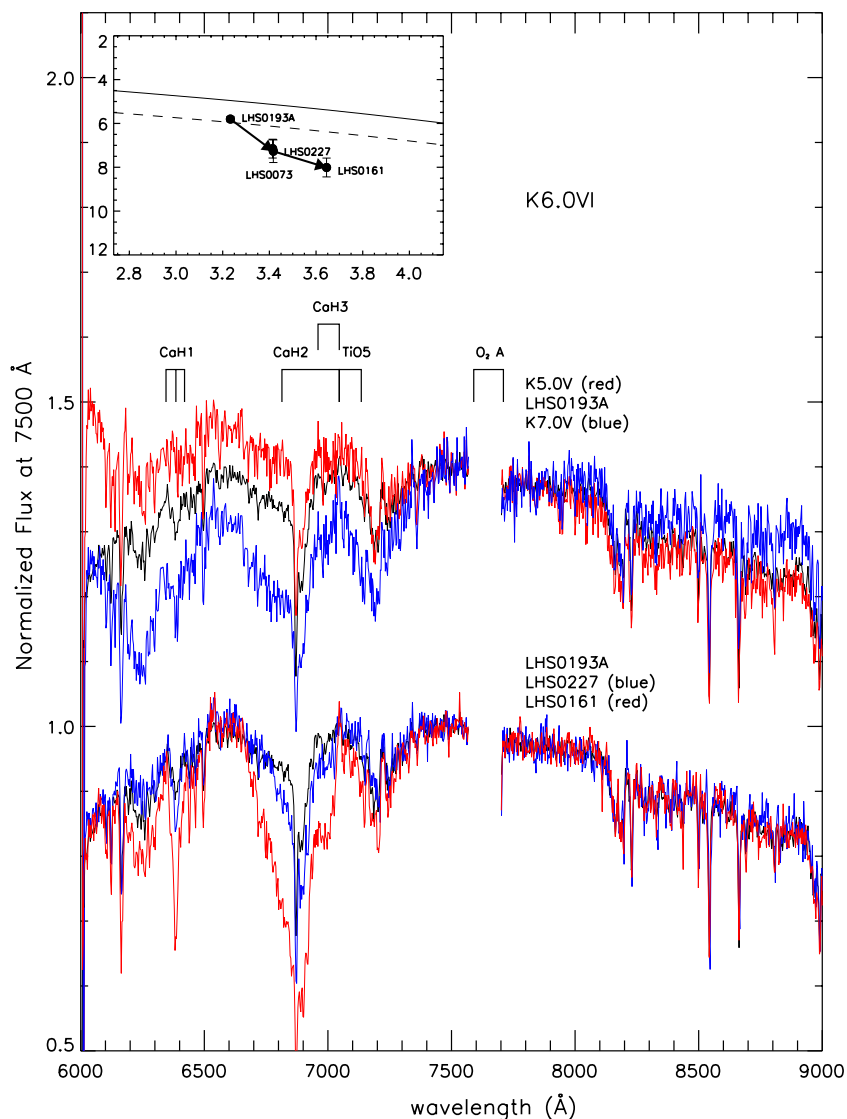


Figure 14. Spectra of LHS 193A, LHS 227, and LHS 161 (all K6.0VI) with our K5.0V and K7.0V standard spectra. The telluric O₂ A band has been removed. The thick arrows in the H-R diagram point toward sequentially higher-gravity subdwarfs. The symbols and lines have the same meanings as in Figure 12. (A color version of this figure is available in the online journal.)

measurements, are required to identify the subdwarfs. An alternative method to separate the subdwarfs from the dwarfs is to obtain spectra that include the MgH bands at 4845 Å, 5211 Å, and 5621 Å that Bessell (1982) pointed are sensitive to metal abundance for temperatures hotter than 4500 K.

Several possibilities may explain the locations of the three subdwarfs, LHS 2467, G 022–015, and GJ 223.1 on the H-R diagram just below or on the main-sequence line: (1) they are subdwarfs with unseen companions that brighten their M_{K_s} magnitudes, (2) they are slightly evolved and have moved significantly from the subdwarf zero age main-sequence line, or (3) their metallicity measurements are not accurate and they are, in fact, main-sequence dwarfs.

LHS 125, LHS 232, and LHS 327. The spectra for these three stars, shown in Figure 13, match neither the LHS 2467 K4.0[VI] spectrum nor a K4.0V spectrum, although the spectra have the overall slopes and the stars have $V - K_s$ colors indicative of K4.0 stars. They are tentatively assigned types of K4.0[VI] based on their locations on the H-R diagram.

7.2.2. K6.0VI

We identify four stars to have spectral type K6.0VI, as shown in Figure 14. Their spectral slopes fall between K5.0V and K7.0V.

LHS 193A. This is a binary with a separation of 12'59 comprised of a cool subdwarf (A) and a DC-type white dwarf (B) with a featureless spectrum (Monteiro et al. 2006). At the system's distance of 31.2 pc, the large separation of the pair corresponds to 393 AU, indicating that significant pollution of the subdwarf by the white dwarf during its planetary nebula phase seems unlikely. From Figure 14, it is clear that LHS 193A's spectral slope is between K5.0V and K7.0V. Although the spectrum is a near match to K5.0V between 8200 Å and 9000 Å, the blue end (6000–7500 Å) is too low to be a K5.0V (as a subdwarf, the blue end of the spectrum would have to be above the dwarf standard). As shown in Figure 9, for a star with 4400 K (a K5.0V from Allen's Astrophysical Quantities 2000), there is effectively no difference in the continua of spectra for

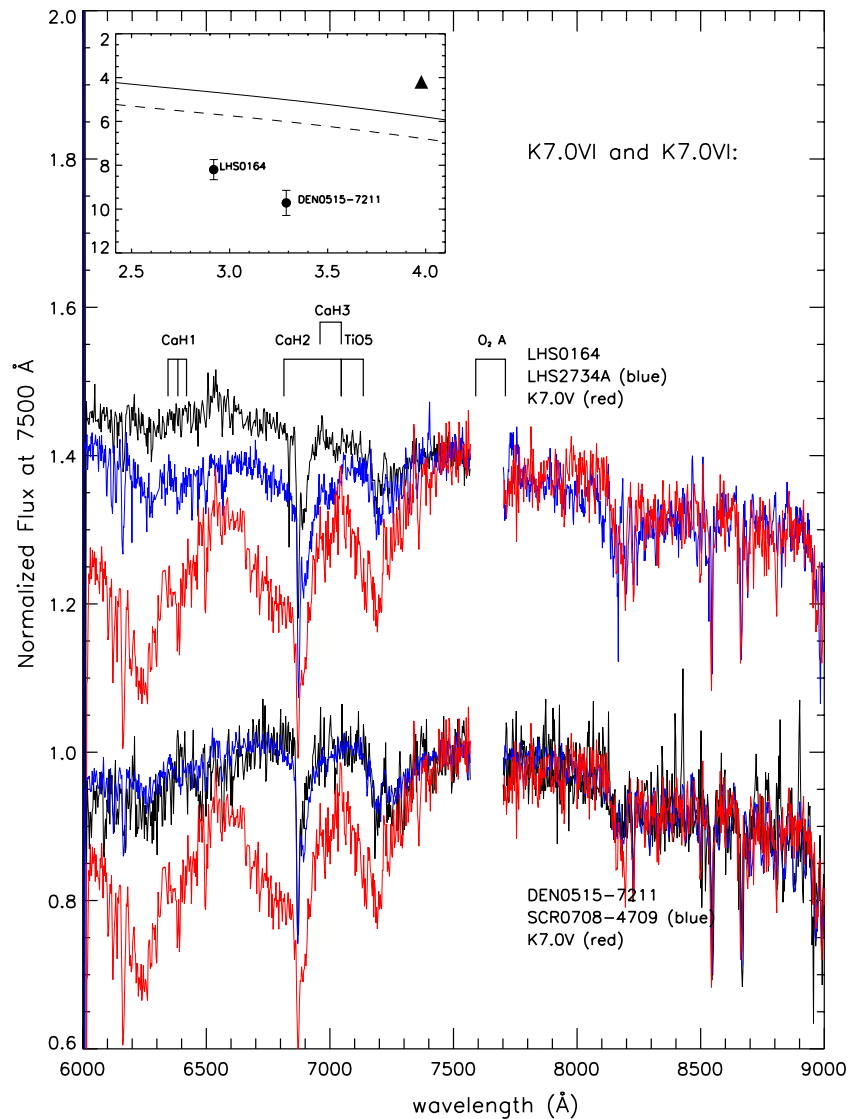


Figure 15. Spectra of LHS 164, LHS 2734A (both K7.0VI), DEN 0515–7211, and SCR0708–4709 (both K7.0VI:), with our K7.0V standard spectrum (represented by a triangle in the inset plot). The telluric O₂ A band has been removed. The symbols and lines have the same meanings as in Figure 12. (A color version of this figure is available in the online journal.)

dwarfs and subdwarfs. Hence, we assign LHS 193A a type of K6.0VI because its TiO5 band is “brightened” (low metallicity), as shown in Figure 9. Given its low metallicity, location on the H-R diagram (as shown in the inset of Figure 14), its $V_{\text{tan}} = 147.3 \text{ km s}^{-1}$ (Jao et al. 2005), and its age of 6–9 Gyr based on its white dwarf companion’s cooling age (Monteiro et al. 2006), it is most likely a thick-disk subdwarf.

LHS 73 and LHS 227. These two objects have virtually identical spectra, so we only show LHS 227 in Figure 14 for clarity. The only differences between these spectra and that of LHS 193A are in CaH. Using results from the top panel of Figure 10, we find that LHS 73 and LHS 227 have higher gravities than LHS 193A.

We have acquired spectra for both LHS 72 and LHS 73, a wide ($\sim 96''$ separation) common proper-motion pair. Unfortunately, the spectrum of LHS 72 ($V - K_s = 3.29$, $M_{K_s} = 6.69$) is poor and requires re-observation, although it would fall in the subdwarf region of the H-R diagram. LHS 73 has $V - K_s = 3.42$ and $M_{K_s} = 7.27$ and is plotted in Figure 14, also clearly in the subdwarf region. Rodgers & Eggen (1974) previously identified both objects as subdwarfs, but no spectral types were

given. Bidelman (1985) identified LHS 72 and LHS 73 as K4 and K5 dwarfs, respectively. Reylé et al. (2006) reported LHS 72/73 (they identified LHS 73 as sdK7) to be the nearest subdwarf binary based on their spectroscopic parallax (18.7 pc), although the trigonometric parallax from YPC is $37.6 \pm 8.9 \text{ mas}$ ($21.5 \text{ pc} < d < 34.8 \text{ pc}$). The nearest known subdwarf binary system is actually μ Cas AB, at a distance of 7.5 pc ($\pi_{\text{trig}} = 132.4 \pm 0.6 \text{ mas}$, ESA 1997).

LHS 161. This star was previously reported to be an esdM2.0 extreme subdwarf (Gizis 1997). However, its slope and spectral features, like LHS 227, are too hot for type M2.0VI. As shown in Figure 14, LHS 161 has stronger CaH than LHS 193A and LHS 227, but the rest of the spectrum is the same. We conclude that LHS 161 has higher gravity than the other two subdwarfs. LHS 161’s very strong CaH lines and consequent CaH and TiO5 indices place it in the previously designated “extreme” subdwarf region, which typically implies that the star has very low metallicity. It appears, from our current understanding, that the strong CaH in LHS 161 may not be linked to metallicity, because the TiO5 band is not significantly different from LHS 193A, LHS 73, or LHS 227.

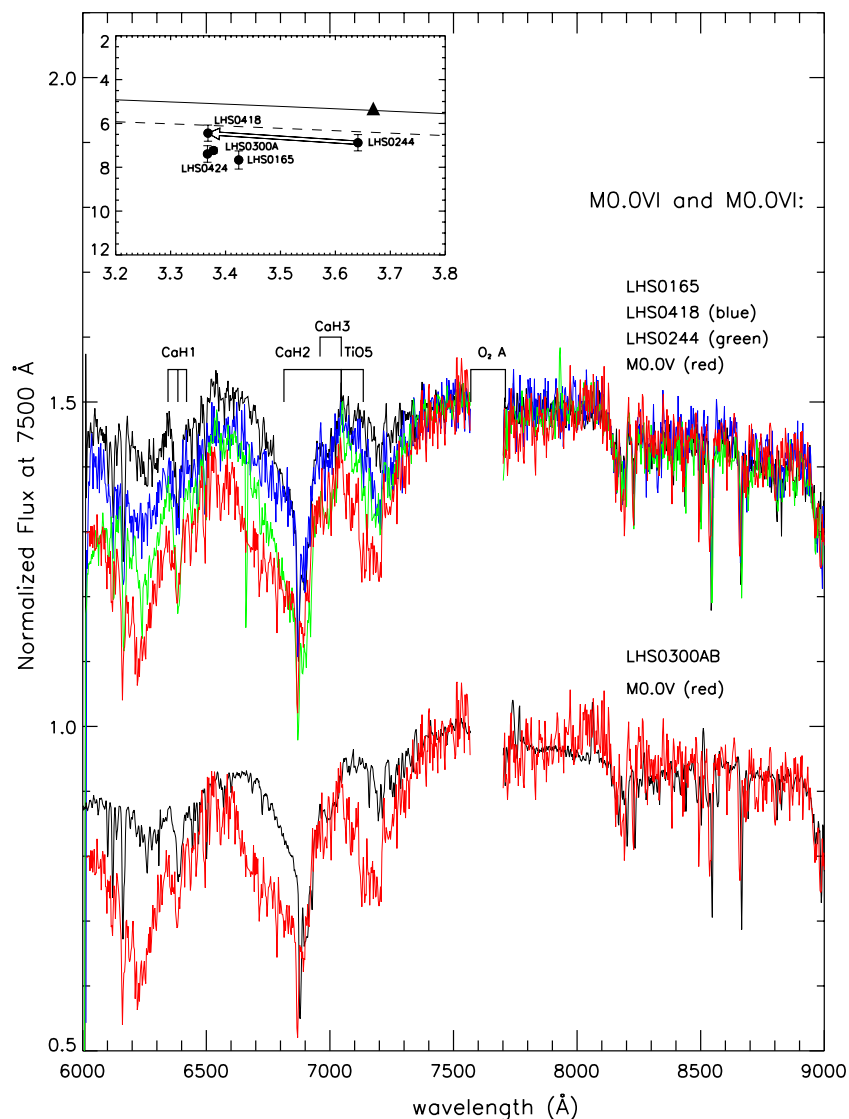


Figure 16. Spectra of LHS 165, LHS 418, LHS 244 (all M0.0VI), and LHS 300AB (M0.0VI) with our M0.0V standard spectrum (represented by a triangle in the inset plot). The telluric O₂ A band has been removed. The hollow arrow indicates the shift on the H-R diagram caused by decreasing metallicity. The symbols and lines have the same meanings as in Figure 12.

(A color version of this figure is available in the online journal.)

In the inset of Figure 14 we connect LHS 193A, LHS 73, LHS 227, and LHS 161 on the H-R diagram with thick arrows to outline a sequence of increasing gravity effects that shift their locations to the lower right (less luminous and redder). We will soon see more such gravity effects, which are always toward lower luminosities.

7.2.3. K7.0VI

We identify four stars to have spectral type K7.0VI, as shown in Figure 15. This is the earliest spectral type for which we see clear metallicity effects in the blue regions of our spectra.

LHS 2734A. This is the primary in a new common proper-motion system discovered during CTIOPI, for which we measure the components to have $\mu = 0''.59$ and $0''.60 \text{ yr}^{-1}$ at position angles 228.2° and 228.4° for the A and B components, respectively. The B component is located $68''.8$ away at position angle 162.4° . Unfortunately, both components are beyond our current trigonometric parallax limit (100 pc), but the A component

provides a useful subdwarf anchor point even though its location on the H-R diagram is unknown.

There are three reasons to adopt LHS 2734A as a reliable subdwarf anchor. First, we measure a zero parallax, implying that its V_{tan} is at least 280 km s^{-1} (assuming a distance of 100 pc). A tangential velocity of this size is indicative of a subdwarf. Second, LHS 2734B ($V - K_s = 3.90$), is redder than LHS 2734A ($V - K_s = 3.23$), and later type subdwarfs are more easily separated from dwarfs, as shown in Figure 9. As discussed in Section 7.2.6, LHS 2734B is clearly a subdwarf. Assuming this common proper-motion pair formed at the same time with similar “genetics,” both components are subdwarfs. Third, Figure 15 shows the comparison between K7.0V and LHS 2734A, in which the blue end of LHS 2734A’s spectrum is clearly “brightened.” This indicates that LHS 2734A has lower metallicity than K7.0V, as expected for a subdwarf.

LHS 164. This star is four full magnitudes below the main-sequence line in the inset in Figure 15. We find a good match at the red end between our K7.0V standard and LHS 164’s

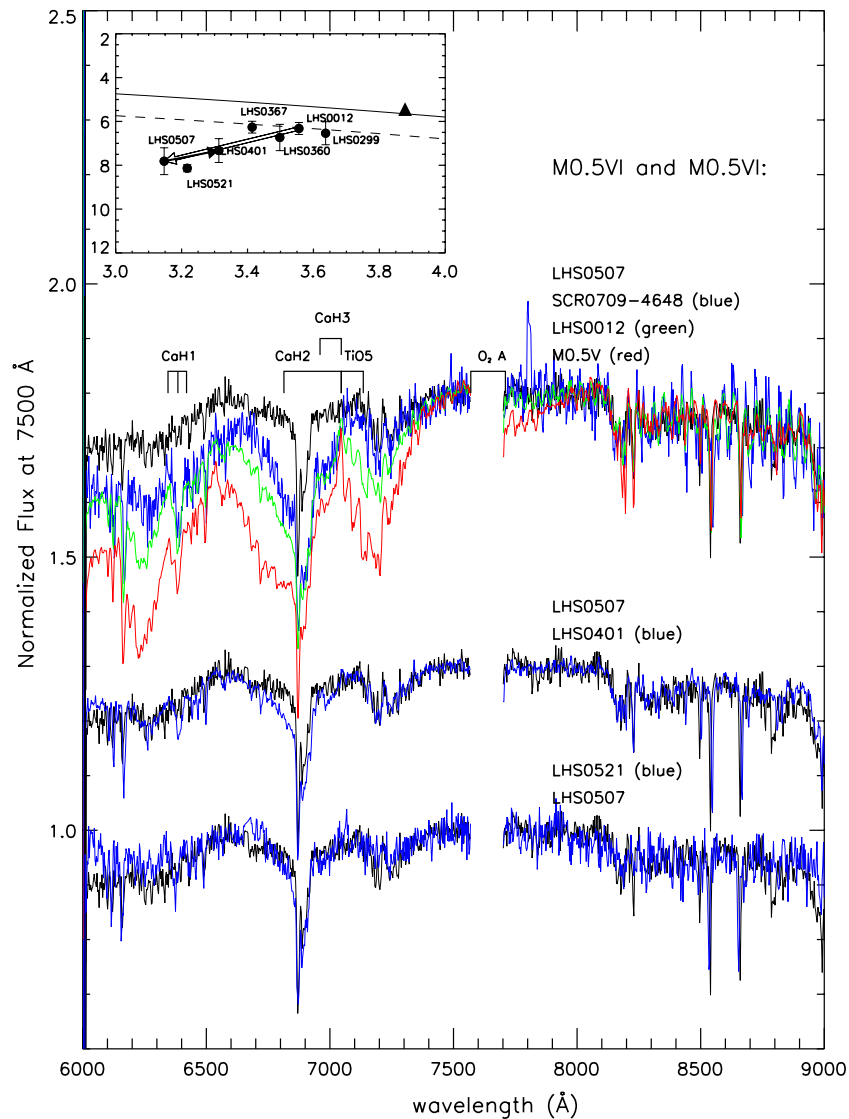


Figure 17. Spectra of LHS 507, SCR 0709-4648, LHS 12, LHS 401 (all M0.5VI), and LHS 521 (M0.5VI) with our M0.5V standard spectrum (represented by a triangle in the inset plot). The telluric O₂ A band has been removed. The hollow arrow indicates the shift on the H-R diagram caused by decreasing metallicity. The solid arrow indicates the shift caused by higher gravity. The symbols and lines have the same meanings as in Figure 12.

(A color version of this figure is available in the online journal.)

spectrum, while the blue end is elevated. We conclude that LHS 164's metallicity is even lower than LHS 2734A's.

Thus, our K7.0V standard, LHS 2734A, and LHS 164 form a sequence of decreasing metallicity. The CaH and TiO5 band depths significantly decrease as the metallicity drops, matching the effects discussed in Section 4.1 and Figure 8.

DEN0515–7211 and SCR 0708–4709. These two spectra are virtually identical and are assigned type K7.0VI: because the spectra do not match either the K7.0V standard, LHS 164, or LHS 2734A (Figure 15). DEN0515–7211 is nearly 5 mag less luminous in M_{K_s} than the main-sequence line, so it is certainly a subdwarf. SCR 0708–4709 ($\mu = 0''.402 \text{ yr}^{-1}$; Subasavage et al. 2005a) has almost the same spectrum as DEN0515–7211 and falls in the subdwarf region on the reduced proper-motion diagram (see Subasavage et al. 2005a).

7.2.4. M0.0VI

We show four stars with spectral type M0.0VI in Figure 16.

LHS 244, LHS 418, and LHS 165. These three spectra have the same continua at the red end but are very different at the blue end.

The differences are caused by metallicity, as seen in Figure 9, with the main-sequence standard–LHS 244–LHS 418–LHS 165 trending to lower metallicities. The blue ends of the subdwarf spectra have clearly “brightened” along this sequence, which is consistent with the theoretical models. In addition, as discussed in Section 4.1, CaH1 absorption decreases (increasing index) as metallicity decreases if T_{eff} is greater than 3500 K. LHS 165 is redder in $V - K_s$ and has stronger CaH1 absorption than LHS 418, so we suspect LHS 165 has a higher gravity (similar to gravity effects shown in Figure 14). We also find that LHS 418 has weaker CaH1 absorption than LHS 244, indicating that LHS 244 could also possibly have higher gravity than LHS 418. LHS 244 is much redder than LHS 418 and LHS 165 in the H-R diagram because of a combination of gravity and metallicity effects.

LHS 424. This star has the same spectrum and color as LHS 418, so we assign the same spectral type. We note that LHS 424 is a full magnitude less luminous in M_{K_s} , perhaps hinting that LHS 418 is a multiple system.

LHS 300AB. This is a close binary with a separation of $\sim 4''.3$ (Jao et al. 2003) comprised of a cool subdwarf (A) and a

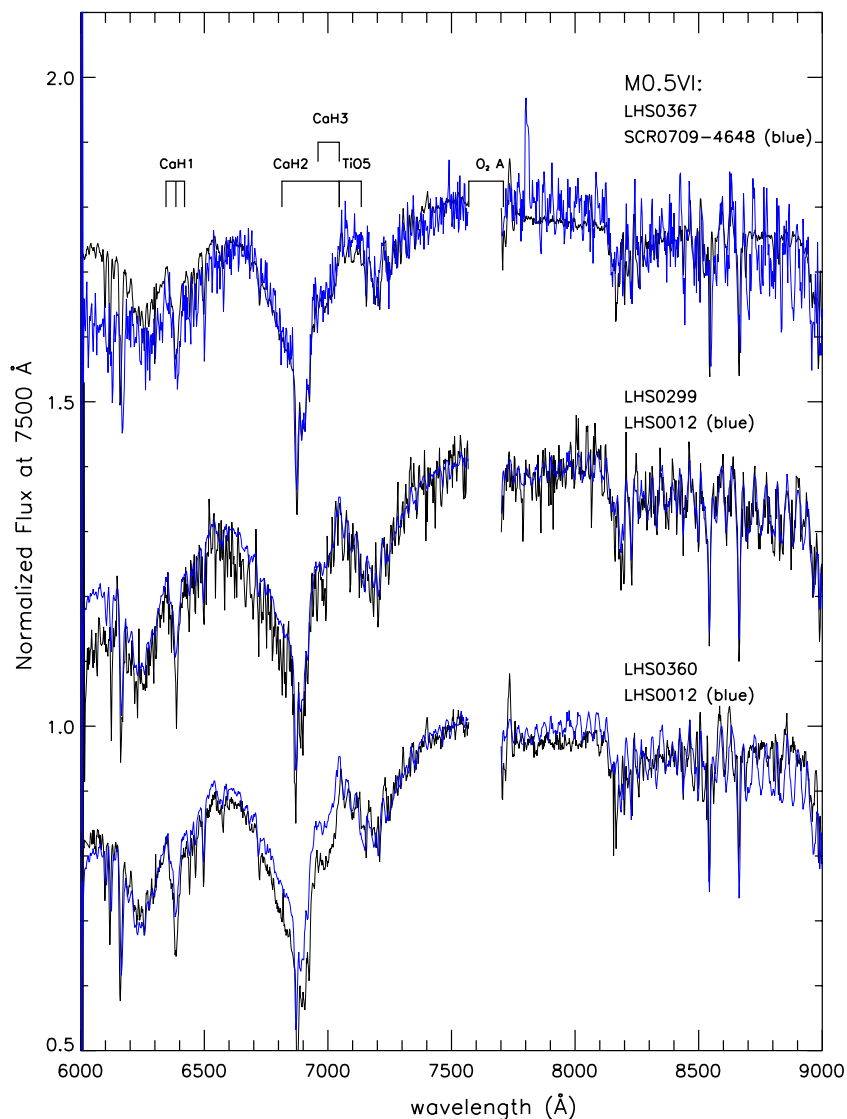


Figure 18. Spectra of LHS 367, LHS 299, and LHS 360 (all M0.5VI). The telluric O₂ A band has been removed. (A color version of this figure is available in the online journal.)

DC-type white dwarf (B) with a featureless spectrum (Monteiro et al. 2006). The spectrum obtained includes both components, but with $\Delta VRI = 4.61, 4.85, 4.96$ mag (Monteiro et al. 2006), the contamination of the cool subdwarf spectrum from the white dwarf is negligible. At a distance of 31.0 pc, the projected separation implies a distance of 133 AU between the two components, indicating that the subdwarf's composition was unlikely to be significantly contaminated by the evolved star during its planetary nebula phase. The spectrum does not match other M0.0VI stars at the blue end, but it matches the red end of M0.0V and M0.0VI well. We therefore assign it a type M0.0VI:

7.2.5. M0.5VI

This is the first half spectral type we currently assign for subdwarfs. We see both metallicity and gravity effects for M0.5VI, as shown in Figures 17 and 18.

LHS 507, SCR 0709–4648, and LHS 12. These three stars, along with our M0.5V standard, illustrate a nice four-step trend in metallicity. With the lowest metallicity, LHS 507 is

significantly bluer than LHS 12, which is, in turn, bluer than our main-sequence standard. We do not yet have a trigonometric parallax for SCR 0709–4648, so we cannot confirm its location on the H-R diagram. LHS 12 was previously reported to be a type sdM0.0 in Gizis (1997).

LHS 401. This star has stronger CaH bands and therefore higher gravity than LHS 507, which has extremely weak CaH1. LHS 401 is redder than LHS 507, as expected, but is slightly more luminous, which is not consistent with the gravity effects seen for types K6.0VI and M0.0VI. We believe this inconsistency is a result of the large absolute magnitude errors for these two objects.

LHS 521. This star has a spectrum nearly identical to LHS 507, except at 6000–6200 Å. Its CaH2 feature is slightly different from LHS 507, so we assign it a type M0.5VI:

LHS 367 and LHS 299. Both objects have trigonometric parallaxes. Their spectra are similar to SCR 0709–4648 and LHS 12, respectively (as shown in Figure 18), so they also have similar offsets in metallicities from one another. We assign them as M0.5VI: because of (1) discrepancies at 6000–6200 Å, (2)

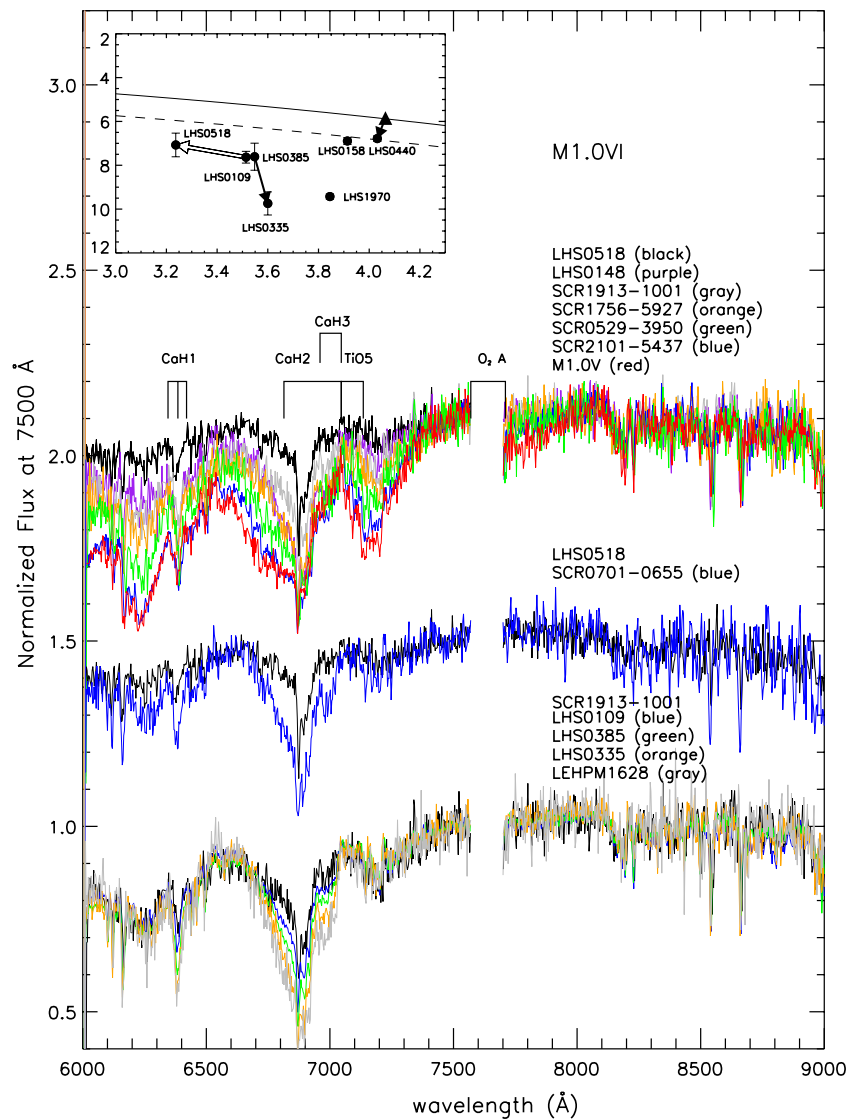


Figure 19. Progressions in metallicity and gravity effects in M1.0VI subdwarf spectra. The top set of spectra illustrates spectra with metallicities increasing from black to red (top to bottom, metallicity scale from m — — — — to m). The red line is our M0.5V standard spectrum (represented by a triangle in the inset plot). The bottom two sets of spectra illustrate gravity effects for metallicity scales m — — — — and m — — —. The telluric O_2 A band has been removed. The symbols and lines have the same meanings as in Figure 17.

(A color version of this figure is available in the online journal.)

LHS 299 has deeper CaH1 absorption than LHS 12 and different CaH2 absorption, and (3) their locations on the H-R diagram are redder than their respective comparison stars. LHS 299 may have a higher gravity than LHS 12, but a smaller absolute magnitude error is needed to confirm this speculation.

LHS 360. This star appears to have higher gravity than LHS 12 because the CaH features are deeper, but its location on the H-R diagram does not match its stronger gravity because its $V - K_s$ color is slightly bluer than LHS 12. Costa et al. (2006) reported that LHS 360 has $V_{\text{tan}} \sim 524 \text{ km s}^{-1}$. Based on its very high V_{tan} and location on the H-R diagram, we assign it a type M0.5VI:

7.2.6. M1.0VI

The M1.0VI type has the largest number (23) of confirmed subdwarfs in our current sample. The spectra of 16 different M1.0VI stars are shown in Figures 19 and 20. Many of these stars have similar colors, as identified in a reduced proper-motion diagram derived using results from our SuperCOSMOS-

RECONS (SCR) survey (Subasavage et al. 2005a, 2005b). Given the rich dataset for this type, we first discuss the sample in terms of metallicity and gravity effects, then discuss individual targets.

Metallicity effects. Perhaps better than for any other spectral type available, the M1.0VI stars show a beautiful trend in metallicity in their spectra, as shown in the top of Figure 19. The red ends of the spectra match the M1.0V standard spectrum, but the blue ends of the spectra are very different because of metallicity effects. We assign their metallicities on a scale of m to m — — — —, where m is indistinguishable from the main-sequence standard and 6 “—” indicate the most severely metal poor subdwarf.

As metallicity drops, the TiO5 band gradually weakens, as predicted in the model spectra of Figure 9 for stars cooler than $\sim 4000 \text{ K}$. Our M1.0V standard (metallicity m), LHS 109 (metallicity scale m — — — —), and LHS 518 (metallicity scale m — — — —) have trigonometric parallaxes, and as predicted from the models, their positions on the H-R

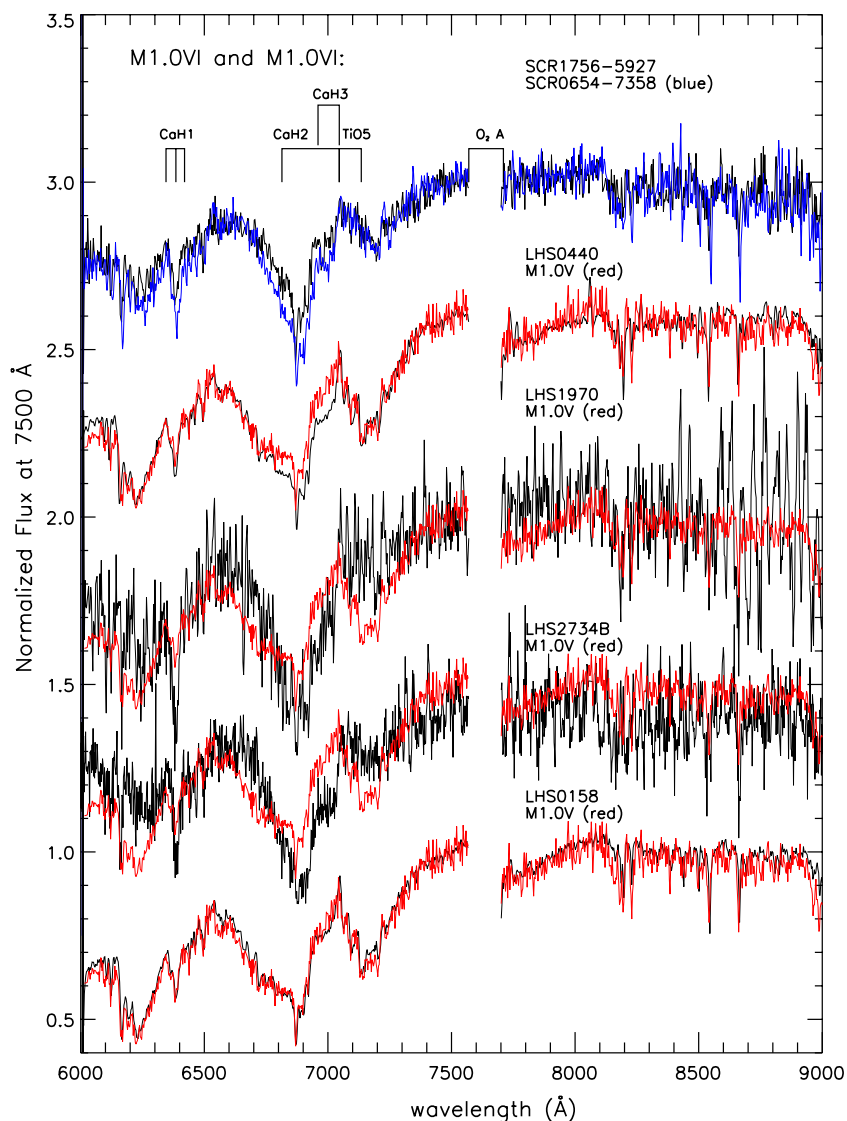


Figure 20. The top set of spectra illustrates gravity effects for metallicity scale $m- - -$. Spectra of LHS 440, LHS 1970, LHS 2734B (all M1.0VI), and LHS 158 (M1.0[VI]) are also shown compared individually to our M1.0V standard. The telluric O₂ A band has been removed.

(A color version of this figure is available in the online journal.)

diagram shift bluer with decreasing metallicity. At metallicity $m- - -$, SCR 2101–5437 is slightly metal poor compared to M1.0V (TiO5) and has slightly higher gravity than M1.0V (CaH). Unfortunately, none of the SCR objects in Figure 19 has trigonometric parallaxes yet. Thus, they cannot be plotted on the H-R diagram, and the progressive trend in metallicity effects for these stars cannot yet be shown.

Gravity effects. The effects of gravity can be seen at three different metallicities for type M1.0VI. Spectra for metallicity scale $m- - - - -$ subdwarfs are shown in the middle of Figure 19. SCR 0701–0655 has higher gravity than LHS 518. Both spectra are identical, except at CaH. Spectra for metallicity scale $m- - - -$ subdwarfs are shown in the bottom of Figure 19. A clear trend can be seen. Three of these five objects have trigonometric parallaxes—LHS 109, LHS 385, and LHS 335—and their gravity differences shift their locations on the H-R diagram toward redder and less luminous territory, as with previously discussed types. (LHS 385’s high parallax error is the likely cause of the slight offset between its H-R diagram position and LHS 109’s.) Finally, as shown at the top of

Figure 20 for metallicity scale $m- - -$, SCR 0654–7358 has higher gravity than SCR 1756–5927.

LHS 440. This was reported by Bidelman (1985) to be type M1.0V. The second set of spectra in Figure 20 shows that LHS 440 has deeper absorptions in all three CaH bands than the M1.0V standard, but is virtually identical at all other wavelengths. This indicates that LHS 440 probably has higher gravity than M1.0V, making it less luminous than main-sequence stars on the H-R diagram. Because it is just barely 1 mag below the main-sequence fit, we currently assign it a type M1.0VI.

LHS 1970 and LHS 2734B. Both have noisy spectra because they are faint. As shown in Figure 20, their strong CaH bands indicate that they are high gravity (strong CaH), low-metallicity (weak TiO5) subdwarfs. LHS 1970’s location on the H-R diagram confirms that it is a subdwarf and Gizis (1997) reported its spectral type is esdM2.5. LHS 2734B’s spectral similarity to LHS 1970 indicates that it also has low metallicity and high gravity. Unfortunately, we measure zero parallax for the LHS 2734AB pair, within the errors, so we cannot plot them

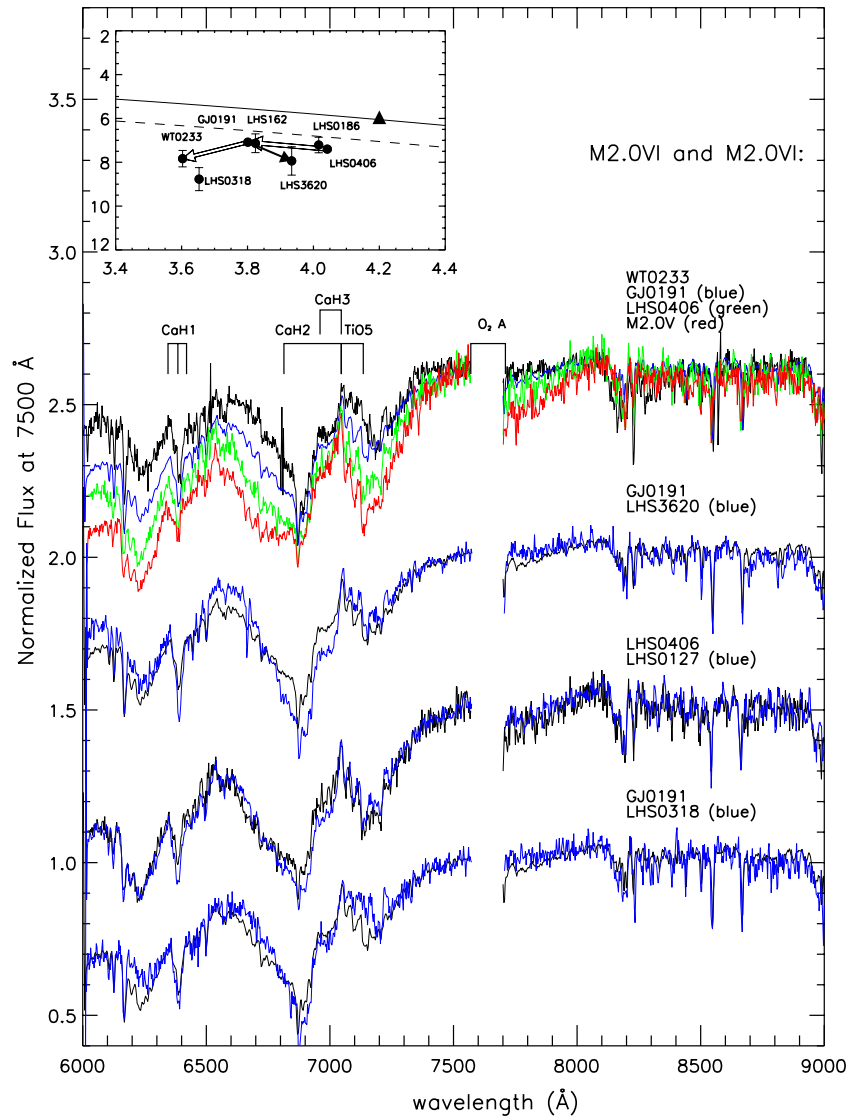


Figure 21. Spectra for WT 233, GJ 191, LHS 406, LHS 3620, LHS 127 (all M2.0VI), and LHS 318 (M2.0VI-) with our M2.0V standard spectrum (represented by a triangle in the inset plot). The telluric O₂ A band has been removed. The symbols and lines have the same meanings as in Figure 17. (A color version of this figure is available in the online journal.)

on the H-R diagram (see Section 7.2.3 for discussion of LHS 2734A). We assign both LHS 1970 and LHS 2734B types M1.0VI: because of their noisy spectra.

LHS 158. This has a spectrum nearly identical to an M1.0V star, but falls 1 mag below the main-sequence line on the H-R diagram. It also has $V_{\text{tan}} = 191 \text{ km s}^{-1}$ (Jao et al. 2005). The low luminosity and tangential velocity together imply that LHS 158 may be a subdwarf, so we assign it a type M1.0[VI], representing its uncertain assignment as a subdwarf, as is the case for the mid-K-type subdwarfs.

7.2.7. M2.0VI

This is the earliest type for which we see that CaH1 absorption deepens as the metallicity decreases, as shown by the curves in Figure 8 for T_{eff} less than 3500 K. Figure 21 shows the spectra for stars discussed in this section.

LHS 406, GJ 191 (Kapteyn’s Star), and WT0233. They form a sequence of decreasing metallicity. These three stars have parallaxes, and their positions on the H-R diagram show a

clear trend toward the blue for stars with decreasing metallicity (shown with open arrows). One of the prototypes of the subdwarf class, Kapteyn’s Star, which has $[\text{Fe}/\text{H}] = -0.99$ from Woolf & Wallerstein (2005), has previously been reported to be a type sdM1.0 in Gizis (1997). We assign a somewhat later type for this famous star, which at 3.9 pc is the nearest known subdwarf of any type.

GJ 191/LHS 3620 and LHS 406/LHS 127. The relative effects of gravity can be seen in the spectra of these two pairs. LHS 3620 has much stronger gravity than GJ 191, while LHS 127 has slightly stronger gravity than LHS 406. On the H-R diagram, LHS 3620 is redder and less luminous than GJ 191, as expected. LHS 162 has a spectrum (not plotted) virtually identical to LHS 3620, but is only slightly redder and less luminous than GJ 191.

LHS 318. It is almost identical to GJ 191 except for weaker TiO5 absorption. This weaker TiO5 indicates LHS 318 is slightly more metal poor than GJ 191, so the blue end of the spectrum should be “brightened”; however, it is not. LHS 318’s location on the H-R diagram in relation to GJ 191 suggests a

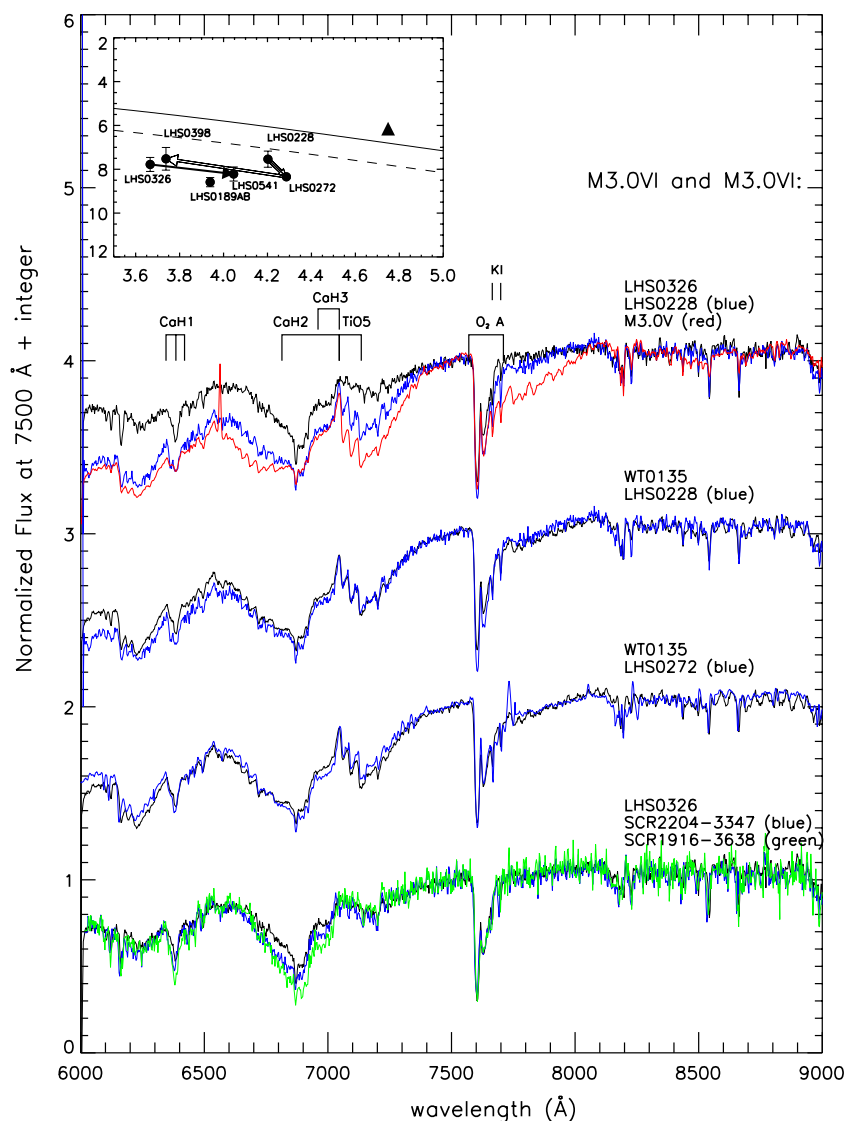


Figure 22. Spectra for six M3.0VI, with our M3.0V standard spectrum in the top set of spectra (represented by a triangle in the inset plot). LHS 326 and LHS 228 show metallicity changes, while LHS 326, SCR2204–3347, and SCR1916–3638 show effects of gravity. WT 135 and LHS 272 are M3.0VI:. Note that the K I lines at 7665 Å and 7699 Å have appeared and blended in the O₂ A band. The symbols and lines have the same meanings as in Figure 17.

(A color version of this figure is available in the online journal.)

higher gravity that is not apparent in its spectrum. We would expect LHS 318 to appear brighter and bluer than GJ 191 if metallicity is the only difference in these two stars, so we assign it as M2.0VI:.

7.2.8. M3.0VI

LHS 228/LHS 189AB and LHS 326/LHS 398. They are pairs of stars with nearly identical spectra. As shown in Figure 22, LHS 326, LHS 228, and our M3.0V standard form a metallicity sequence. As in the case of M2.0VI, CaH1 absorption deepens for M3.0VI stars with decreasing metallicity. In the case of LHS189AB, Costa et al. (2006) reported their separation as about 3'' and their $\Delta R \sim 0.5$ mag. At a distance of 22.1 pc, the projected separation implies a distance of ~ 66 AU between the two components. This spectrum has combined both components, so we assign it type M3.0VI: until completely “clean” data can be acquired for the components, and their individual metallicity scales can be determined.

WT 135. It was previously identified by Henry et al. (2002) as type M2.5V. We assign its metallicity m–: because its

band is the same as seen in LHS 228, but the blue end of its spectrum is “brightened” (making it somewhat metal poor compared to LHS 228). It lacks a trigonometric parallax, so we cannot plot it on the H-R diagram.

LHS 272. It with $V - I = 4.29$ is similar in color to WT 135 ($V - I = 4.32$) but appears to have slightly higher gravity (deeper CaH bands). Overall, the blue end of its spectrum (6000–6300 Å) is comparable to WT 135, although with portions slightly brighter and portions slightly fainter. We therefore assign its metallicity to be the same as WT 135, at m–:. It is slightly redder and less luminous than LHS 228. We use both hollow (metallicity) and solid (gravity) arrows to indicate its location relative to LHS 228. The competition between metallicity and gravity effects in this case seems to indicate that gravity is the dominant factor because LHS 272’s position moves to the red, rather than the blue. LHS 272 was reported as sdM3.0 in Gizis (1997).

LHS 326, SCR 2204–3347/LHS 541, and SCR 1916–3638. They form a clear sequence of gravity effects. Other than having a noisier spectrum (not shown), LHS 541 appears to be identical

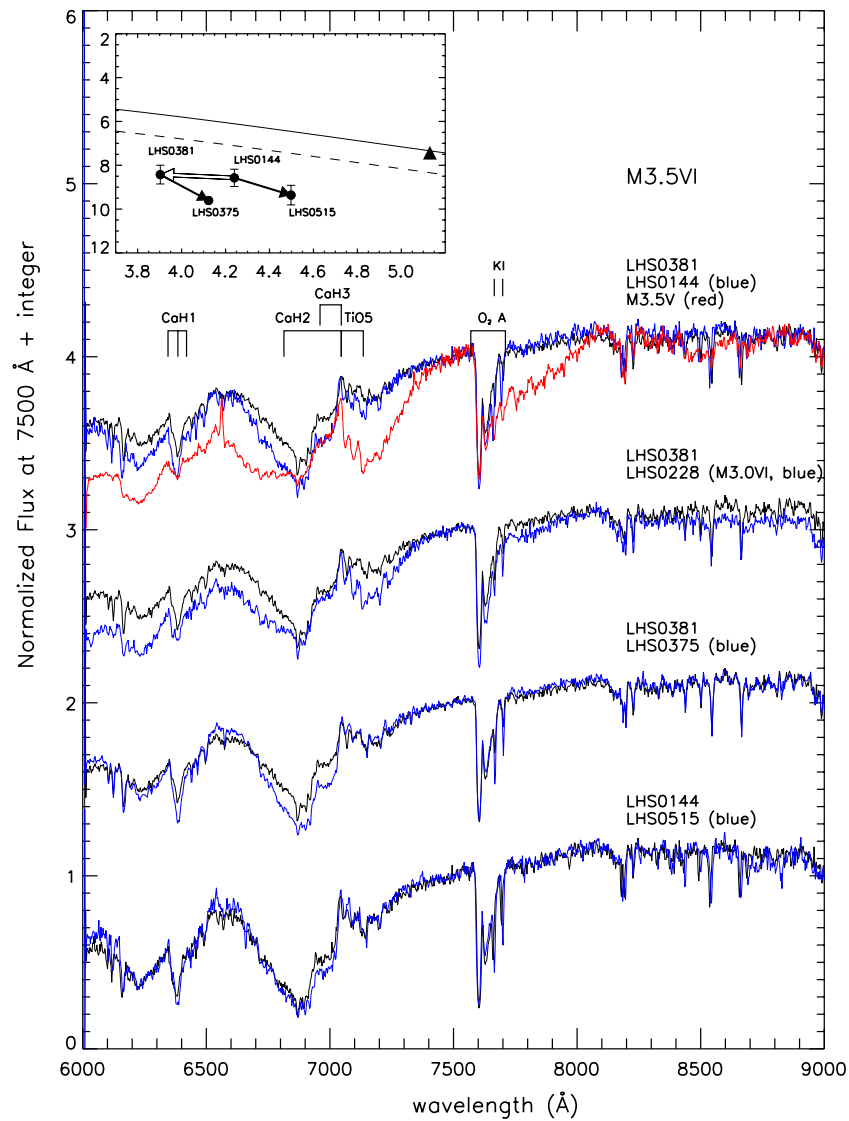


Figure 23. Spectra for LHS 381 and LHS 144 (both M3.5VI) with our M3.5V standard spectrum (represented by a triangle in the inset plot). These three stars show a dramatic metallicity sequence for M3.5. The spectrum of LHS 228 (M3.0VI) is compared to that of LHS 381 to illustrate the slope difference between M3.0VI and M3.5VI (8200–9000 Å). LHS 375 and LHS 515 have higher gravities than LHS 381 and LHS 144, respectively. Note that K I lines (7665 Å and 7699 Å) have appeared and blended in the O₂ A band. The symbols and lines have the same meanings as in Figure 17.

(A color version of this figure is available in the online journal.)

to SCR 2204–3347. LHS 541’s location on the H-R diagram relative to LHS 326 reflects the effects of gravity.

7.2.9. M3.5VI

This half type is assigned because four stars have spectra shown in Figure 23 with redder slopes than M3.0VI (compare to LHS 228, a M3.0VI subdwarf in the second set of spectra), but not as steep as M4.0VI (see the next section). Conveniently, all four stars of this type have trigonometric parallaxes.

LHS 381 and LHS 144. Both have lower metallicities than observed for our M3.5V standard. Their spectra redward of 8200 Å match M3.5V relatively well and show the same trends predicted by the *GAIA* models (Figure 9) for stars with temperatures of about 3200 K. Their CaH1 indices also match the trend discussed in Section 4.1.

LHS 375 and LHS 515. Both have higher gravities than LHS 381 and LHS 144, respectively. Both objects are redder and less luminous than their low-gravity counterparts on the H-R dia-

gram. Gizis (1997) reported LHS 375 to be an esdM4.0 subdwarf and Reid & Gizis (2005) reported LHS 515 to be an esdM5.0 subdwarf. We classify both as M3.5VI with high gravities.

7.2.10. M4.0VI to M6.0VI

We identify only four subdwarfs with types M4.0VI to M6.0VI, only one of which, LHS 2067A, currently has a trigonometric parallax. Because of the paucity of such objects, we do not yet have a sample sufficiently large to map out the effects of metallicity and gravity.

When stars are cooler than ~ 3200 K, their spectra redward of 7500 Å change radically between $[m/H] = 0.0$ and -1.0 (see Figure 9), but are rather more stable between $[m/H] = -1.0$ and -2.0 . For example, Figure 24 shows comparisons between LEHPM 3861 (M4.0VI) and our M3.0V and M4.0V standards. Clearly, if its spectral type is incorrectly assigned to be M3.0VI, there is excess red flux. Lodieu et al. (2005) reported LEHPM 3861 to be a sdM6.0 subdwarf.

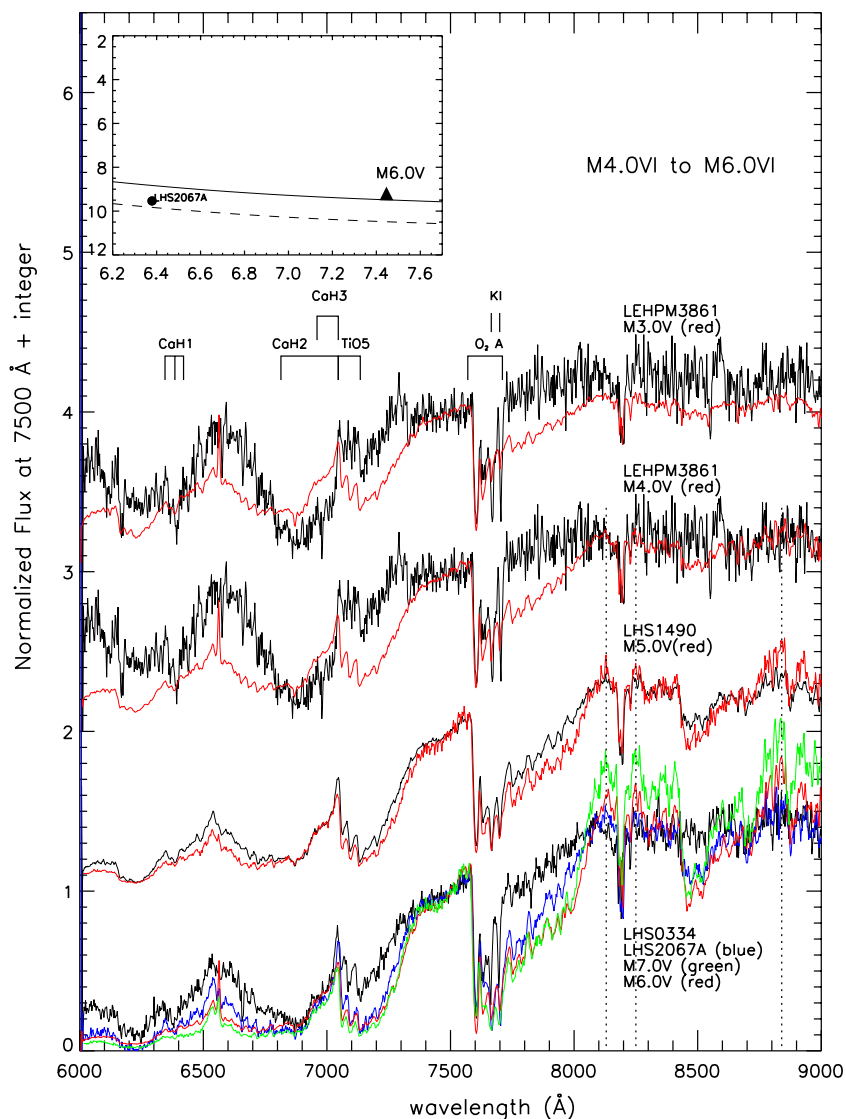


Figure 24. LEHPM 3861 (M4.0VI), LHS 1490 (M5.0VI), LHS 334 (M6.0VI), and LHS 2067A (M6.0VI) subdwarf spectra compared to our standard M3.0-7.0V standards. Only LHS 2067A and the M6.0V standard (filled triangle) are shown in the H-R diagram. The vertical dotted lines represent the three peaks we use to assist us to assign spectral types. The K I lines at 7665 Å and 7699 Å are clearly seen blended in the O₂ A band. The symbols and lines have the same meanings as in Figure 17.

(A color version of this figure is available in the online journal.)

LEHPM 3861 (M4.0VI), *LHS 1490* (M5.0VI), *LHS 334* (M6.0VI), and *LHS 2067A* (M6.0VI), whose spectra are shown in Figure 24 are assigned subdwarf spectral types later than M3.5VI. The types are based on fluxes redward of 7500 Å, with emphasis on three pseudo-continuum peak points at 8130, 8250, and 8840 Å (marked in Figure 24 with dotted lines). As shown in Figure 9 for stars cooler than 3200 K, the flux decreases at these three points as the metallicity drops from $[m/H] = 0.0$ to -1.0 and this trend becomes even more prominent as T_{eff} decreases. Thus, these three peaks for a low-metallicity subdwarf will not be brighter than a dwarf with a comparable spectral type.

LHS 2067A. This is bluer than M6.0V on the H-R diagram and is slightly below the main-sequence line. LHS 2067A was previously identified to be a subdwarf in Kirkpatrick et al. (1995), but no spectral type was given. Although its CaH1 and CaH2 + CaH3 indices are not in the subdwarf region (see Figure 3 and Table 1), its spectrum is clearly different from M6.0V and M7.0V, with stronger CaH1 absorption. It forms a wide ($\sim 55''$ NE) common proper-motion pair with a white

dwarf, LHS 2067B, so it, like LHS 193AB and LHS 300AB, forms an intriguing pair that can be used for comparing metallicity and white dwarf ages. At the system's distance of 25.5 pc, the large separation of the pair corresponds to 472 AU, indicating that significant pollution of the subdwarf by the white dwarf during its planetary nebula phase seems unlikely.

LHS 334. It was reported to be a sdM4.5 subdwarf in Reid & Gizis (2005). We assign it a type of M6.0VI because of the good match of the three pseudo-continuum peak points to LHS 2067A, which appears to be slightly more metal rich than LHS 334.

8. APPLICATION TO SDSS SUBDWARFS

It is useful to apply our spectral typing methodology to the recent work of West et al. (2004), who have provided a significant sample of 60 new subdwarf spectra, all acquired and reduced in a homogeneous way. The subdwarfs were selected

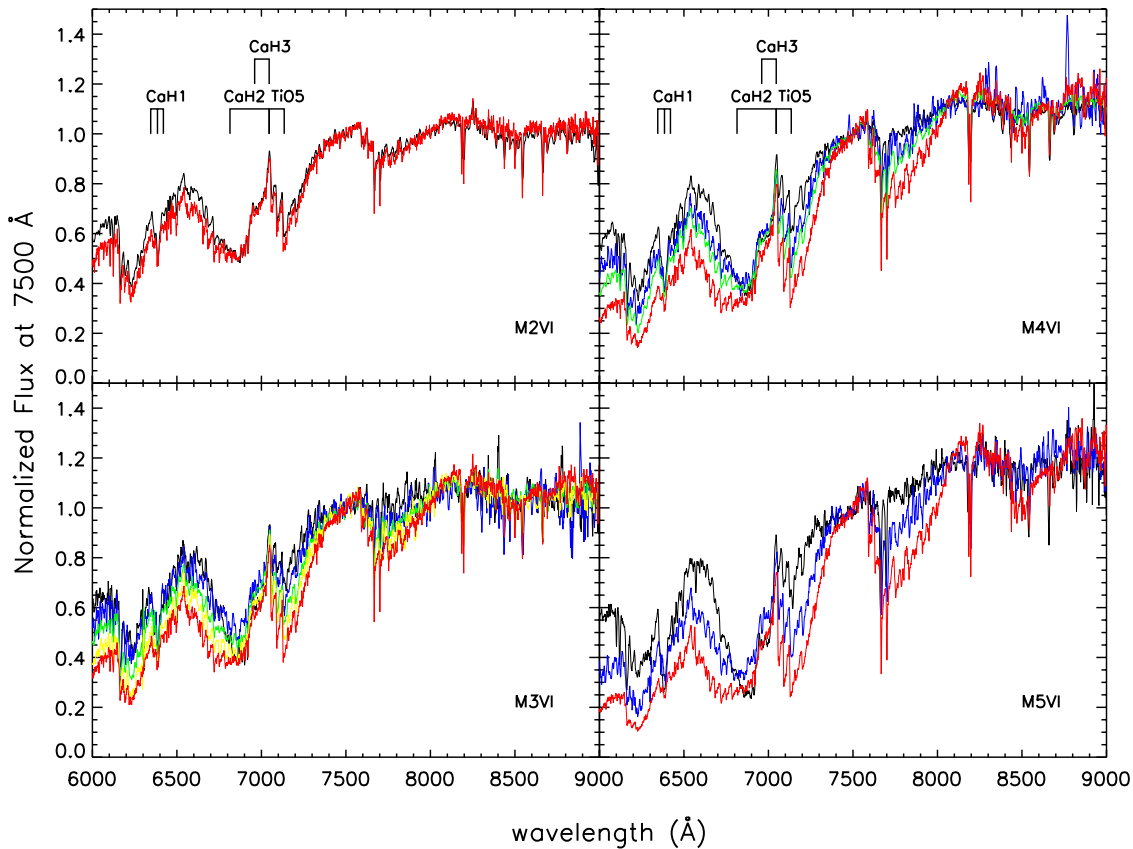


Figure 25. Spectra for subdwarfs from West et al. (2004) separated into types assigned by us by matching standard spectra (red) from Bochanski et al. (2007) in the region 8200–9000 Å. Other colors (black, blue, green, and yellow) represent different metallicities at each type. Metallicity increases from black to red. (A color version of this figure is available in the online journal.)

and spectral types were assigned via their CaH and TiO indices. For comparison, we retrieved 50⁹ of the publicly available spectra and use our new method to assign types. The brightest star among these subdwarfs has $r = 17.0$, resulting in somewhat noisy spectra for the sample, so we smoothed the spectra by averaging the flux over five pixels and normalizing at 7500 Å. Representative spectra are shown in Figures 25 and 26.

The SDSS spectra have telluric lines removed, so we use M dwarf standard spectra from Bochanski et al. (2007) that also omit the telluric lines, rather than our own standards. In addition, Bochanski et al. (2007) do not present half-type standard spectra, so we do not present any half-type spectra for the SDSS subdwarfs. Previous and current types are listed in Table 3. The subdwarfs have types between M1.0 and M3.0 in Bochanski et al. (2007), while our efforts yield types between M2.0 and M5.0.

Our point here is not to assign definitive spectral types, but to illustrate the gravity and metallicity effects in the SDSS dataset, and provide examples of the application of our proposed spectral typing method. Stars of a given spectral type, of course, may have a range of metallicities, as discussed at length in previous sections, and as is evident in Figure 25. Gravity effects are also seen, as shown in Figure 26. Three stars (SDSSJ085843.89+511210.1, SDSSJ093141.85+453914.5, and SDSSJ145447.32+011006.8) previously identified as subdwarfs have spectra identical to

SDSS M dwarfs. Two other stars, SDSSJ083217.77+522408.2 and SDSSJ113501.76+033720.3, appear to have slightly higher gravities (stronger CaH1 line) than dwarfs, but the rest of these two spectra are almost identical to SDSS M dwarfs. Therefore, to these two stars we assign types of M2.0VI: and M3.0VI: with $g+z$, respectively.

Unfortunately, the SDSS dwarfs do not have parallaxes that can be used to confirm their locations on the H-R diagram. In addition, we find many SDSS subdwarfs with identical spectral types that have $g - z$ colors as different as 0.53. It is therefore difficult to verify how metallicities and gravities affect the SDSS absolute magnitudes and colors. Nonetheless, the robust sample of West et al. (2004) provides many additional subdwarfs that can be targeted for further work.

9. DISCUSSION

9.1. Why Subdwarfs' Physical Parameters are Not Listed Explicitly

Stellar spectra follow trends primarily defined by temperature, yet as we have seen, metallicities and gravities also have significant effects on the spectra of cool subdwarfs. Here, we have provided a consistent spectral sequence for subdwarfs that is based on linking observed subdwarf spectra to spectra acquired for main-sequence dwarfs using the same telescope/instrument/observing protocols. Here we compare synthetic to observed spectra to evaluate how well we can assign values for the temperatures, metallicities, and gravities of cool dwarfs and subdwarfs.

⁹ The remaining ten subdwarfs could not be retrieved using the SDSS DR4 Web site, even though we used a 1' search radius and coordinates from their table.

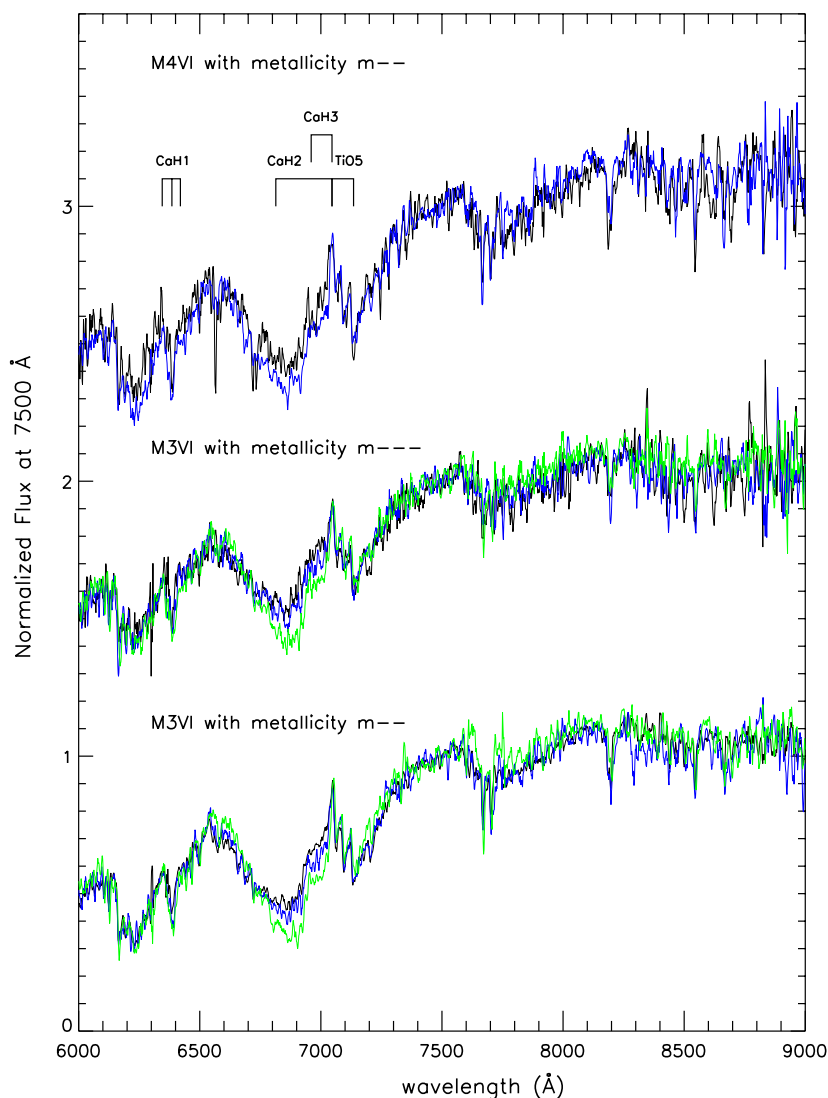


Figure 26. Gravity effects for SDSS subdwarfs of types M3VI and M4VI. The black, blue and green lines represent increasing gravities: g, g+ and g++. (A color version of this figure is available in the online journal.)

9.1.1. Matching Synthetic and Observed Spectra

To test the reliability of the model grids and our fitting procedures, we use our six standard spectral sequence dwarfs with types M0.0V to M5.0V as test spectra (see Figure 27). All are currently believed to be uncorrupted single red dwarfs because they show no evidence of multiplicity from combinations of (1) *HST/NICMOS* observations, (2) optical speckle observations, (3) optical CCD imaging, and/or (4) three or more years of astrometric observations that would reveal perturbations from unseen companions that contributed significant light to the system.

We compared the spectral region from 6000 Å to 9000 Å after normalizing both the *GAIA* grid spectra and ours at 7500 Å, and applying a Gaussian function to the much higher resolution *GAIA* model spectra to match our resolution. If a star had a significant spectral shift because of radial velocity, we manually offset the spectrum to match features obvious in the synthetic spectra. We then calculated the reduced χ^2 differences (hereafter, simply χ^2) between the model grid spectra and ours. Because the synthetic spectra do not have the telluric lines of $O_2\alpha$ (6270–6330 Å), $O_2 B$ (6860–6980 Å), $O_2 A$ (7590–7710 Å), and water (7150–7330 Å and 8952–9000 Å),

these absorption regions were excluded in the χ^2 calculations.

The selected model grids have effective temperatures of 2400–4500 K, $[m/H]$ from -2.0 to $+0.5$, and $\log g$ from 4.0 to 5.5 in steps of 100 K, 0.5 dex, and 0.5 dex, respectively. The upper panel of Figure 10 shows that for a metallicity of -1.0 and temperature 3500 K, varying the gravity causes changes in only certain wavelength regions (and some specific lines). This means χ^2 is only sensitive to $\log g$ in relatively small spectral regions, but not for the overall spectrum. On the other hand, as shown in the lower panel of Figure 10, for the same temperature star with $\log g$ fixed at 5.0, there are large differences between spectra when the metallicity is varied.

Thus, for a star of a given temperature, the gravity changes the overall spectral shape minimally while the metallicity changes it a great deal, so we first secure a star’s metallicity and then its gravity. Figure 28 is an example for M1.0V standard star, showing χ^2 curves at various metallicities and gravities. Each curve represents a specific $\log g$ and grid spectra have temperatures incremented by 100 K. The smallest scatter in the plots is found when $[m/H]$ is -0.5 , which is adopted as the star’s metallicity. We then examine each point in the $[m/H] = -0.5$ panel to find the best fit with the smallest χ^2 at this

Table 3
SDSS Subdwarfs

Object	r	$g - r$	$g - z$	Old type	New type	Metallicity	Gravity
SDSS J085843.89+511210.1	20.00	1.53	3.10	M2.0VI	M2.0V	m	...
SDSS J093141.85+453914.5	19.45	1.58	3.08	M2.0VI	M2.0V	m	...
SDSS J145447.32+011006.8	20.35	1.44	3.45	M3.0VI	M3.0V	m	...
SDSS J003755.20-002134.2	18.70			M1.0VI	M2.0VI	m-	σ
SDSS J083217.77+522408.2	19.61	1.49	3.14	M2.0VI	M2.0VI:	m	$g+$:
SDSS J033408.64-072349.2	20.21	1.89	3.35	M2.0VI	M3.0VI	m- - - -	$g+$:
SDSS J090434.02+513153.9	19.40	1.78	3.29	M1.0VI	M3.0VI	m- - - -	$g+$:
SDSS J161348.84+482016.0	18.30	1.72	3.19	M1.0VI	M3.0VI	m- - - -	$g+$:
SDSS J112751.35-001246.8	20.03			M1.0VI	M3.0VI	m- - -	σ
SDSS J092708.10+561648.1	19.37	1.62	3.02	M1.0VI	M3.0VI	m- - -	$g+$
SDSS J100109.54+015450.2	19.12	1.71	3.25	M2.0VI	M3.0VI	m- - -	$g++$
SDSS J101031.13+651327.6	19.39	1.68	3.30	M1.0VI	M3.0VI	m- - -	$g++$
SDSS J002228.00-091444.8	18.92	-0.89	3.03	M1.0VI	M3.0VI	m- -	σ
SDSS J024501.77+003315.8	19.38	1.54	3.15	M1.0VI	M3.0VI	m- -	σ
SDSS J081329.95+443945.6	19.39	1.68	3.35	M2.0VI	M3.0VI	m- -	σ
SDSS J090238.75+471813.6	19.97	1.73	3.21	M2.0VI	M3.0VI	m- -	σ
SDSS J092534.16+524442.4	19.79	1.71	3.31	M3.0VI	M3.0VI	m- -	σ
SDSS J092745.78+582122.7	20.47	1.78	3.56	M3.0VI	M3.0VI	m- -	σ
SDSS J095147.77+003612.0	18.27	1.58	3.15	M2.0VI	M3.0VI	m- -	σ
SDSS J115900.70+665214.3	19.37	1.61	3.35	M3.0VI	M3.0VI	m- -	σ
SDSS J125919.29-025402.3				M2.0VI	M3.0VI	m- -	σ
SDSS J173452.52+603603.1	18.78	1.71	3.36	M2.0VI	M3.0VI	m- -	σ
SDSS J215937.69+005536.2	18.96	1.61	3.22	M2.0VI	M3.0VI	m- -	σ
SDSS J221500.88+005217.2	19.08	1.60	3.33	M2.0VI	M3.0VI	m- -	σ
SDSS J145547.00+602837.3	19.18	1.70	3.39	M2.0VI	M3.0VI	m- -	$g+$
SDSS J104320.47+010439.4	19.16	1.66	3.37	M2.0VI	M3.0VI	m- -	$g++$
SDSS J084105.39+032109.6	20.05	1.45	3.18	M3.0VI	M3.0VI	m-	σ
SDSS J091451.98+453152.8	19.02	1.64	3.49	M3.0VI	M3.0VI	m-	σ
SDSS J093024.66+554447.7	19.14	1.56	2.96	M3.0VI	M3.0VI	m-	σ
SDSS J094306.37+465701.4	19.74	1.59	3.29	M3.0VI	M3.0VI	m-	σ
SDSS J224854.83-091723.2	19.85	1.57	3.39	M3.0VI	M3.0VI	m-	σ
SDSS J235830.60-011413.2	19.99	1.54	3.33	M2.0VI	M3.0VI	m-	σ
SDSS J113501.76+033720.3				M3.0VI	M3.0VI:	m	$g+$:
SDSS J105122.43+603844.8	17.15	1.65	3.21	M2.0VI	M4.0VI	m- - -	σ
SDSS J092429.76+523410.7	18.70	1.67	3.21	M2.0VI	M4.0VI	m- - -	σ
SDSS J031314.28-000619.8	20.33	1.48	3.39	M2.0VI	M4.0VI	m- -	σ
SDSS J082230.00+471645.8	19.39	1.67	3.38	M2.0VI	M4.0VI	m- -	σ
SDSS J143930.77+033317.3	19.38	1.80	3.58	M3.0VI	M4.0VI	m- -	$g+$
SDSS J003541.84+003210.1	20.15	1.64	3.37	M3.0VI	M4.0VI	m-	σ
SDSS J003701.37-003248.3	20.15	1.60	3.50	M3.0VI	M4.0VI	m-	σ
SDSS J010811.89+003042.4	17.34	1.61	3.43	M3.0VI	M4.0VI	m-	σ
SDSS J083002.73+483251.6	19.92	1.90	3.69	M3.0VI	M4.0VI	m-	σ
SDSS J171745.22+625337.0	18.66	1.65	3.57	M3.0VI	M4.0VI	m-	σ
SDSS J221625.03-003122.5	19.28	1.58	3.37	M3.0VI	M4.0VI	m-	σ
SDSS J223802.82-082532.4	19.71	1.78	3.59	M3.0VI	M4.0VI	m-	σ
SDSS J224605.41+141640.6	17.00	1.57	3.48	M3.0VI	M4.0VI	m-	σ
SDSS J230303.49-010656.7	18.95	1.62	3.42	M3.0VI	M4.0VI	m-	σ
SDSS J235116.25-003104.8	19.48	1.49	3.31	M3.0VI	M4.0VI	m-	σ
SDSS J150511.33+620926.3	18.61	1.81	3.45	M3.0VI	M5.0VI	m- -	σ
SDSS J230805.24+001812.7	19.36	1.70	3.72	M3.0VI	M5.0VI	m-	σ

Note. Column definitions are the same as in Table 2. Double lines separate each type.

fixed metallicity. In this case, the best fit has $T_{\text{eff}} = 3600$ K, $\log g = 4.5$, and $[m/H] = -0.5$.

9.1.2. Discrepancies Between the Best-Fitting Synthetic and Observed Spectra

In this paper, we do not explicitly list temperatures, metallicities, or $\log g$ values for subdwarfs. A few examples support our reasoning for not listing these physical parameters.

Figure 27 shows observed spectra and the best-fit synthetic spectra for six main-sequence spectral standard stars with types M0.0V to M5.0V (in steps of 1.0 subtypes). In general, the overall slopes of the model spectra fit fairly well, especially for the earlier types. However, we discuss here six regions labeled at the top of Figure 27 that do not match, which are particularly relevant for the subdwarfs that are the focus of this paper.

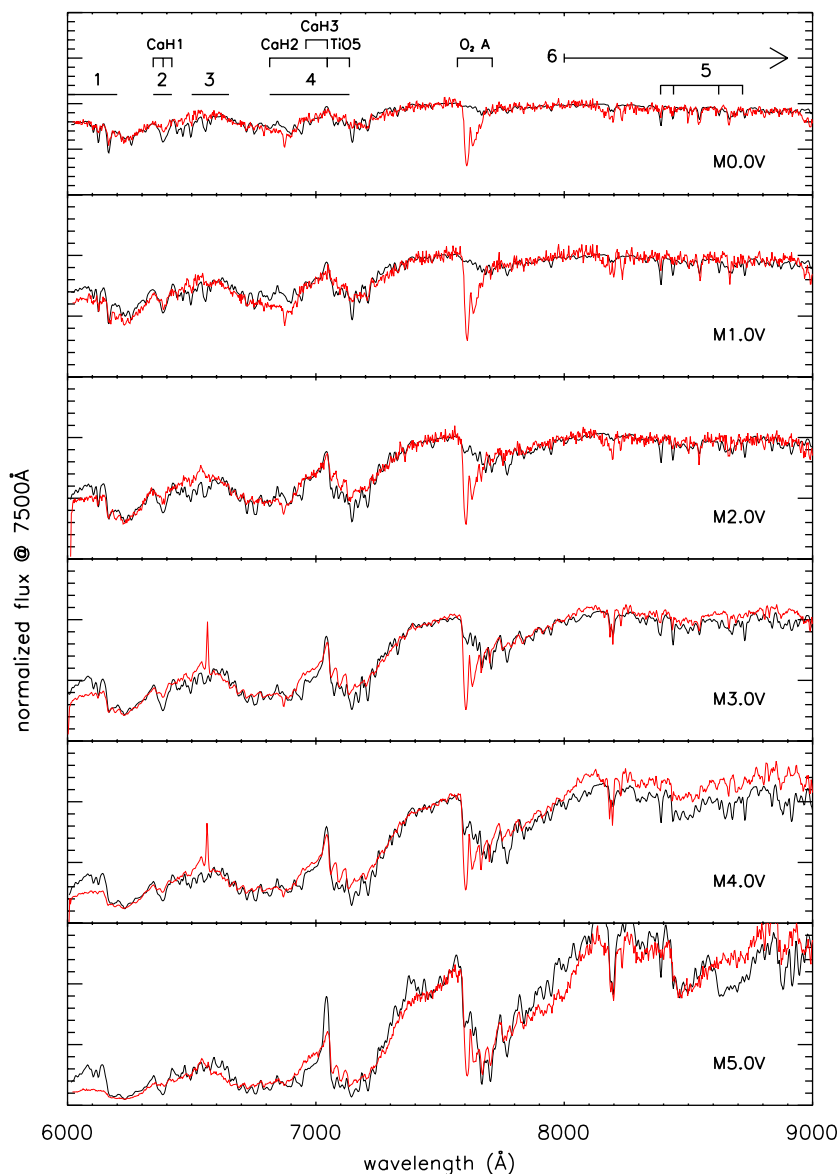


Figure 27. Observed spectra of dwarf standard stars (red lines) compared with the best-fitting synthetic spectra (black lines). Telluric lines are not present in the synthetic spectra. The regions labeled from 1 to 6 are discussed in the text.

(A color version of this figure is available in the online journal.)

1. *Region 1.* The observed spectrum is always less luminous than the model, except for M0.0V.
2. *Region 2.* This is the CaH1 absorption region. Observed spectra have shallower CaH1 features than the models. The depth of CaH1 is determined by a combination of gravity and metallicity. Decreasing CaH1 absorption can be caused by either decreasing gravity or decreasing metallicity. However, fine tuning the gravity or metallicity affects not only the CaH1 feature, but the TiO5 feature in region 4.
3. *Region 3.* The pseudo-continuum always peaks near 6530 Å in the observed spectra. However, the synthetic spectra have this peak “red-shifted” to ~6650 Å.
4. *Region 4.* Containing the CaH2, CaH3 and TiO5 features, this is the most important region for examining the interplay of metallicity and gravity in cool dwarfs. Unfortunately, the CaH2 feature is blended with O₂ B so it is not entirely reliable for analysis of spectra taken through the Earth’s

atmosphere. The CaH3 and TiO5 features are usually weaker in observed spectra than in the models. The strength of TiO5 is primarily driven by metallicity, not gravity (see the bottom panel of Figure 10). Therefore, this region reveals valuable information about a star’s metallicity, in particular at types later than M2.0.

5. *Region 5.* Several Fe I absorption lines (8388 Å, 8440 Å, and 8718 Å) and a Mg I line (8718 Å) in the model spectra redward of 8300 Å are deeper than observed. This indicates poor metallicity matches and/or poor modeling of those particular lines.
6. *Region 6.* Overall, redward of 8000 Å the M4.0V and M5.0V matches are not as good as other regions. This likely indicates fundamental problems with the strengths of some opacity sources (e.g., H₂O and TiO) in the models.

The top panel of Figure 29 shows the two best fitting synthetic spectra for our M1.0V standard. The red spectrum (3600 K,

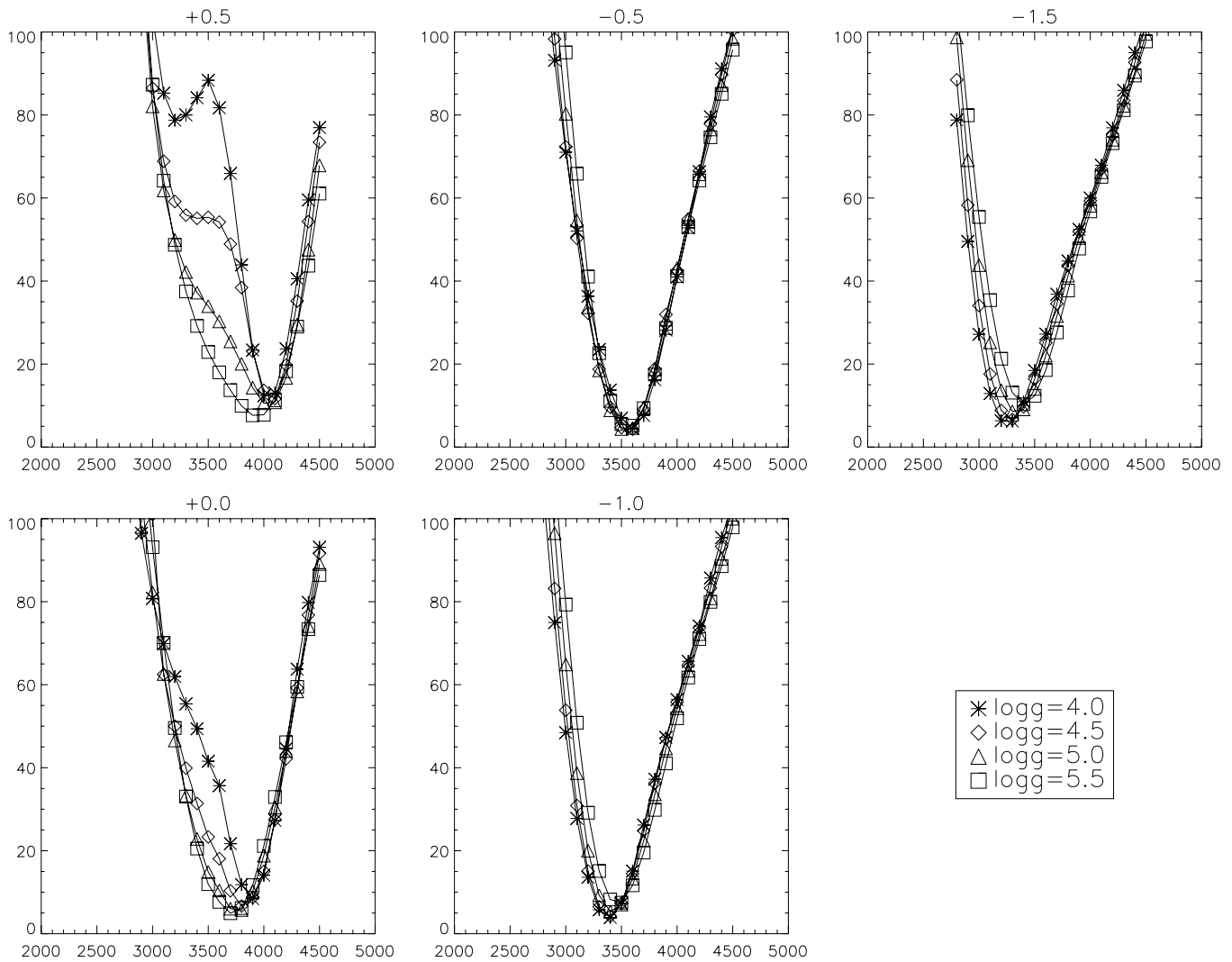


Figure 28. Synthetic models were compared to the observed spectrum of our M1.0V standard. The resulting χ^2 values are plotted against temperature for models with five different metallicities, at four different gravities each. The $[m/H] = -0.5$ plot has the tightest curves at different $\log g$.

$[m/H] = -0.5$, $\log g = 4.5$) provides the best fit and the blue spectrum (3400 K, $[m/H] = -1.0$, $\log g = 4.0$) is second best. There are only slight differences between the two synthetic spectra—the CaH1 strengths and continuum fluxes redward of 8000 Å are the only notable differences. However, the effective temperatures for the two models differ by 200 K, while the metallicities and $\log g$ each differ by 0.5 dex. The lower panel of Figure 29 shows the two best fit spectra for our M3.0V standard. The best fit (red line) yields 3200 K, $[m/H] = -0.5$, $\log g = 4.5$ and the second best fit (blue line) yields 3300 K, $[m/H] = 0.5$, $\log g = 5.5$. However, neither model fit is an ideal match to the observed spectrum (which is why the $[m/H]$ value for the two best matches differs by an order of magnitude), and matches become even poorer for cooler stars.

As a whole, many of the best fits for the main-sequence dwarfs in Figure 27 are for metallicities of -0.5 , which is somewhat lower than studies that have specifically attempted to assign metallicities to cool dwarfs in the solar neighborhood. For example, the mean $[Fe/H]$ from 21 M dwarf secondaries in Bonfils et al. (2005) is -0.09 , and the mean $[Fe/H]$ from five M dwarf secondaries in Bean et al. (2006) is -0.17 . Also worthy of note is that the fits were made for metallicities incremented by 0.5 dex, and stars with metallicities between

-0.5 and 0.0 may have slightly better fits for -0.5 . One might think that interpolation from existing model grids would allow better fits. There are, however, degeneracy problems in matching model spectra to observations—when fitting the three-dimensional space of temperature, metallicity, and gravity, two or more synthetic spectra yield low points with similar χ^2 , as is the case for the M1.0V example discussed above. More worrisome is that the overall discrepancies discussed above (items 1–6) cannot be removed through interpolation in the existing model grids.

Figure 30 illustrates how the χ^2 values change for best fit matches of the *GAIA* models to our spectral standards with types M0.0V through M5.5V. Spectral type M3.0V is the latest type for which a reasonably tight plot like that shown in Figure 28 can be identified. The dotted line in Figure 30 provides a dividing point between reasonable matches and poor matches, indicating that once χ^2 exceeds 10, the χ^2 plots are too scattered to choose a unique set of model spectra parameters to match observed spectra.

A specific example of applying the models to one of our subdwarfs illustrates the large discrepancies that must be overcome to derive reliable parameter values for metallicity and gravity. When we applied our fitting algorithm to our observed spectrum

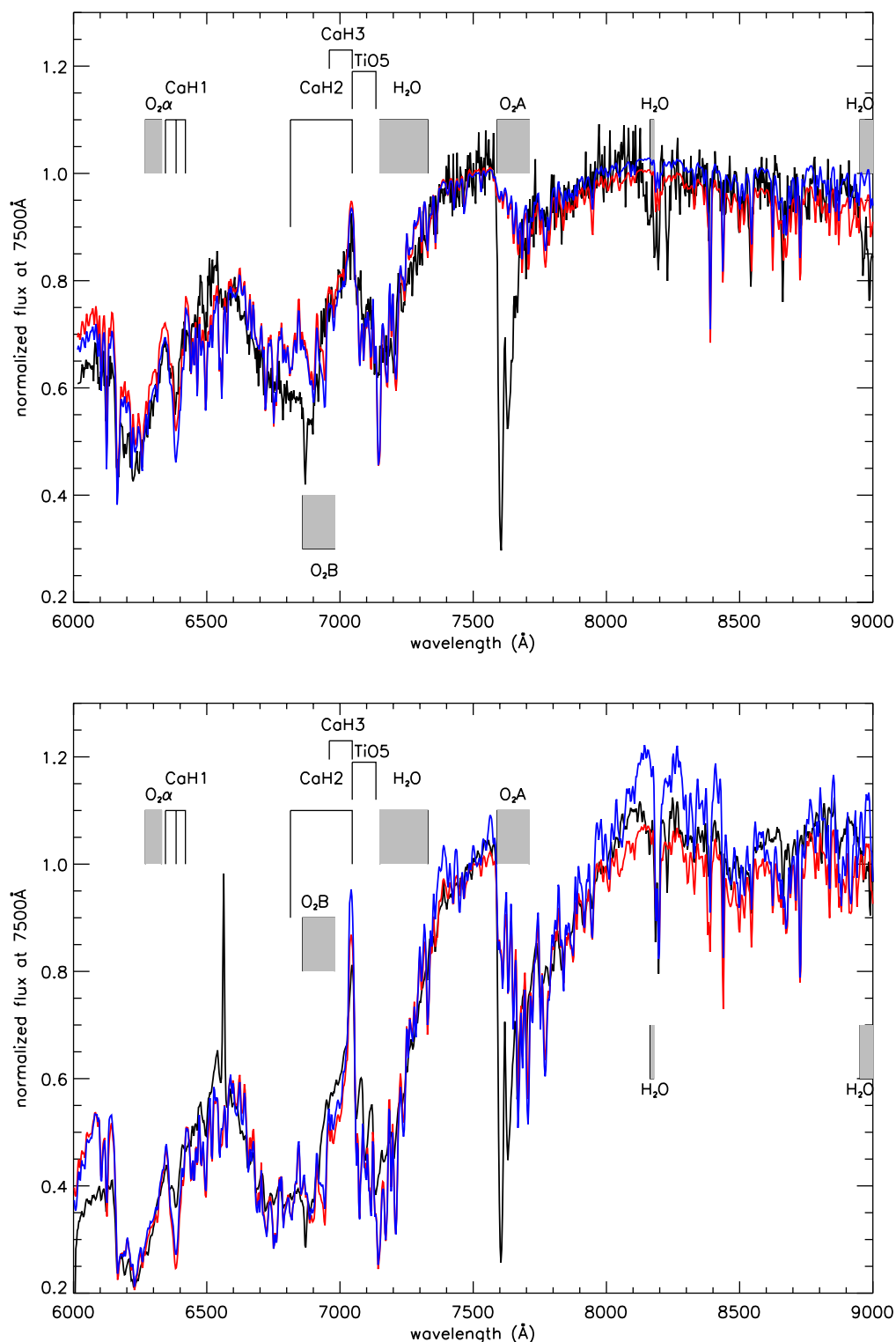


Figure 29. Comparisons of observed spectra for M1.0V (top) and M3.0V (bottom) are shown against the two best-fitting synthetic spectra for each. The red line is the best fit, where $T_{\text{eff}}/[\text{m}/\text{H}]/\log g = 3600/-0.5/4.5$ for M1.0, and $3200/-0.5/4.5$ for M3.0. The blue line is the second best fit, where the values are $3400/-1.0/4.0$ for M1.0 and $3300/0.5/5.5$ for M3.0. Telluric bands are marked as the gray boxes.

(A color version of this figure is available in the online journal.)

for LHS 335 (M1.0VI, as shown in Figure 31), we discovered that the “best fit” was quite poor. Although the formal χ^2 value was 5.9 (less than our cutoff of 10, indicating a reliable fit), the model’s CaH3 band is not deep enough, the TiO5 band is too deep, and the continuum flux redward of 7700 Å is less than observed.

For myriad reasons we conclude that we cannot strictly determine reliable metallicities and log g values for cool dwarfs using the fitting method discussed here. Thus, until improved model grids are available, we defer assignment of numerical values for temperatures, metallicities, and log g values. However, we certainly *can* use the *GAIA* model grids to mimic *trends*

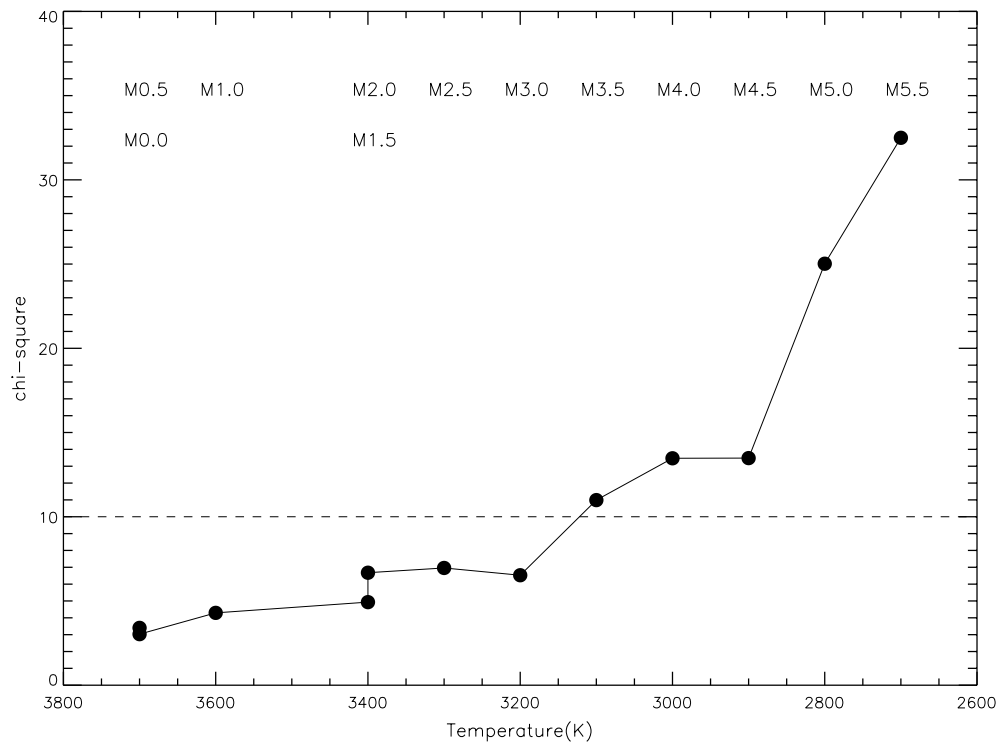


Figure 30. The best χ^2 values are shown for synthetic spectra fits to observed spectra for stars of types M0.0V to M5.5V (labeled relative to each type). The dashed line indicates the selected limit for reliability of fitting model spectra to observed spectra—above this line fits are deemed unreliable.

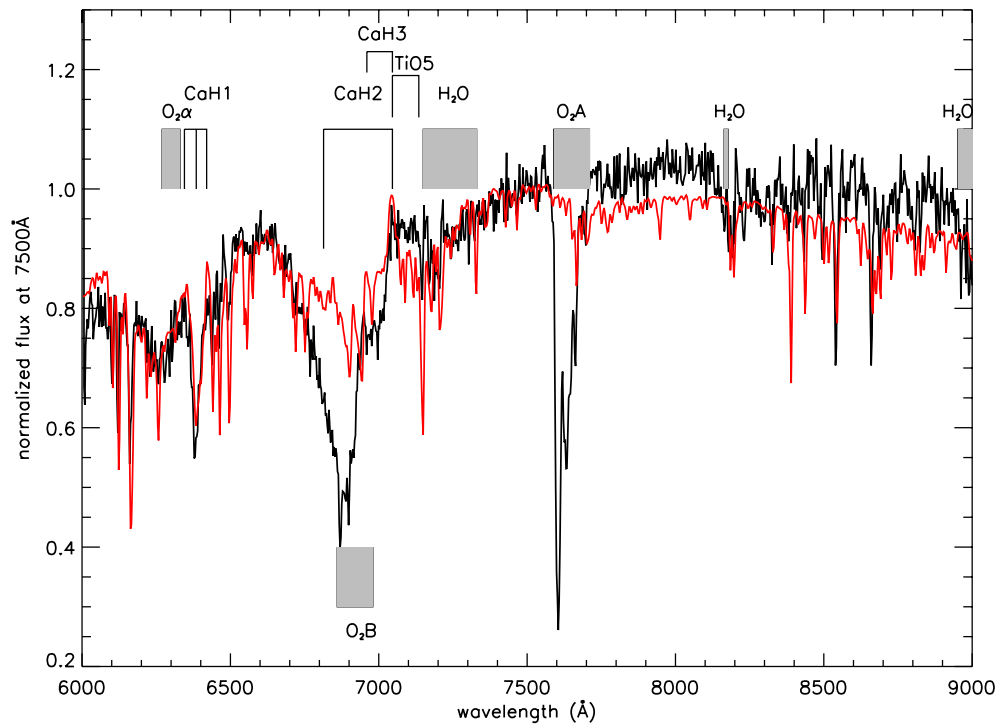


Figure 31. The spectrum of the subdwarf LHS 335 (black) with the corresponding best fitting synthetic spectrum (red).
(A color version of this figure is available in the online journal.)

(as discussed in Sections 5 and 6) in the spectra of subdwarfs to compare the stars within a framework of changing physical parameters.

9.2. The Confusion Between *sd*, *esd* and *usd* Prefixes

Gizis (1997) proposed that subdwarfs have two subclasses, “subdwarfs” (*sd*) and “extreme subdwarfs” (*esd*), based on their

CaH and TiO5 band strengths. He separated the two classes using the line shown in the top panel of Figure 3. Another term, “ultra subdwarf,” was proposed by Caldwell et al. (1984) to describe GJ 59B ($V - K_s = 3.42$, $M_{K_s} = 7.89$), which is ~ 2.5 mag underluminous compared to main-sequence stars of similar color. This star falls in the region including “extreme subdwarfs” in Gizis (1997). More recently, Lépine et al. (2007)

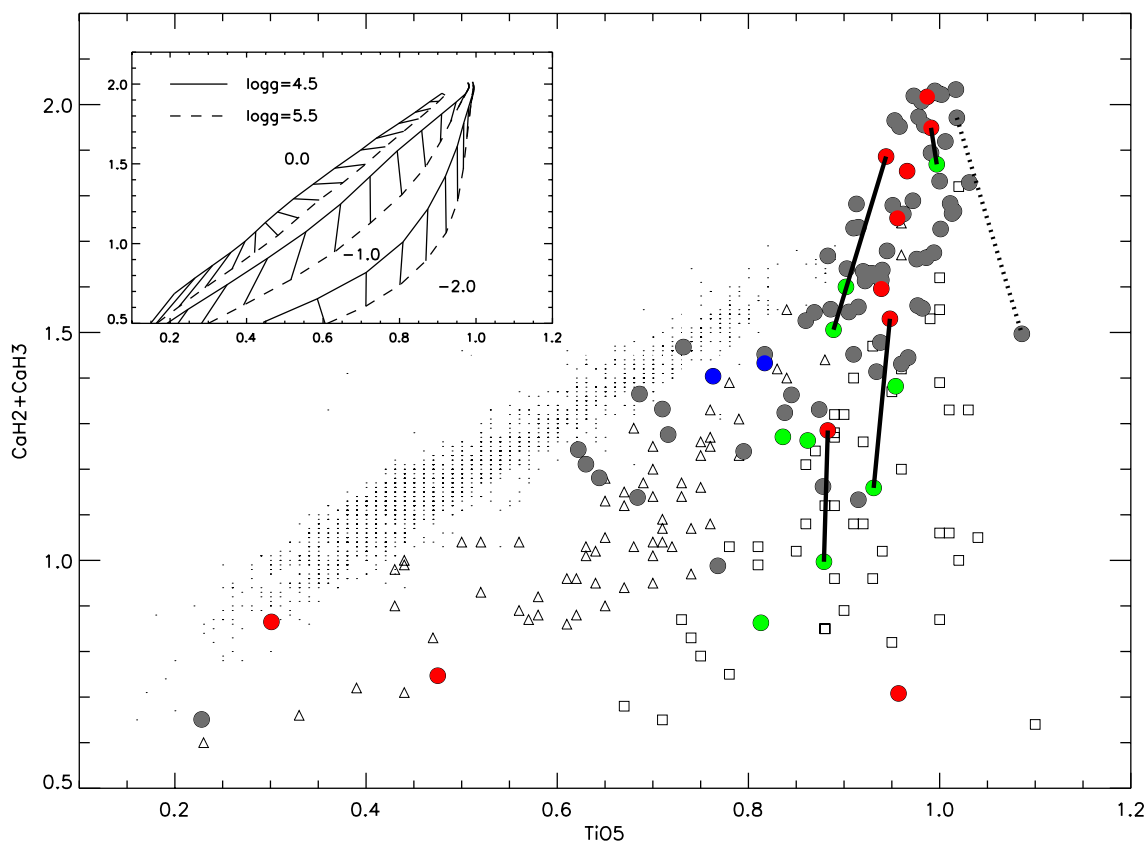


Figure 32. The CaH2+CaH3 vs. TiO5 indices plotted for subdwarfs discussed in this paper (filled circles). For comparison, known cool dwarfs (dots), subdwarfs (open triangles), and “extreme” subdwarfs (open boxes) from Hawley et al. (1996), Gizis (1997), and Reid & Gizis (2005) are also shown. The green circles are subdwarfs with the highest gravities at a given type (g with most +) in Table 2. The two blue circles represent LHS 400 and SCR 1822–4542, which have higher gravities than M dwarfs. The red circles represent the lowest metallicity stars in Table 2 at a given type (m with most –). The solid lines indicate pairs of stars having the same number of – in metallicity, but different gravities. A dotted line connects LHS 2734A and LHS 2734B, which is the only wide CPM binary in our sample. For comparison, the inset plot illustrates the indices (TiO5 vs. CaH2 + CaH3) calculated from *GAIA* models for temperatures 2800–4400 K. Axis labels are omitted, but both axes have the same ranges as the main figure. Three different metallicities, 0.0, –1.0, and –2.0, and two gravities, $\log g = 4.5$ (solid line) and 5.5 (dash line), are shown. Connections are drawn for stars with the same temperatures but different gravities.

(A color version of this figure is available in the online journal.)

adopted the “ultra subdwarf” (*usd*) term for subdwarfs found to have stronger CaH features than “extreme subdwarfs.” We believe these terms confuse the situation and do not address the underlying astrophysics. We recommend that they be not used for the following reasons.

1. These terms can only be applied to M-type subdwarfs, not K-type subdwarfs. Both observed spectra and models show that K subdwarfs do not follow the trends in CaH absorption with metallicity that M subdwarfs follow. Thus, there is no clear delineation for K-type subdwarfs.
2. Empirically, the values of the indices are affected by a complicated interplay of temperature, metallicity, and gravity effects. One cannot separate these three factors simply based on the indices. Typically, when the term “extreme” subdwarf is used, it refers to “very low metallicity” alone. But that is only one part of the portrait that needs to be painted for a given subdwarf. For example, the filled boxes shown in Figure 4 indicate stars previously identified as extreme subdwarfs from their indices. Note that the spread for “extreme” subdwarfs at a given color ($V - K_s \sim 3.5$) is 3.5 mag, or a factor of ~ 25 in luminosity. There is no clear separation in the fundamental H-R diagram between stars termed “subdwarfs” and “extreme subdwarfs” classified using spectral indices.

In Figure 32, we take a detailed look at astrophysical causes that shift points in the CaH2 + CaH3/TiO5 indices plot. The

red circles in Figure 32 represent the lowest metallicity stars of each spectral type we have presented here. Some of these very low-metallicity stars are not located in the “extreme” subdwarf region. The green circles represent subdwarfs in our sample that have highest gravity at a given type. The solid lines connect stars having the same metallicity rankings in Table 2 (components of the common proper-motion binary LHS 2734 AB are connected by a dotted line because they presumably have the same metallicity). It is clear from these three pairs that high gravity can push a subdwarf toward or into the extreme subdwarf region, even if the metallicities of the two objects are similar. In addition, many other high-gravity subdwarfs (green circles) that do not have particularly low metallicities are also in the subdwarf region. Finally, the two blue circles represent LHS 440 and SCR 1822-45542, which subdwarfs having the same metallicities but higher gravities than dwarfs. Their spectroscopic features indicate that they are subdwarfs, but they do not have low metallicity at all. Yet, they fall in the subdwarf region of the indices plot, which has traditionally indicated low metallicity.

The inset in Figure 32 helps explain this phenomenon. We have calculated the spectral indices from the *GAIA* synthetic spectra with $[m/H] = 0.0, -1.0, \text{ and } -2.0$ and temperatures of 2800–4400 K. Two different gravities were

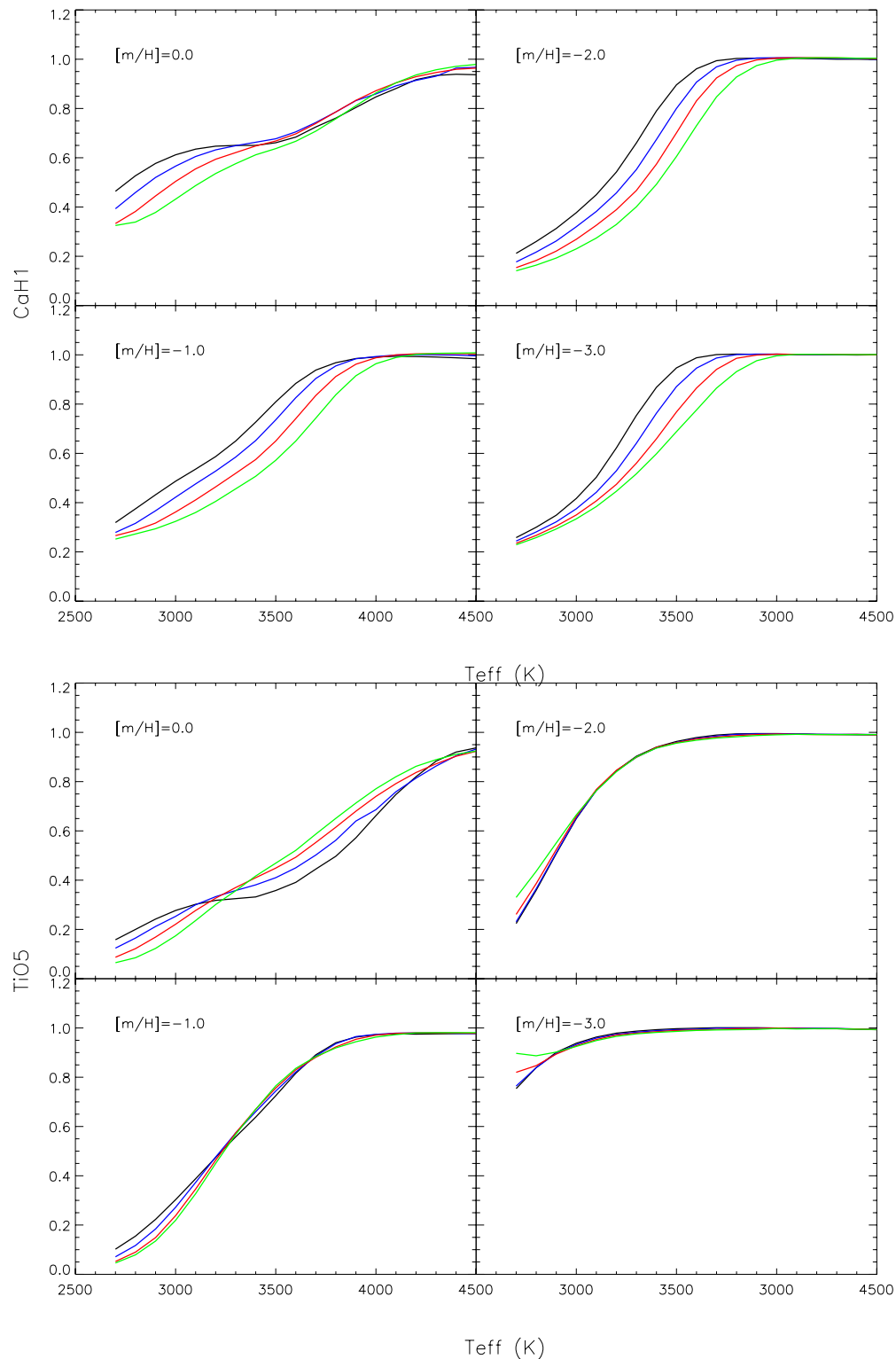


Figure 33. CaH1 and TiO5 indices from *GAIA* model grids plotted against effective temperature. The black, blue, red, and green lines indicate $\log g = 4.0, 4.5, 5.0,$ and $5.5,$ respectively. Note that a given CaH1 and TiO5 value may correspond to many combinations of metallicities and gravities.

(A color version of this figure is available in the online journal.)

selected for each metallicity. The models indicate that both low metallicity and high gravity push stars toward the extreme subdwarf region. Thus, if two stars have the same metallicity, the one with higher gravity will be pushed more toward the extreme subdwarf region, indicating that this spectral indices plot is not a clear indicator of metallicity alone.

3. Theoretically, in order to show how complicated the TiO5 versus CaH1 plot is astrophysically, we use *GAIA* model grids to do a demonstration. We have chosen models with $2700 \text{ K} < T_{\text{eff}} < 4500 \text{ K}$, $-3.0 < [m/H] < 0.0$, and $4.0 < \log g < 5.5$, and have calculated the output CaH and TiO5 indices, as shown in Figure 33. As is apparent in the plots, for a given (TiO5, CaH1) indices pair, there

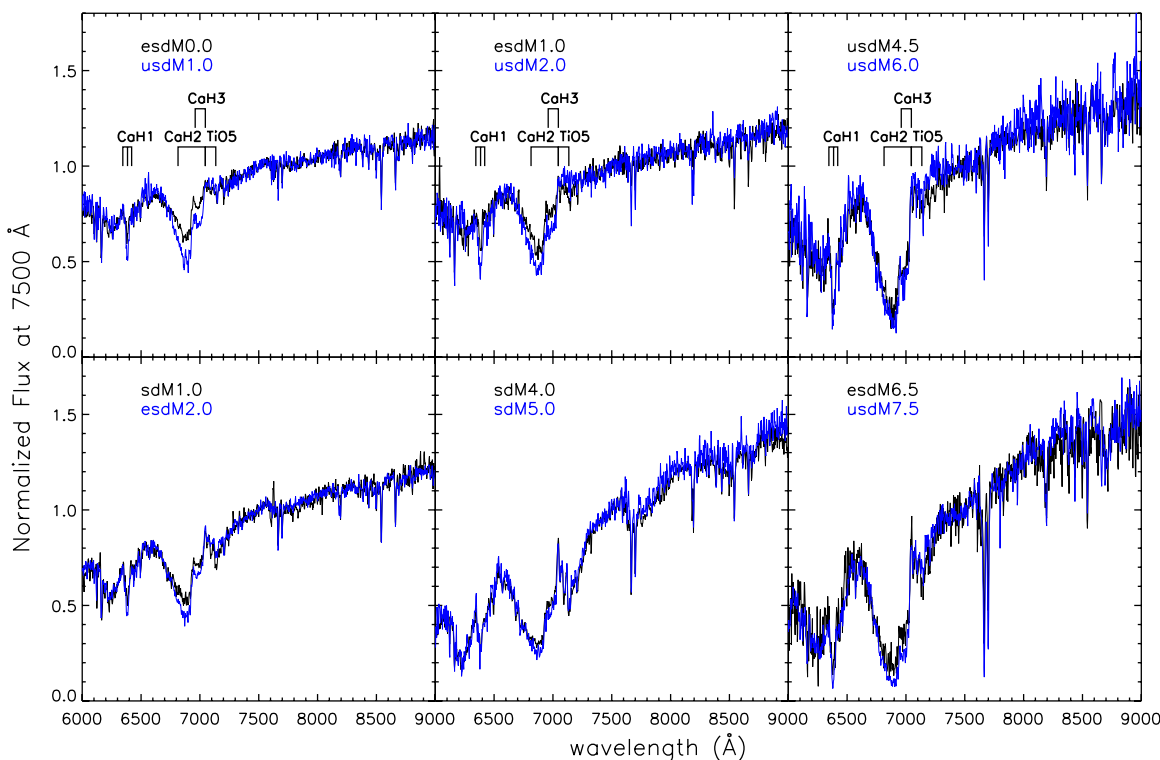


Figure 34. Spectra from Lépine et al. (2007) with their published types. The colors (black and blue) represent different spectra, and their colors match with labels. Each pair has almost the same overall spectral shape, but each star is assigned a different subtype and identification as extreme or ultra. Spectra are normalized at 7500 Å.

(A color version of this figure is available in the online journal.)

are many possible parameter combinations. Both indices are a function of temperature, gravity, and metallicity, which would require a 6D plot to describe TiO5 versus CaH. Unfortunately, one cannot classify stars as subdwarfs, extreme subdwarfs, or ultra subdwarfs using 2D index plots that infer trends in metallicity alone.

For these reasons, the indices only indicate a star’s location on these particular spectroscopic indices plots. They do not address low or very low metallicity only, as implied by past usage, but instead incorporate effects of both metallicity and gravity for stars of a given temperature. They do not provide obvious or direct links to positions on H-R diagrams, which provide the astrophysical meaning underlying stellar classification. Finally, the modifiers “extreme” and “ultra” themselves have effectively the same meaning and do not provide meaningful information about their differences.

9.3. Why Previous Methods Work for Dwarfs but Not Subdwarfs

In the Palomar-MSU spectroscopy survey, Reid et al. (1995) used the TiO5 index and polynomial equations to assign subtypes for M dwarfs. Gizis (1997) then applied the same methodology to M subdwarfs. As can be seen in Figure 33, TiO5 versus temperature is effectively linear, especially for $\log g = 5.0$ and $[m/H] = 0.0$, so this typing method works successfully for a fairly homogeneous set of dwarfs (possibly with somewhat different gravities)—temperature is the main factor affecting the overall slope of red dwarf spectra. However, it is not as simple for subdwarfs because both low-metallicity and high-gravity stars are sorted into the same TiO5

values for various combinations. Thus, the same methodology that works for dwarfs cannot straightforwardly be applied to subdwarfs.

9.4. The Subdwarf Spectral Standards from Lépine et al. (2007)

Lépine et al. (2007) recently released a set of spectral standards for the sdM, esdM, and usdM subclasses using wider spectral coverage than used by Gizis (1997) and revised polynomial equations. Their project is contemporaneous with ours, but unfortunately there is only one star in both samples, LHS 228. We assign it a type of M3.0VI while their type is sdM2.0. As shown in Figure 34, gravity effects come into play in their spectra.¹⁰ Each pair of spectra shown have nearly identical continua, with CaH bands being the only significant spectral difference. Using their method, each of the pairs of subdwarfs shown is assigned a different subtype. We believe that by using the overall shape of the spectrum, with knowledge that both metallicity and gravity affect certain regions, each pair should have the same spectral subtypes. Based on the trends from GAIA models, the pairs of spectra shown have different gravities, as we have also seen in our spectra and those from SDSS (as shown in Section 8). Figure 35 illustrates spectral differences at types M3.0, M5.0, and M7.5. Although the spectra in each panel have the same subtypes for sdM, esdM, and usdM subdwarfs, they show very different continua between 6000 Å and 9000 Å. When examining the overall spectra, there is no clear morphology trend for each subtype. We conclude that using spectral indices alone omits important information evident in the overall morphology of the spectra that is useful to spectral classification.

¹⁰ Their telluric lines have been removed.

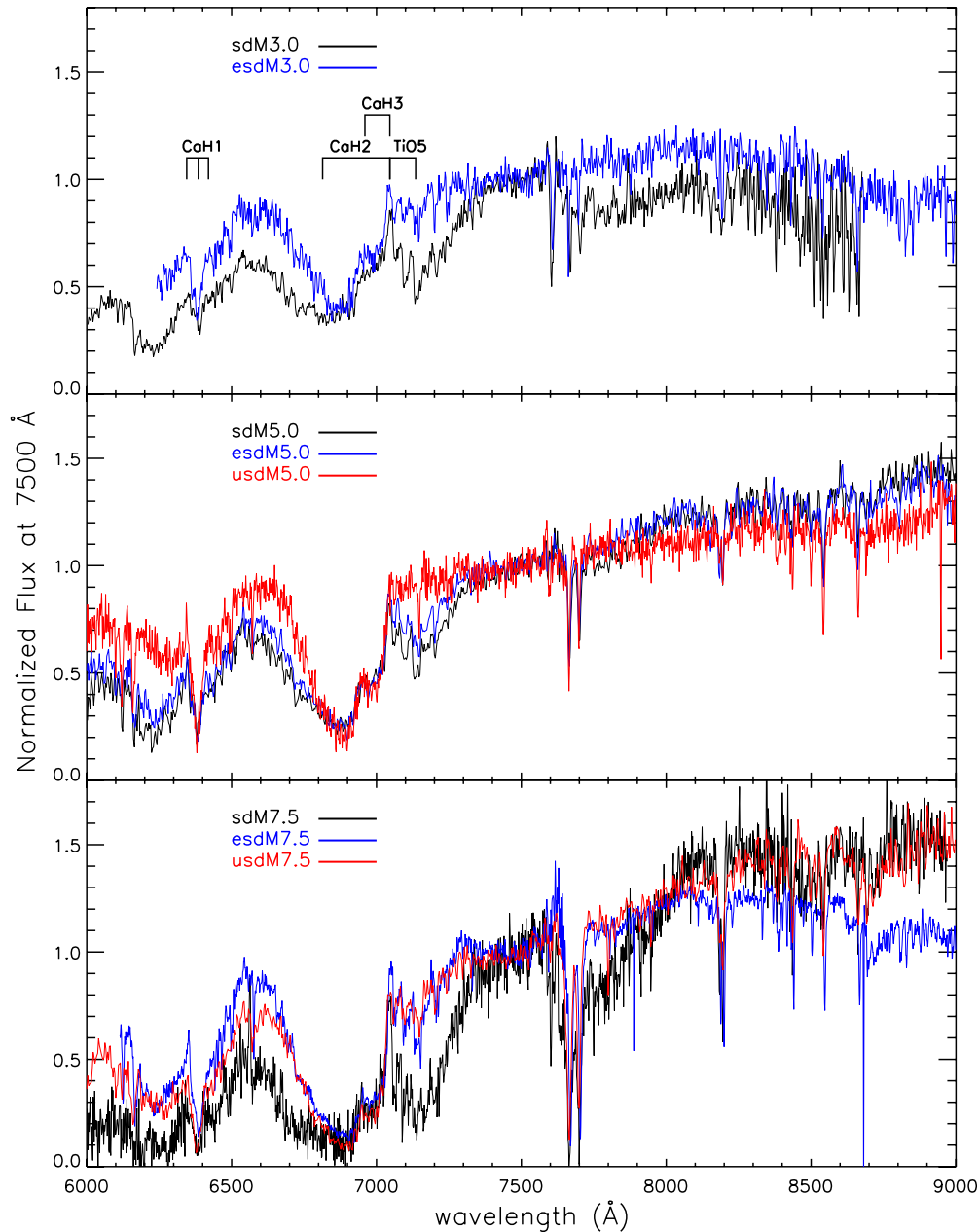


Figure 35. Spectra from Lépine et al. (2007) for spectral types for M3.0, M5.0, and M7.5. The black, blue, and red spectra represent sdM, esdM, and usdM, respectively. Spectra are normalized at 7500 Å.

(A color version of this figure is available in the online journal.)

10. CONCLUSIONS

We have discussed 88 cool subdwarfs using spectra covering 6000–9000 Å. Based on these spectra and the trends from *GAIA* model grids, we have redefined the subdwarf spectral sequence, spanning types K3.0 to M6.0. We find that wide spectral coverage is the key to defining a subdwarf’s spectral type. We consider this to be an important, but not final, step in defining the subdwarf spectral sequence.

Through the understanding of *GAIA* model grids, we find that the key to assigning a subdwarf spectral type is to compare the spectrum to dwarf spectral standards in regions affected minimally by metallicity and gravity, thereby making a direct link between the dwarf and subdwarf sequences. Even so, it remains difficult to establish a definitive sequence for subdwarfs because of the multifaceted nature of their spectra. Until we have

surveyed a large number of subdwarfs and covered a multitude of possible temperatures, metallicities, and gravities, a definitive sequence will remain elusive.

From an analysis of the history of the term “subdwarf,” and the layout of the fundamental H-R diagram, we propose that the suffix “VI” be used, rather than the “sd” prefix, as the preferred spectral classification notation. This reduces the confusion between cool subdwarfs and hot OB subdwarfs. This is also prudent because subdwarfs really do form an independent class of stars on the H-R diagram, for which five Roman numerals are in common use, with cool subdwarfs naturally falling beneath the main-sequence V types.

Overall, we find that trigonometric parallaxes are crucial for identifying mid-K-type subdwarfs, and allow us to understand how the complex interplay of temperatures, metallicities, and gravities affects the positions of cool dwarfs on the H-R

diagram. We found that mid-K-type subdwarfs cannot be identified spectroscopically using our data. There are many G- and M-type subdwarfs, so K-type subdwarfs presumably exist, but additional information is needed to identify them. Consequently, we use metallicities, kinematics, and parallaxes to ascertain their true natures and use their locations on the H-R diagram to flag them as “subdwarfs” (other spectroscopic wavelength and resolution combinations could also be used). Because they are not spectroscopically identified as subdwarfs in our spectra, we use a conservative notation, [VI], for subdwarfs of types K3.0 through K5.0 to indicate their questionable status.

We have confirmed that spectroscopic indices are useful in separating late K- to late M-type subdwarfs from dwarfs, but that the indices have limitations when attempting to understand the astrophysical causes leading to observed subdwarf spectra. When combined with trigonometric parallax and photometric information, our results show that for lower metallicities, subdwarfs are generally bluer and brighter at optical wavelengths, so they slide up and to the left on the H-R diagram (using axes $V - K_s$ versus M_{K_s}). In contrast, higher gravities make stars redder and less luminous at optical wavelengths, so subdwarfs generally slide down and to the right on the same H-R diagram. Because of the complex, and not yet completely mapped out, interplay of temperatures, metallicities, and gravities, we conclude that the “extreme” and “ultra” prefixes *only* outline locations on spectroscopic indices plots, and do not successfully differentiate the underlying astrophysical causes for shifts on CaH/TiO5 plots.

Improvements in the subdwarf spectral sequence can be made by observing wide common proper-motion subdwarf binaries, like LHS 2734AB discussed here. Assuming identical metallicities, such binaries allow us to constrain one of the three variables that affects cool dwarf spectral types. The ultimate subdwarf spectral sequence will be three dimensional, with temperature, metallicity, and gravity as independent variables (see Kirkpatrick 2005, Figure 11).

Previously, gravity effects in cool subdwarfs have been almost entirely ignored, as metallicity was the factor considered to describe changing CaH features. Our results clearly show the importance of gravity effects. An additional factor, contamination from an unseen, evolved, i.e. white dwarf, companion, could also change the slope of subdwarf spectra. Thus, comprehensive surveys of subdwarfs for companions are warranted.¹¹ Finally, this work also shows that current synthetic spectra provide a useful framework in which to evaluate cool dwarf spectra, but they do not yet provide perfect matches, indicating that atmospheric models still require fine-tuning to make additional advances in the future characterization of cool dwarfs (P. Hauschildt 2008, private communication).

We would like to thank the referee, Sandy Leggett, for her very helpful comments that improved this paper. We also thank Pat Boeshaar and Doug Gies for their comments and suggestions. Peter Hauschildt was instrumental in helping us use the *GAIA* model grids, and Vincent Woolf contributed the old version of synthetic spectra. We thank Sebastien Lepine for providing his subdwarf spectra to us before they were publicly available and for his comments on Section 9.4. We appreciate the help of many members of the Georgia State University (GSU) RECONS team

in their data acquisition and reduction efforts, especially Charlie Finch and Jennifer Winters. This work has been supported at GSU by NASA’s Space Interferometry Mission, the National Science Foundation (NSF, grant AST-0507711), and GSU. Finally, we wish to thank the other members of the SMARTS Consortium, without whom the telescopes at CTIO used for this effort might not be available.

This research has made use of the SIMBAD database, operated at CDS, Strasbourg, France. This paper has also made use of data from the SDSS. Funding for the SDSS and SDSS-II has been provided by the Alfred P. Sloan Foundation, the Participating Institutions, NSF, the U.S. Department of Energy, NASA, the Japanese Monbukagakusho, the Max Planck Society, and the Higher Education Funding Council for England. This work has used data products from the Two Micron All Sky Survey, which is a joint project of the University of Massachusetts and the Infrared Processing and Analysis Center at California Institute of Technology funded by NASA and NSF. This research has also made use of NASA’s Astrophysics Data System.

REFERENCES

- Adams, W. S., & Joy, A. H. 1922, *ApJ*, 56, 242
 Adams, W. S., Joy, A. H., Humason, M. L., & Brayton, A. M. 1935, *ApJ*, 81, 187
 Allard, F., & Hauschildt, P. H. 1995, *ApJ*, 445, 433
 Allen, C., Poveda, A., & Herrera, M. A. 2000, *A&A*, 356, 529
 Bean, J. L., Sneden, C., Hauschildt, P. H., Johns-Krull, C. M., & Benedict, G. F. 2006, *ApJ*, 652, 1604
 Bessell, M. S. 1982, *PASA*, 4, 417
 Bessell, M. S. 1990, *A&AS*, 83, 357
 Bessel, M. S., & Wickramasinghe, D. T. 1979, *ApJ*, 227, 232
 Bidelman, W. P. 1985, *ApJS*, 59, 197
 Bochanski, J. J., West, A. A., Hawley, S. L., & Covey, K. R. 2007, *AJ*, 133, 531
 Boeshaar, P. C. 1976, PhD thesis, The Ohio State University
 Bonfils, X., Delfosse, X., Udry, S., Santos, N. C., Forveille, T., & Ségransan, D. 2005, *A&A*, 442, 635
 Brott, I., & Hauschildt, P. H. 2005, *The Three-Dimensional Universe with Gaia*, 576, 565
 Burgasser, A. J., & Kirkpatrick, J. D. 2006, *ApJ*, 645, 1485
 Burgasser, A. J., et al. 2003, *ApJ*, 592, 1186
 Caldwell, J. A. R., Spencer Jones, J. H., & Menzies, J. W. 1984, *MNRAS*, 209, 51
 Carney, B. W., Latham, D. W., Laird, J. B., & Aguilar, L. A. 1994, *AJ*, 107, 2240
 Cayrel de Strobel, G., Soubiran, C., Friel, E. D., Ralite, N., & Francois, P. 1997, *A&AS*, 124, 299
 Cayrel de Strobel, G., Soubiran, C., & Ralite, N. 2001, *A&A*, 373, 159
 Chamberlain, J. W., & Aller, L. H. 1951, *ApJ*, 114, 52
 Costa, E., & Méndez, R. A. 2003, *A&A*, 402, 541
 Costa, E., Méndez, R. A., Jao, W.-C., Henry, T. J., Subasavage, J. P., Brown, M. A., Ianna, P. A., & Bartlett, J. 2005, *AJ*, 130, 337
 Costa, E., Méndez, R. A., Jao, W.-C., Henry, T. J., Subasavage, J. P., & Ianna, P. A. 2006, *AJ*, 132, 1234
 Cox, N. 2000, *Allen’s Astrophysical Quantities* (New York: AIP Press/Springer)
 Deacon, N. R., Hambly, N. C., & Cooke, J. A. 2005, *A&A*, 435, 363
 Digby, A. P., Hambly, N. C., Cooke, J. A., Reid, I. N., & Cannon, R. D. 2003, *MNRAS*, 344, 583
 ESA 1997, *The Hipparcos and Tycho Catalogues*, ESA SP-1200 (Noordwijk: ESA)
 Feige, J. 1958, *ApJ*, 128, 267
 Giclas, H. L., Burnham, R., & Thomas, N. G. 1971, *Lowell Obs. Bull. (Flagstaff, AZ: Lowell Obs.)*
 Giclas, H. L., Burnham, R. Jr., & Thomas, N. G. 1978, *Lowell Obs. Bull.*, 8, 89
 Gizis, J. E. 1997, *AJ*, 113, 806
 Gray, R. O., Corbally, C. J., Garrison, R. F., McFadden, M. T., Bubar, E. J., McGahee, C. E., O’Donoghue, A. A., & Knox, E. R. 2006, *AJ*, 132, 161
 Gray, R. O., Corbally, C. J., Garrison, R. F., McFadden, M. T., & Robinson, P. E. 2003, *AJ*, 126, 2048
 Greenstein, J. L. 1966, *ApJ*, 144, 496
 Greenstein, J. L., & Eggen, O. J. 1966, *Vistas Astron.*, 8, 63
 Greenstein, J. L., & Münch, G. 1966, *ApJ*, 146, 618

¹¹ We have an ongoing project to survey cool subdwarfs for companions. To date, we have found that cool subdwarfs have a lower binary fraction than cool dwarfs as reported by Riaz et al. (2008), so the contamination assumption from possible unseen companions appears unlikely.

- Goldberg, D., Mazeh, T., Latham, D. W., Stefanik, R. P., Carney, B. W., & Laird, J. B. 2002, *AJ*, **124**, 1132
- Hartwick, F. D. A., Cowley, A. P., & Mould, J. R. 1984, *ApJ*, **286**, 269
- Hawley, S. L., Gizis, J. E., & Reid, I. N. 1996, *AJ*, **112**, 2799
- Heber, U. 1992, LNP Vol. 401: The Atmospheres of Early-Type Stars, **401**, 233
- Henry, T. J., Jao, W.-C., Subasavage, J. P., Beaulieu, T. D., Ianna, P. A., Costa, E., & Méndez, R. A. 2006, *AJ*, **132**, 2360
- Henry, T. J., Subasavage, J. P., Brown, M. A., Beaulieu, T. D., Jao, W.-C., & Hambly, N. C. 2004, *AJ*, **128**, 2460
- Henry, T. J., Walkowicz, L. M., Barto, T. C., & Golimowski, D. A. 2002, *AJ*, **123**, 2002
- Houk, N., & Cowley, A. P. 1975, Michigan Catalogue of Two-dimensional Spectral Types for the HD Star (Ann Arbor, MI: Department of Astronomy Univ. Michigan)
- Humason, M. L., & Zwicky, F. 1947, *ApJ*, **105**, 85
- Jacoby, G. H., Hunter, D. A., & Christian, C. A. 1984, *ApJS*, **56**, 257
- Jao, W.-C., Henry, T. J., Subasavage, J. P., Bean, J. L., Costa, E., Ianna, P. A., & Méndez, R. A. 2003, *AJ*, **125**, 332
- Jao, W.-C., Henry, T. J., Subasavage, J. P., Brown, M. A., Ianna, P. A., Bartlett, J. L., Costa, E., & Méndez, R. A. 2005, *AJ*, **129**, 1954
- Jaschek, C., & Jaschek, M. 1987, *The Classification of Stars* (Cambridge: Cambridge Univ. Press)
- Joy, A. H. 1947, *ApJ*, **105**, 96
- Kazarovets, E. V., Samus, N. N., Durlевич, O. V., Kireeva, N. N., & Pastukhova, E. N. 2006, *Inf. Bull. Var. Stars*, 5721, 1
- Kirkpatrick, J. D. 2005, *ARA&A*, **43**, 195
- Kirkpatrick, J. D., Henry, T. J., & McCarthy, D. W. Jr. 1991, *ApJS*, **77**, 417
- Kirkpatrick, J. D., Henry, T. J., & Simons, D. A. 1995, *AJ*, **109**, 797
- Kuiper, G. P. 1939, *ApJ*, **89**, 548
- Kuiper, G. P. 1940, *ApJ*, **91**, 269
- Laird, J. B., Carney, B. W., & Latham, D. W. 1988, *AJ*, **95**, 1843
- Leggett, S. K. 1992, *ApJS*, **82**, 351
- Lépine, S., Rich, R. M., & Shara, M. M. 2003, *AJ*, **125**, 1598
- Lépine, S., Rich, R. M., & Shara, M. M. 2007, *ApJ*, **669**, 1235
- Lépine, S., & Shara, M. M. 2005, *AJ*, **129**, 1483
- Lodieu, N., Scholz, R.-D., McCaughrean, M. J., Ibata, R., Irwin, M., & Zinnecker, H. 2005, *A&A*, **440**, 1061
- López-Morales, M. 2007, *ApJ*, **660**, 732
- Luyten, W. J. 1979, LHS Catalog (2nd ed.; Minneapolis, MN: Univ. Minnesota)
- Monet, D. G., Dahn, C. C., Vrba, F. J., Harris, H. C., Pier, J. R., Luginbuhl, C. B., & Ables, H. D. 1992, *AJ*, **103**, 638
- Monteiro, H., Jao, W.-C., Henry, T., Subasavage, J., & Beaulieu, T. 2006, *ApJ*, **638**, 446
- Morrison, H. L., et al. 2003, *AJ*, **125**, 2502
- Mould, J. R. 1976, *A&A*, **48**, 443
- Nordström, B., et al. 2004, *A&A*, **418**, 989
- Öhman, Y. 1934, *ApJ*, **80**, 171
- Peterson, R. C., Willmarth, D. W., Carney, B. W., & Chaffee, F. H. Jr. 1980, *ApJ*, **239**, 928
- Reid, I. N., & Gizis, J. E. 2005, *PASP*, **117**, 676
- Reid, I. N., Hawley, S. L., & Gizis, J. E. 1995, *AJ*, **110**, 1838
- Reylé, C., Scholz, R.-D., Schultheis, M., Robin, A. C., & Irwin, M. 2006, *MNRAS*, **373**, 705
- Riaz, B., Gizis, J. E., & Samadgar, D. 2008, *ApJ*, **672**, 1153
- Rodgers, A. W., & Eggen, O. J. 1974, *PASP*, **86**, 742
- Roman, N. G. 1955, *ApJS*, **2**, 195
- Ryan, S. G., & Norris, J. E. 1991, *AJ*, **101**, 1835
- Sandage, A. R., & Eggen, O. J. 1959, *MNRAS*, **119**, 278
- Silva, D. R., & Cornell, M. E. 1992, *ApJS*, **81**, 865
- Smart, R. L., Lattanzi, M. G., Jahreiß, H., Bucciarelli, B., & Massone, G. 2007, *A&A*, **464**, 787
- Subasavage, J. P., Henry, T. J., Hambly, N. C., Brown, M. A., & Jao, W.-C. 2005a, *AJ*, **129**, 413
- Subasavage, J. P., Henry, T. J., Hambly, N. C., Brown, M. A., Jao, W.-C., & Finch, C. T. 2005b, *AJ*, **130**, 1658
- Turnshek, D. E., Turnshek, D. A., & Craine, E. R. 1985, *Astronomy and Astrophysics Series* (Tucson, AZ: Western Research Company)
- Valenti, J. A., Piskunov, N., & Johns-Krull, C. M. 1998, *ApJ*, **498**, 851
- van Altena, W. F., Lee, J. T., & Hoffleit, D. 1995, *The General Catalogue of Trigonometric Stellar Parallaxes* (4th ed.; New Haven, CT: Yale Univ. Obs.)
- Weis, E. W. 1996, *AJ*, **112**, 2300
- West, A. A., et al. 2004, *AJ*, **128**, 426
- Wolf, V. M., & Wallerstein, G. 2005, *MNRAS*, **356**, 963